DOT/FAA/RD-79-103, II
DOT-TSC-FAA-79-18, II

Chicago Monostatic Acoustic Vortex Sensing System

Volume II: Decay of B-707 and DC-8 Vortices

D.C. Burnham
J.N. Hallock

Transportation Systems Center
Cambridge MA 02142

September 1981
Final Report

U.S. Department of Transportation
Federal Aviation Administration

Systems Research and Development Service
Washington DC 20590

Technical Report Documentation Page

1. Report No.	2. Government Accession No.	3. Recipient's Catalog No.
FAA-RD-79-103,II		

4. Title and Subtitle	5. Report Date
CHICAGO MONOSTATIC ACOUSTIC VORTEX SENSING SYSTEM Volume II: Decay of B-707 and DC-8 Vortices	September 1981
	6. Performing Organization Code
	8. Performing Organization Report No. DOT-TSC-FAA-79-18,II
7. Author(s) D.C. Burnham, J.N. Hallock	
9. Performing Organization Name and Address U.S. Department of Transportation Research and Special Programs Administration Transportation Systems Center Cambridge MA 02142	10. Work Unit No. (TRAIS) FA186/R1116 11. Contract or Grant No.
12. Sponsoring Agency Name and Address U.S. Department of Transportation Federal Aviation Administration Systems Research and Development Service Washington DC 20590	13. Type of Report and Period Covered Final Report Oct. 1976-Dec. 1979 14. Sponsoring Agency Code

15. Supplementary Notes

16. Abstract

A Monostatic Acoustic Vortex Sensing System (MAVSS) was installed at Chicago's O'Hare International Airport to measure the strength and decay of aircraft wake vortices from landing aircraft. The MAVSS consists of an array of acoustic antennas which measure the vertical profile up to 60-m altitude of the vertical component of the wind. The decay in wake vortex strength is measured as the vortex passes over successive antennas in the array. In this volume, the data are analyzed to examine whether landing B-707 and DC-8 aircraft need to be divided into Heavy and non-Heavy categories on the basis of wake vortex hazard. Volume I (published in October 1979) described the MAVSS principles of operation, the hardware developed, and the data reduction methods employed. Volume III (to be published at a later date) describes the statistical methods used to understand wake vortex decay and presents the data on all common jet transport aircraft.

17. Key Words	18. Distribution Statement
Wake Vortices Acoustics B-707 DC-8	DOCUMENT IS AVAILABLE TO THE PUBLIC THROUGH THE NATIONAL TECHNICAL INFORMATION SERVICE, SPRINGFIELD, VIRGINIA 22161

19. Security Classif. (of this report)	20. Security Classif. (of this page)	21. No. of Pages	22. Price
Unclassified	Unclassified	140	

Form DOT F 1700.7 (8-72) Reproduction of completed page authorized

PREFACE

An understanding of the statistical nature of aircraft wake vortex behavior can lead to improved airport capacity. This report presents statistical data on the decay of wake vortex strength measured with the Monostatic Acoustic Vortex Sensing System (MAVSS). The data might be used to refine the wake vortex aircraft categories (of specific interest is the current division of B-707s and DC-8s into two categories) and to assess the influence of various meteorological conditions on wake vortex decay.

The authors would like to acknowledge the efforts of their colleagues Tom Sullivan and Berl Winston. Tom Sullivan arranged with the airlines to obtain the landing weights of the aircraft discussed herein. Berl Winston made sure that all the vortex and weight data were correctly stored in a data base and obtained a number of retrievals for the authors. We thank United, TWA, and American Airlines for their cooperation at O'Hare. The continuing interest of Oliver St. John, Chief Scientist of the British Civil Aviation Authority, is acknowledged. We especially thank Myron Clark and Malcolm Burgess, FAA, for their patience and comments on improving the clarity of the report.

METRIC CONVERSION FACTORS

Approximate Conversions to Metric Measures

Symbol	When You Know	Multiply by	To Find	Symbol
		LENGTH		
in	inches	*2.5	centimeters	cm
ft	feet	30	centimeters	cm
yd	yards	0.9	meters	m
mi	miles	1.6	kilometers	km
		AREA		
in^2	square inches	6.5	square centimeters	cm^2
ft^2	square feet	0.09	square meters	m^2
yd^2	square yards	0.8	square meters	m^2
mi^2	square miles	2.6	square kilometers	km^2
	acres	0.4	hectares	ha
		MASS (weight)		
oz	ounces	28	grams	g
lb	pounds	0.45	kilograms	kg
	short tons (2000 lb)	0.9	tonnes	t
		VOLUME		
tsp	teaspoons	5	milliliters	ml
Tbsp	tablespoons	15	milliliters	ml
fl oz	fluid ounces	30	milliliters	ml
c	cups	0.24	liters	l
pt	pints	0.47	liters	l
qt	quarts	0.95	liters	l
gal	gallons	3.8	liters	l
ft^3	cubic feet	0.03	cubic meters	m^3
yd^3	cubic yards	0.76	cubic meters	m^3
		TEMPERATURE (exact)		
°F	Fahrenheit temperature	5/9 (after subtracting 32)	Celsius temperature	°C

*1 in = 2.54 (exactly). For other exact conversions and more detailed tables, see NBS Misc. Publ. 286, Units of Weights and Measures, Price $2.25, SD Catalog No. C13.10:286

Approximate Conversions from Metric Measures

Symbol	When You Know	Multiply by	To Find	Symbol
		LENGTH		
mm	millimeters	0.04	inches	in
cm	centimeters	0.4	inches	in
m	meters	3.3	feet	ft
m	meters	1.1	yards	yd
km	kilometers	0.6	miles	mi
		AREA		
cm^2	square centimeters	0.16	square inches	in^2
m^2	square meters	1.2	square yards	yd^2
km^2	square kilometers	0.4	square miles	mi^2
ha	hectares (10,000 m^2)	2.5	acres	
		MASS (weight)		
g	grams	0.035	ounces	oz
kg	kilograms	2.2	pounds	lb
t	tonnes (1000 kg)	1.1	short tons	
		VOLUME		
ml	milliliters	0.03	fluid ounces	fl oz
l	liters	2.1	pints	pt
l	liters	1.06	quarts	qt
l	liters	0.26	gallons	gal
m^3	cubic meters	35	cubic feet	ft^3
m^3	cubic meters	1.3	cubic yards	yd^3
		TEMPERATURE (exact)		
°C	Celsius temperature	9/5 (then add 32)	Fahrenheit temperature	°F

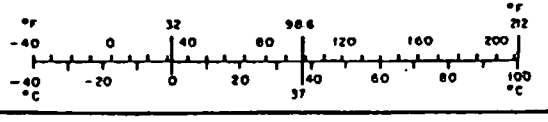

TABLE OF CONTENTS

TABLE OF CONTENTS (CONT.)

LIST OF ILLUSTRATIONS

LIST OF ILLUSTRATIONS (CONT.)

LIST OF ILLUSTRATIONS (CONT.)

LIST OF ILLUSTRATIONS (CONT.)

LIST OF ILLUSTRATIONS (CONT.)

LIST OF ILLUSTRATIONS (CONT.)

LIST OF TABLES

1. INTRODUCTION AND SUMMARY

1.1 INTRODUCTION

The Federal Aviation Administration (FAA) categorizes aircraft for separation purposes into three groups according to the maximum certificated gross takeoff weight:

CATEGORY	MAX. CERTIFICATED GROSS TAKEOFF WEIGHT, W
Small	$W \leq 12{,}500$ lb
Large	12,500 lb $< W <$ 300,000 lb
Heavy	300,000 lb $\leq W$.

The selection of the boundaries between the categories was determined both by the original intent of the categories and by the aircraft types existing at the time of the selection. The division between Small and Large at 12,500 lb (5700 kg) was formally made in Amendment 10 to Civil Air Regulation (CAR) 3 in 1953 which limited the applicability of CAR 3 to airplanes having a maximum weight of 12,500 lb or less. The weight division fell in the middle of the large gap between the few thousand-pound general aviation aircraft and the approximately 28,000 lb (12,700 kg) DC-3. Subsequent development of aircraft has filled in this gap so that one of the original selection criteria no longer pertains.

The introduction of jet transports into airline service in 1959 increased the concern about the effects of successively larger aircraft on traffic spacing. With the advent of the jumbo jet, concern was again expressed over the possibility that the wake vortices generated by these aircraft would be a hazard to other aircraft flying within the terminal area. The division between Large and Heavy aircraft was made in 1970 at 300,000 lb (136,000 kg) in order to deal with the wake vortex hazard. The introduction of the Boeing 747 more than doubled the maximum certificated gross takeoff weight of jet transport aircraft. Flight tests (Ref. 1) showed the B-747 vortices could produce a

significant hazard to following aircraft at the 3-nautical-mile Instrument Flight Rules (IFR) separation standard in use at that time. In order to eliminate the apparent hazard, the separation standards were increased behind the newly created category of Heavy aircraft.

At that time (1970) new heavy versions of the B-707 and DC-8 had already been introduced. The dividing line between Large and Heavy was set at 300,000 lb to include these heavier aircraft with the B-747 in order to minimize the vortex hazard to following aircraft. Subsequently, the weight gap between the B-707/DC-8 and B-747 was filled by the L-1011, DC-10, and A-300.

At the present time, the original decision to split both the B-707 and DC-8 aircraft into two weight categories appears to be arbitrary and confusing. If all B-707 and DC-8 aircraft could be safely classified as Large, reductions could be achieved in the wake vortex-caused delays at congested airports. Reference 2 indicated that placing the stretched versions of the DC-8s and B-707s in the Large category would result in a capacity increase of about 3 to 6 percent at the major airports. It is worth noting that such a classification was used in the United Kingdom (UK); the UK used 375,000 lb (170,000 kg) as the weight for separating between Large (the UK call this group Medium) and Heavy up to August 1978 when the Ninth Air Navigation Commission Meeting of the International Civil Aviation Organization (ICAO) formalized 300,000 lb (136,000 kg) as the weight dividing Large and Heavy.

Between July 1976 and September 1977 TSC collected data at Chicago's O'Hare airport on the decay of wake vortex strength. The Monostatic Acoustic Vortex Sensing System (MAVSS), the remote sensing technique employed, makes use of sound energy scattered from temperature fluctuations to measure the velocity profile of a vortex. Volume I of this report described the hardware and data processing involved in these measurements. The data reported herein were collected during normal airport landing operations. Volume III of this report will present the data for all the common jet transport aircraft and will describe in depth the analysis techniques developed to study the data.

Section 2 outlines the data collection procedures and describes the methods used to identify the aircraft types and models and to obtain the landing weights of the B-707s and DC-8s. Section 3 examines the theory of vortex strength and decay to identify the relevant aircraft parameters. Section 4 contains the data analysis. The correlation of vortex strength with aircraft weight is examined statistically. A primary issue addressed is whether there are any differences between the vortices generated by the landing Large and Heavy versions of the B-707 or DC-8. The issues in the wake vortex categorization of aircraft are studied in Section 5. In Section 6 the observations by the British through their incident reporting system are discussed; prior to August 1978, they classified all models of the B-707 and DC-8 into the Large category.

It is envisioned that eventually aircraft categories will be set based on an understanding of what aircraft parameters in addition to weight should be included. Wingspan must certainly play a role, and engine placement is also likely to be important. If vortex decay can be characterized by a few aircraft parameters, then one can hope to have a more rational system of dealing with the wake vortex hazard. Volume III of this report will address the merits of such a revision of the wake vortex separation categories.

1.2 SUMMARY

The results of this study indicate little possibility of an adverse effect on safety from classifying all landing B-707 and DC-8 aircraft as Large. First, prior to the introduction of the widebody jets in 1970, the standard separation was 3 nautical miles and no problems were experienced even with millions of B-707 and DC-8 landings (including B-707/DC-8 aircraft that are now designated as Heavy). Second, the B-707/DC-8 aircraft classified as Heavy show wake vortex hazards similar to those from the DC-8 aircraft classified as Large. The data indicate similar vortex hazards for jet transport aircraft following Large B-707s, but lower vortex hazards for General Aviation aircraft following Large

B-707s. The net safety impact of reclassifying the B-707H and DC-8H aircraft as Large is to increase the frequency of exposure of following aircraft to the most persistent vortices currently generated by Large aircraft (i.e., DC-8 vortices).

Third, the analysis of the weight dependence of the vortex hazard indicated that the heaviest B-707/DC-8 aircraft would have a vortex hazard midway between the average hazard of the Large DC-8 and that of the B-747/L-1011. This effect of actual aircraft weight is not large enough compared to the other variables affecting the vortex hazard to warrant the complexity of using actual aircraft landing weights to determine aircraft category. This conclusion could be invalid if the landing weights at O'Hare were abnormally low; however, the data in Appendix A show that the O'Hare DC-8H weights are typical of other airports. Fourth, the UK incident reporting system statistics show that the incident rate behind Heavy B-707/DC-8 aircraft at Large separations is reasonable, and is in fact similar to the incident rate behind widebody aircraft at Heavy separations leading to a well balanced system.

The results of this study could contribute to a decision to change the wake vortex separation standards behind landing B-707H and DC-8H aircraft to achieve reduced wake vortex delays. It should be noted that, this study only addressed the B-707H and DC-8H aircraft; raising the dividing line between Large and Heavy to, say, 375,000 lb maximum certificated gross takeoff weight would have the virtue of being consistent with the former UK categories, which are supported by their incident reporting system, but would deal with the A-300 and IL-62 (as well as the A-310 and B-767) with some uncertainty since no experimental vortex strength data are available on these aircraft.

2. DATA COLLECTION AND PROCESSING

The details of the Monostatic Acoustic Vortex Sensing System (MAVSS) data collection are discussed in Volume I (Ref. 3) of this report. The procedures used will be outlined here. A detailed discussion will be presentcd on the methods for obtaining and verifying the aircraft weights and the category (Heavy or Large) of the landing B-707s and DC-8s.

2.1 MAVSS DATA COLLECTION AND PROCESSINC

Each MAVSS antenna measures the vertical profile of the vertical component of the wind above the antenna. As a vortex drifts past an antenna, the vertical velocity profile of the vortex is measured. This measurement is particularly appropriate for aircraft wake vortices since the ambient wind has virtually no vertical velocity component. The vertical velocity signature of a vortex is thus easily and accurately measured as the vortex drifts over a MAVSS antenna. The decay of a vortex can be monitored as it passes successively over several antennas located on a baseline oriented perpendicular to the aircraft flight path. Vortex arrivals are detected by means of their characteristic signatures, including a rapid reversal of velocity as the vortex core passes over the antenna.

The MAVSS baselines were located 610 m (2000 ft) from the runway threshold for runway 32L and 472 m (1550 ft) from the runway threshold for runway 14R. The extent of the baselines made use of the available real estate. Only two antennas were located on the starboard side (looking toward the threshold) of the runway at 61-m (200-ft) and 122-m (400-ft) displacements from the extended runway centerline. On the port side, four (14R) and five (32L) antennas were installed at 61-m (200-ft) spacings. The final edited data base contains MAVSS data for 773 B-707s, 103 B-707Hs, 305 DC-8s, and 183 DC-8Hs.

Figure 1 shows computer-identified detections (the vertical lines) of DC-8H vortices in three of the five antennas on one side of the extended runway centerline (speaker 5 is closest to the extended certerline, speaker 4 is next, etc.). The horizontal axes for each speaker represent different heights or range gates above the MAVSS antenna. The first vortex detected (termed vortex 1) is on the downwind side of the flight path and is detected by three antennas (speakers 5, 4, and 3, respectively). The second vortex detected (termed vortex 2) is from the upwind side of the flight path and is detected by only two antennas (speakers 5 and 4, respectively).

Figure 2 shows the tangential or vertical velocity profiles for each detected DC-8H vortex in Figure 1. The vortex is seen to weaken as it passes successively over the antennas. Figure 3a shows the arrival times of the vortices at the antenna positions.

The velocity profiles (v(r'), where r' is the vortex radius) are used to determine the average vortex strength Γ' according to the equation:

$$\Gamma'(r) = \frac{1}{2r} \int_{-r}^{r} 2\pi r' \, v(r') \, dr', \qquad (1)$$

where r is the averaging radius. The average strength is a useful measurement since it can be related to the vortex-induced rolling moment on a wing of span 2r. The velocity profiles in Figure 2 were used to generate the vortex strength points plotted in Figure 3b for an averaging radius of 5 meters. Each valid vortex detection leads to a value of strength. The average circulation $\Gamma'(r)$ was calculated for four averaging radii: 5, 10, 20, and 30 meters. Later, average circulations for 15 meters were obtained by interpolation.

Some of the data analysis techniques used in this report require more information than is contained in Figure 3b. An interpolation and extrapolation procedure was developed to give the vortex strength history, i.e., the vortex strength at any particular time. The most difficult part of determining the

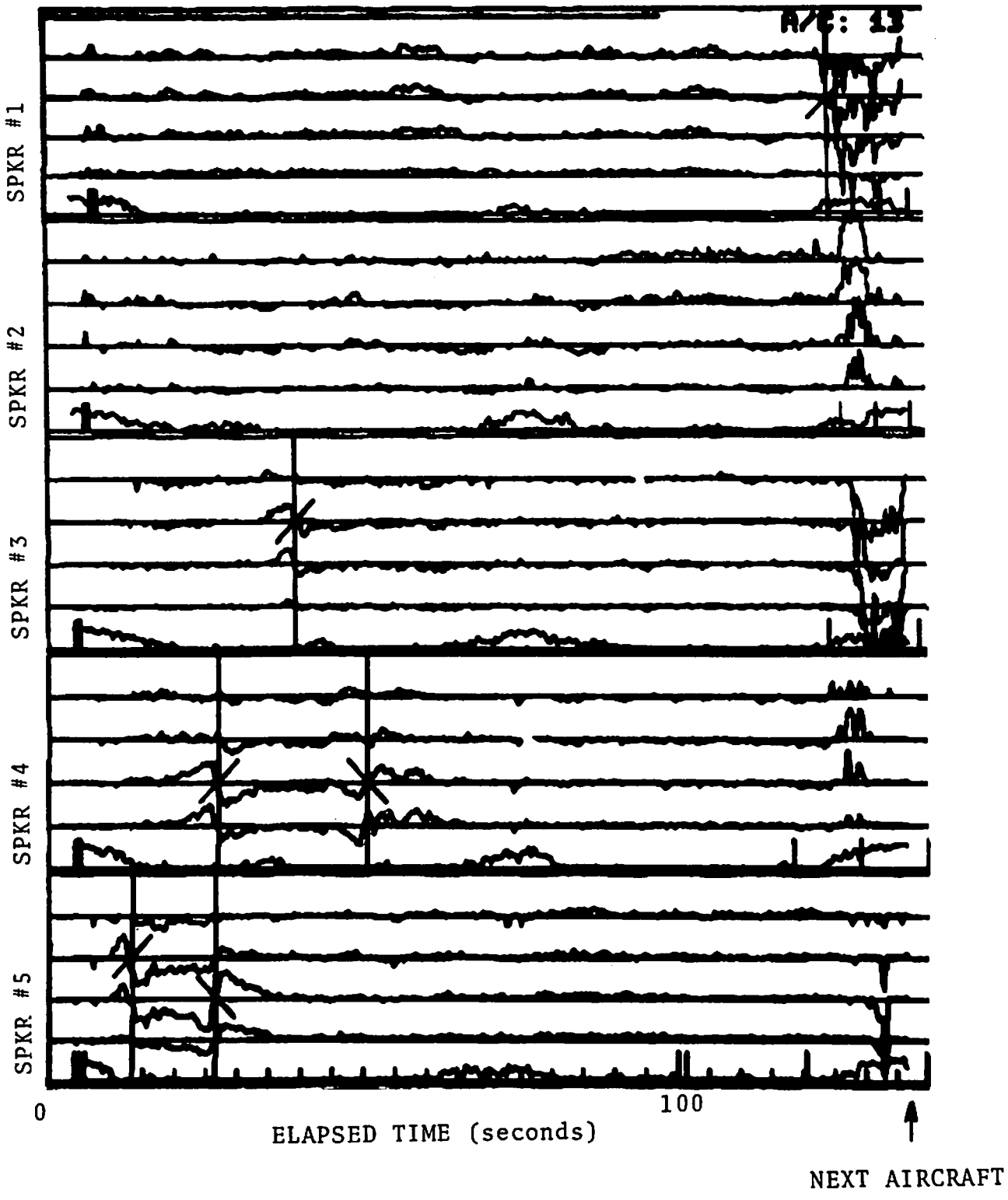

FIGURE 1. VORTEX DETECTIONS FOR A DC-8H AIRCRAFT

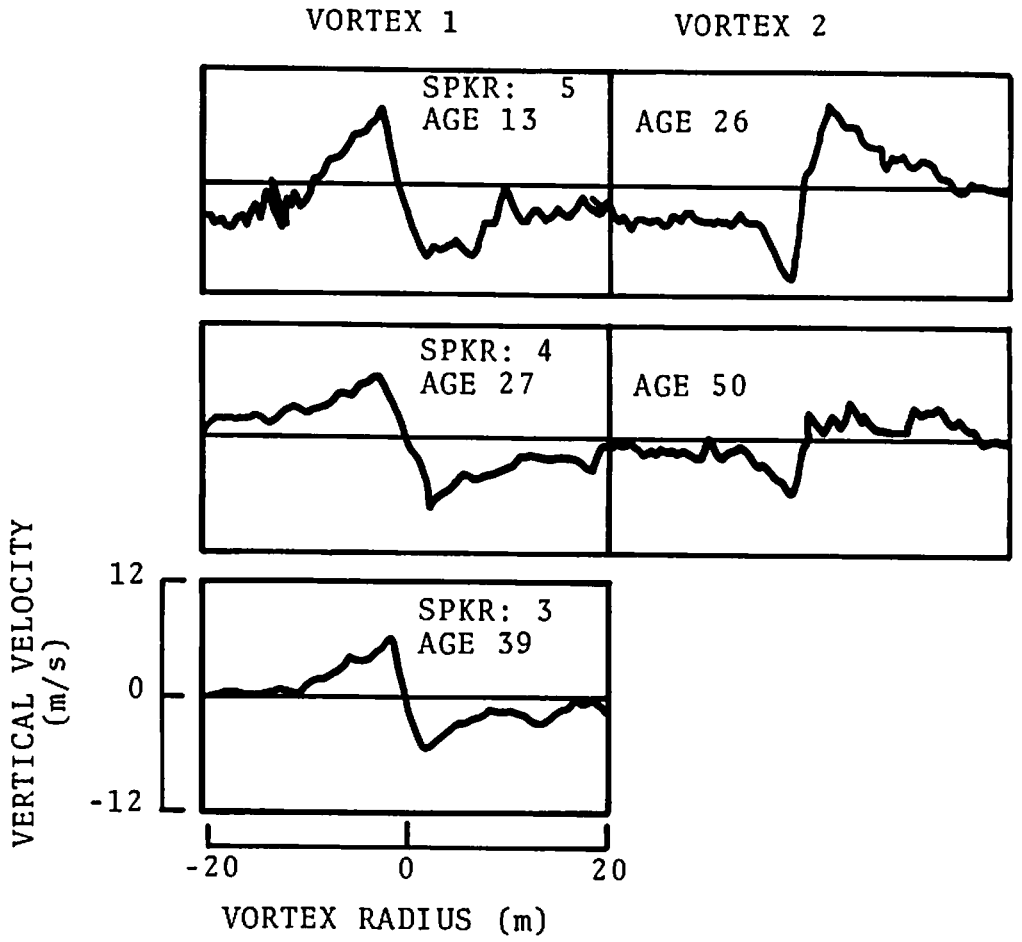

FIGURE 2. VORTEX VELOCITY PROFILES FOR EACH VORTEX DETECTION IN FIGURE 1

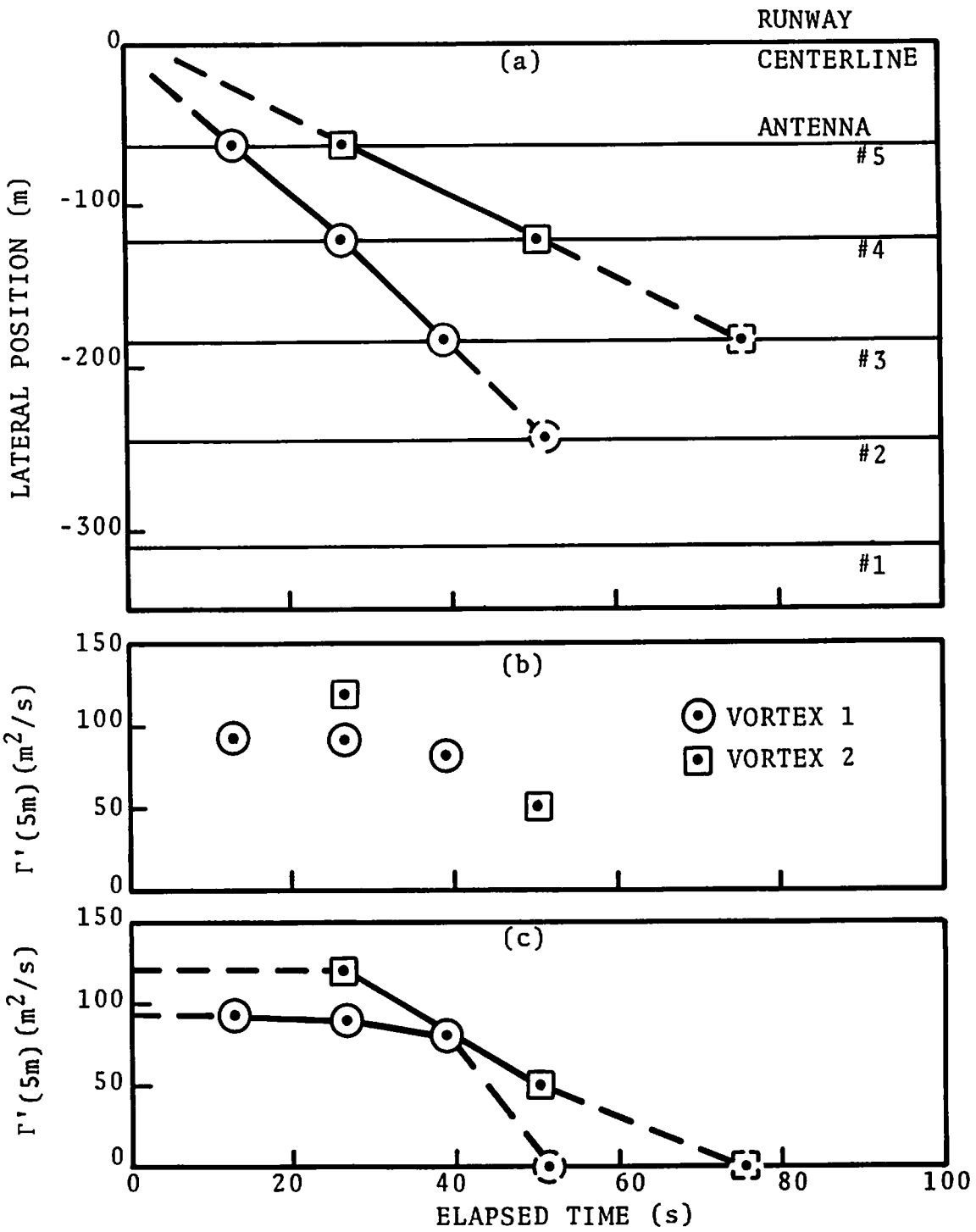

FIGURE 3. VORTEX TIME HISTORIES FOR THE SAME RUN AS IN FIGURES 1 AND 2; (a) Vortex Lateral Position, (b) Average Strength (5-m averaging radius), and (c) Extrapolated and Interpolated Average Strength

vortex strength history is the problem of dealing with the demise of a vortex. The MAVSS cannot detect vortices when their strength falls below the MAVSS detection threshold, which is approximately 30, 40, and 55 m^2/s for averaging radii of 5, 10, and 20 meters, respectively. Figure 3c shows the vortex strength histories obtained by means of the following assumptions:

1) The vortex strength is constant until it is first detected and has the strength value determined from the first detection.

2) The vortex strength is obtained by interpolation between successive vortex detections.

3) The vortex strength is assumed to be zero if it cannot be detected at the next antenna after the last detection. The vortex strength is then extrapolated to zero at the time it would be expected to reach the next antenna, moving at constant velocity (see the extrapolated lines in Figure 3a). This extrapolation is excluded if the last detection is in the last antenna of the array (e.g., antenna 1 for the case in Figure 3a) or if the expected arrival time is too close to the next aircraft landing (not a problem here according to Figure 1). These restrictions were implemented to avoid introducing systematic biases into the data. Nevertheless, it is difficult to assess the errors generated by extrapolating the data to zero strength. For example, the residue of vortex 1 can be seen in speaker 2 of Figure 1, even though the extrapolation procedure assumes zero strength there.

Only vortices detected in at least two antennas are included in later analyses.

The vortex data were edited to remove spurious vortex detections and strength measurements corrupted by noise, and were then entered into a data base. Anomalous data which passed through the first editing process were subsequently eliminated from the data base. The MAVSS data base consists of a number of strength

measurements made on each vortex generated by a landing aircraft. The landing time, aircraft type, weight (if known), and weather conditions are also recorded for each landing.

2.2 AIRCRAFT WEIGHTS

Both the B-707 and the DC-8 consist of a number of models. Table 1 presents the pertinent physical characteristics (Refs. 4 to 6) for the models of interest here. FAA Type Certification for the first B-707 (Series 120) was approved in September 1958 and the last model (Series 320C) in April 1963 (Ref. 5). FAA Type Certification for the first DC-8 (Series 10) was approved in August 1959 and the last model (Series 63) in June 1967 (Ref. 5).

Identification of the aircraft type was the responsibility of the vortex test site operators. The primary means of identification was the airline operating the aircraft. At Chicago O'Hare, knowing the airline uniquely identified whether an aircraft was a DC-8 or a B-707. The landing weights were obtained by telephoning representatives of United, TWA, or American Airlines shortly after the respective aircraft landed. United operates DC-8s, and TWA and American Airlines operate B-707s. According to Reference 5, United owns DC-8 Series 10, 20, 50, 61 and 62; TWA owns B-707 Series 120, 120B, 320, 320B, and 320C; and American owns B-707 Series 120B, 320B, and 320C.

At the beginning of the data collection, an aircraft was determined to be Heavy whenever the test site operator heard a pilot or controller announce an aircraft to be a Heavy (e.g., "United 773 Heavy by the outer marker..." or "American 321 Heavy cleared to land..."). However, a number of Heavy/Large inconsistencies were noted. Subsequently, the site operators requested both the landing weights and the aircraft series or class from the respective airline. Many of the previous inconsistencies were corrected by comparing the Heavy or Large designation for the same flight number over a period of several days. Some inconsistencies remained, however, and these will be discussed later.

TABLE 1. CHARACTERISTICS OF B-707 AND DC-8 MODELS

Model	Wingspan (ft)	Maximum Takeoff Weight (lb)	Maximum Landing Weight (lb)
B-707-120	130.9	258,000	185,000
B-707-120B	130.9	258,000	190,000
B-707-220	130.9	247,000	185,000
B-070-320	142.4	316,000	207,000
B-707-320B	145.8	336,000	247,000
B-707-320C	145.8	336,000	247,000
B-707-420	142.4	316,000	207,000
DC-8-10	142.3	273,000	193,000
DC-8-20	142.3	276,000	199,500
DC-8-30	142.3	315,000	207,000
DC-8-40	142.3	315,000	207,000
DC-8-50	142.3	325,000	207,000
DC-8-61	142.3	325,000	240,000
DC-8-62	148.4	335,000	240,000
DC-8-63	148.4	350,000	245,000

Table 2 shows the landing weight data obtained at O'Hare. Figures 4 and 5 are histograms of the weight data. The arrows indicate the maximum landing weights (Refs. 4 to 6). No aircraft designated Heavy had a landing weight in excess of the published maximum landing weight. The Large B-707 and DC-8 weights did indicate a number of cases where the landing weights were more than the published maximum landing weights. Either the published values are too low (supplementary certificates may have permitted raising the maximum landing weight) or some of the Heavy aircraft were designated as Large. The effect of this inconsistency is examined in Section 4 by means of the following reassignments:

1) All B-707s with landing weights greater than 190,000 lb are declared Heavies.

2) All DC-8s with landing weights greater than 200,000 lb are declared Heavies.

This reassignment was found to have minimal influence on the results of this study.

To demonstrate the representativeness of the weights of the aircraft landing at O'Hare, the weight data for Heavy DC-8s landing at other airports were obtained and are presented in Appendix A. For these 52 landing DC-8Hs, the maximum weight recorded was 233,000 lb and the minimum weight was 178,100 lb; the mean weight was 205,900 lb with a standard deviation of 11,500 lb. These values are consistent with those reported at O'Hare (Table 2).

TABLE 2. LANDING WEIGHTS

Aircraft Type	No. of Cases	Maximum Weight (lb)	Minimum Weight (lb)	Mean Weight (lb)	σ (lb)
B-707	668	208000	151000	171000	10000
B-707H	106	246000	154000	193000	18000
DC-8	307	229000	151000	183000	15000
DC-8H	247	240000	160000	202000	15000

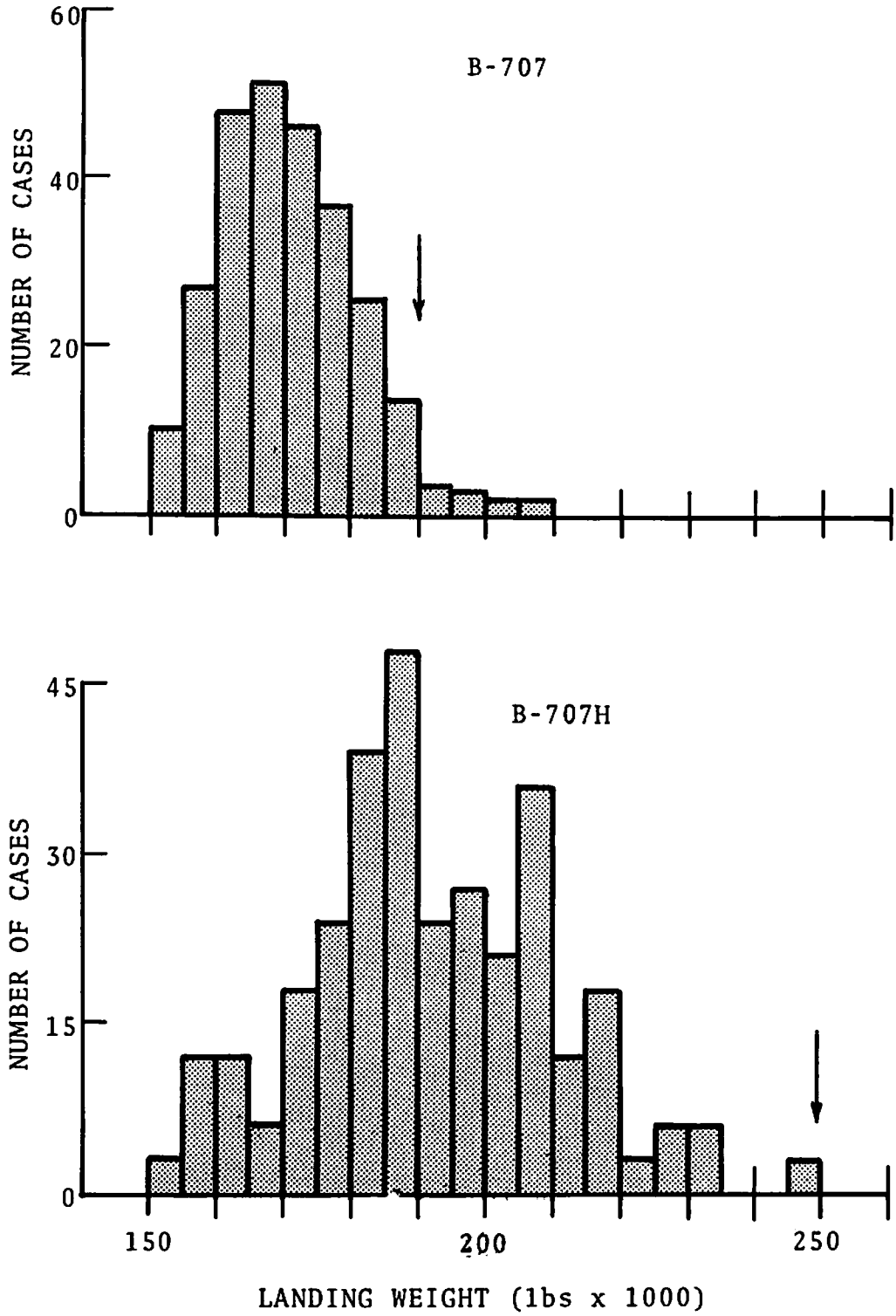

FIGURE 4. LANDING WEIGHT HISTOGRAMS FOR B-707 AND B-707H AIRCRAFT

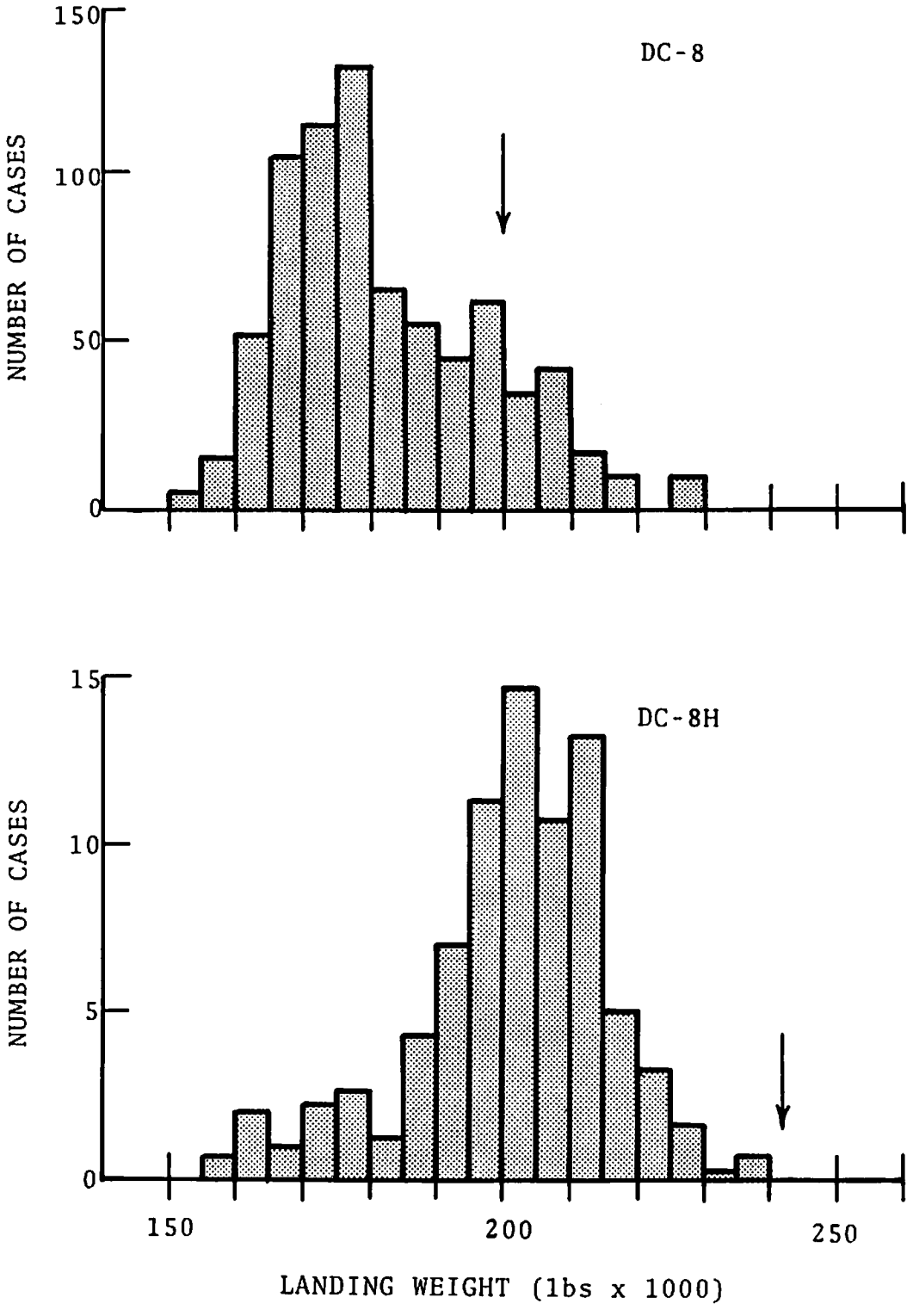

FIGURE 5. LANDING WEIGHT HISTOGRAMS FOR DC-8 AND DC-8H AIRCRAFT

3. THEORY OF VORTEX STRENGTH

Aerodynamic theory has produced a simple understanding of the initial total circulation or strength of a wake vortex. Unfortunately, no such understanding is available for vortex decay. This section examines the implications of available theory for the correlation of vortex strength and decay with aircraft parameters.

3.1 INITIAL VORTEX STRENGTH

The classical expression for the dependence of total wake vortex strength upon aircraft parameters (Ref. 7) is:

$$\Gamma_\infty = CW/\rho bV \qquad (2)$$

where W is the aircraft weight, b is the wingspan, V is the airspeed, ρ is the air density, and C is a constant depending upon the wing loading distribution ($C = 4/\pi$ for elliptic loading). The total strength Γ_∞ increases with aircraft weight and decreases with airspeed and wingspan. The Heavy aircraft tend to have larger wingspans as well as weights. Thus, some of the effect of heavier weight is cancelled by the larger wingspans.

Since aircraft weight data were collected but not data on airspeed or air density, it will be of particular interest to examine how the vortex strength might depend upon aircraft weight under the assumption of fixed wingspan and fixed air density. If the wing loading distribution is also fixed (i.e., the same flap setting), a pilot can respond to changes in weight in two ways. The first is to keep the same airspeed V and change the aircraft pitch angle so as to change the coefficient of lift. This procedure yields an initial vortex strength that is proportional to the weight. The second possible response is to keep the pitch attitude fixed and vary the airspeed to accommodate the weight change. (This method is normally used.) Since the lift is proportional to the square of the airspeed, the latter procedure yields a strength that is proportional to the square root of the weight. Equation (2) also

predicts that the ratio of vortex strength to aircraft weight will be inversely proportional to the wingspan assuming a similar lift distribution and the same airspeed. These predictions will be compared to the observed weight dependence of vortex strength in Section 4.2.

The use of Equation (1) to describe the average vortex strength $\Gamma'(r)$ is strictly valid only in the limit as the averaging radius r approaches infinity. However, if the velocity profiles are similar, as one would expect for similar lift distributions, the value of $\Gamma'(r)$ will be proportional to Γ_∞ for all values of r.

3.2 VORTEX DECAY

Persistence of the wake vortex hazard depends upon aircraft parameters (wingspan, weight, configuration, engine location, etc.) meteorological parameters (wind velocity, wind shear, turbulence, atmospheric stability, pressure, etc.), and decay processes (vortex linking, bursting, and turbulent diffusion). Since the decay processes occur at random even when all the parameters are fixed, the persistence of a vortex can be defined only through a probability.

The current designation of wake vortex separation categories assigns the wake vortex hazard to a single aircraft parameter, the maximum certificated gross takeoff weight. Of necessity, this simplified procedure gives only a rough indication of the wake vortex hazard. The actual hazard persistence for a specified aircraft has a wide spread because of variation in the actual weight (as well as in the other aircraft parameters), varation in the meteorological conditions, and the stochastic nature of vortex decay. Because of this spread, the change in the vortex hazard probability will be relatively small for small percentage changes in the maximum certificated gross takeoff weight (e.g., an increase from 300,000 lb to 375,000 lb or a 25 percent change).

A theory of wake vortex decay must depend both upon the properties of the vortex wake and upon the properties of the atmosphere. Although some progress has been made in understanding

the characteristics of two decay mechanisms, linking (Ref. 8) and bursting (Ref. 9), no simple functional dependence, such as Equation (2), has been found to describe the dependence of vortex decay upon aircraft parameters. In the next section the following statement concerning vortex decay from a particular aircraft type will be proffered, namely that the vortex strength $\Gamma(t)$ at a time t is simply a fraction $F(t)$ of the initial vortex strength, $\Gamma(t=0) = \Gamma(0)$:

$$\Gamma(t) = F(t)\ \Gamma(0). \qquad (3)$$

Therefore, the distribution of vortex strengths for all times is similar to the initial distribution of strengths.

4. DATA ANALYSIS AND DISCUSSION

Two methods of analyzing the MAVSS strength data will be presented herein; additional methods will be described in Volume III. The first and simpler analysis uses the measurements on only detected vortices with no extrapolation or interpolation (as in Figure 3b). Each detection is treated as a separate data point. This method of analysis is useful only for vortex ages or times less than 40 or 50 seconds; after 40 or 50 seconds many vortices have decayed below the MAVSS detection threshold. The second method is for later times and makes use of interpolated and extrapolated vortex histories (as in Figure 3c). These histories are used to determine the probability for the vortex strength to remain above a selected strength value at a particular vortex age.

4.1 STATISTICAL ANALYSIS

Section 4.1 examines the applicability of Equation (2), the classical expression for the dependence of wake strength on aircraft parameters. The dependence on vortex age and aircraft type (Section 4.1.1), on average aircraft weight (Section 4.1.2), and on weight (Section 4.1.3) is calculated from the MAVSS data.

4.1.1 Dependence of Vortex Strength on Vortex Age and Aircraft Type

The analysis herein makes use of all vortex measurements for a particular aircraft class. For example, Figure 6 shows the 5-m average strength measurements for B-707H aircraft. Statistical analysis is applied to all detections in a 10- or 20-second time interval. There may be some redundancy in the data since the same vortex could be detected at more than one antenna within the 10- or 20-second time interval. This redundancy, however, has no effect on the statistics since the large strength variation shown in Figure 6 is caused by variations in decay and measurement errors, not by the variation of aircraft parameters.

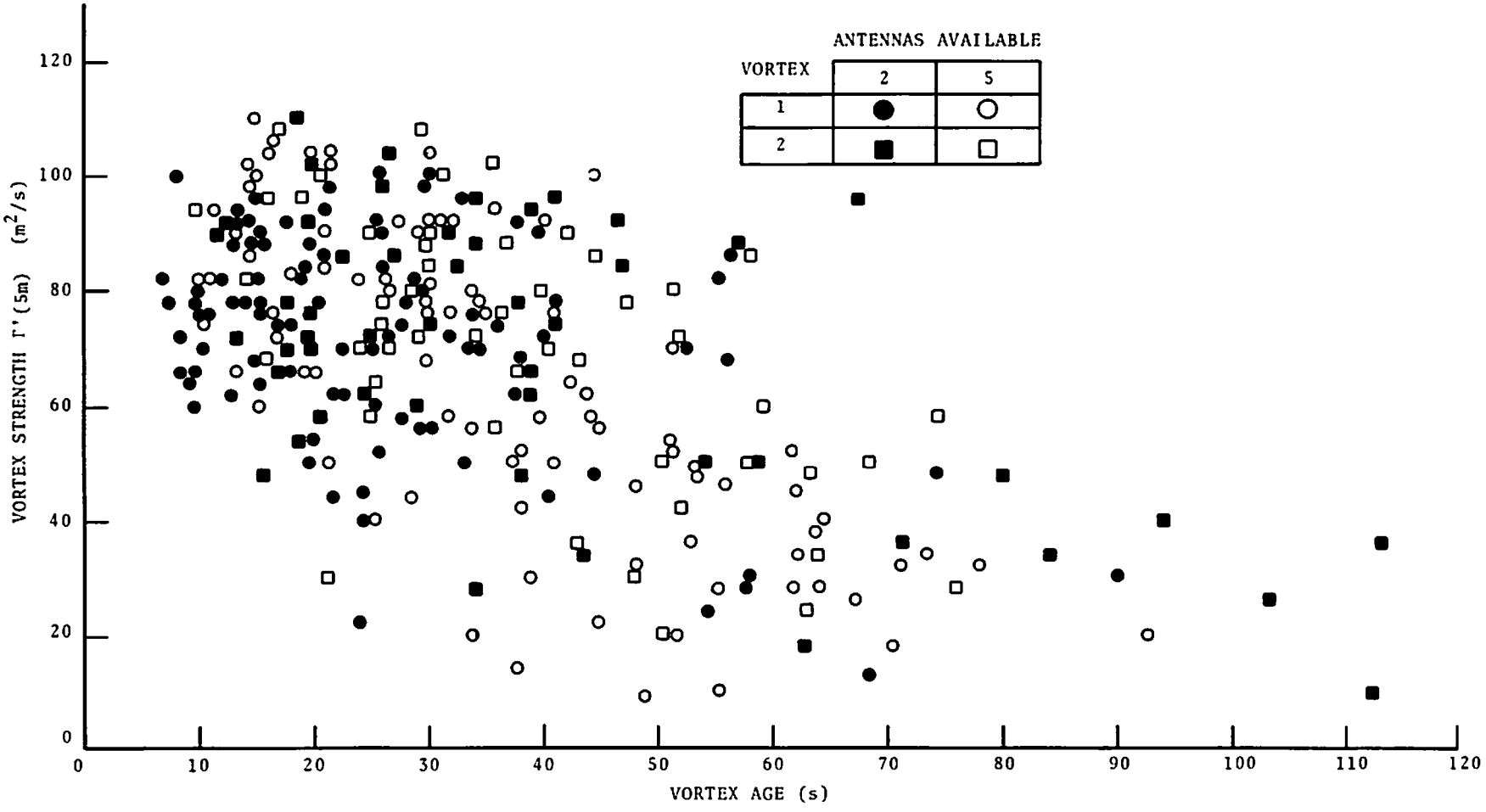

FIGURE 6. STRENGTH MEASUREMENTS (5-m AVERAGING RADIUS) OF B-707H VORTICES

The number of vortex detections per unit time decreases for long times because of two effects: (1) Vortex decay brings the vortex strength below the MAVSS detection threshold. (2) Because there are only two antennas on one side of the extended runway centerline (four or five on the other), many vortices are lost after two detections even though the vortices may not have decayed. The second effect can be seen in Figure 6 where relatively few solid points (only 2 antennas available) are seen after 40 seconds. Figure 7 shows the number of strength measurements per second versus vortex age in Figure 6. Since few vortices were lost off the end of the five-antenna line, the open symbol points reflect the effect of vortex decay.

Because the statistical fluctuations in Figure 7 tend to obscure the trends in the data, Figure 8 is included to show the total number of measurements per second for the B-707 (which had the most data). The reduction in the number of measurements for older vortices is similar for the other aircraft types. The number of measurements for the B-707H, DC-8, and DC-8H is 15, 40, and 40 percent, respectively, of that for the B-707.

The two loss mechanisms described above have different effects on vortex strength statistics. The effect of a short baseline (the loss of vortices off the end of the two-antenna array, effect 2) introduces little bias to the data, but simply reduces the number of data points. The effect of a detection threshold (i.e., eliminating the vortices below the detection threshold) introduces significant biases into the vortex strength distribution when a large fraction of the vortices are undetected. Figure 8 shows that half the vortices are lost after 45 seconds. Since many of these are lost due to the short baseline (effect 2), the data before 45 seconds can be considered to be relatively unbiased.

Figure 9 shows the decay of mean vortex strength with time for the four aircraft. The error bars indicate the rms deviation in strength. These plots represent a statistical analysis of the scatter plots (e.g., Figure 6) for each aircraft type and averaging radius. The same 20-second time intervals were used for all

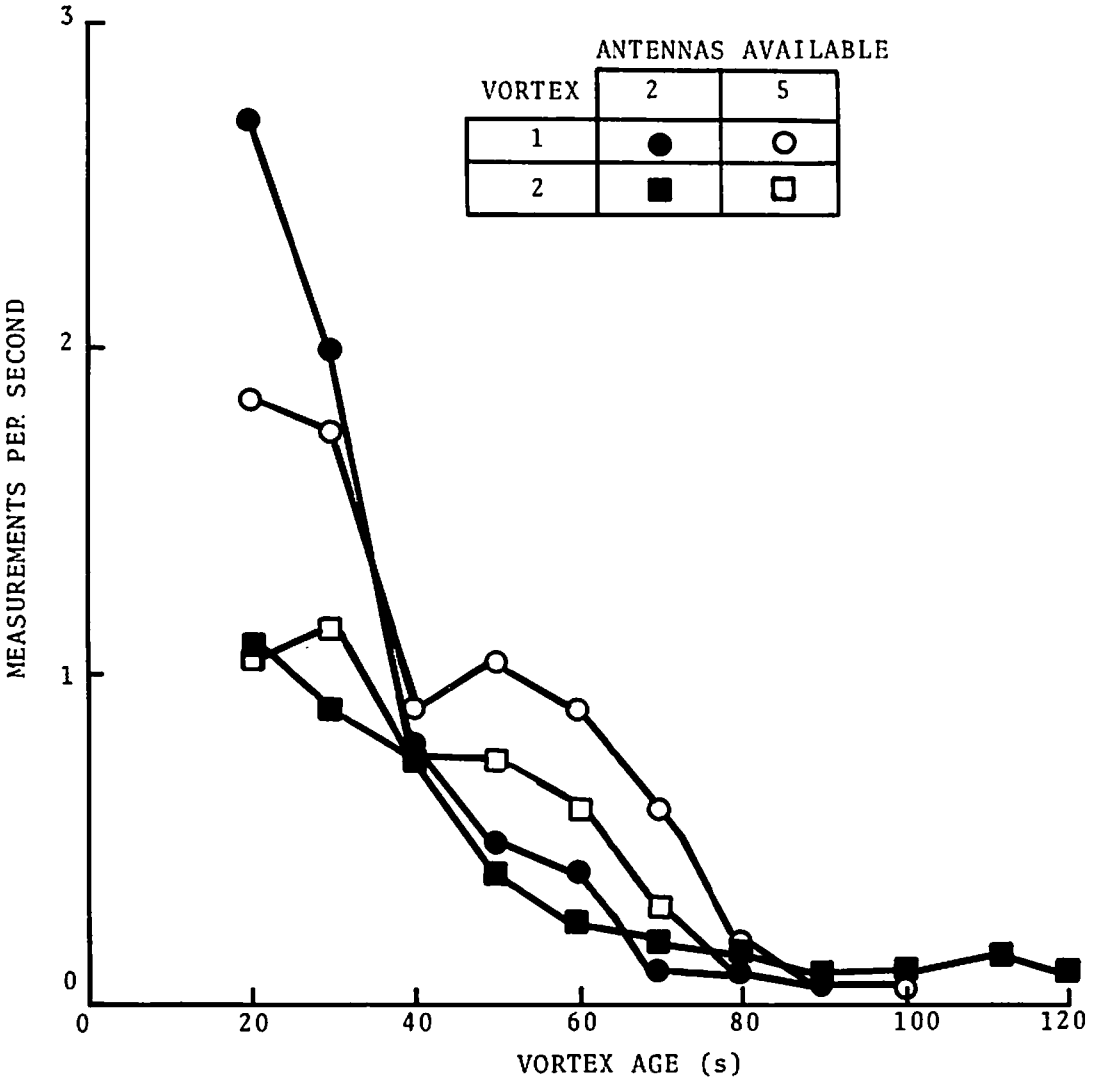

FIGURE 7. NUMBER OF MEASUREMENTS PER SECOND VERSUS VORTEX AGE IN FIGURE 6. (Each point represents a 20-second interval.)

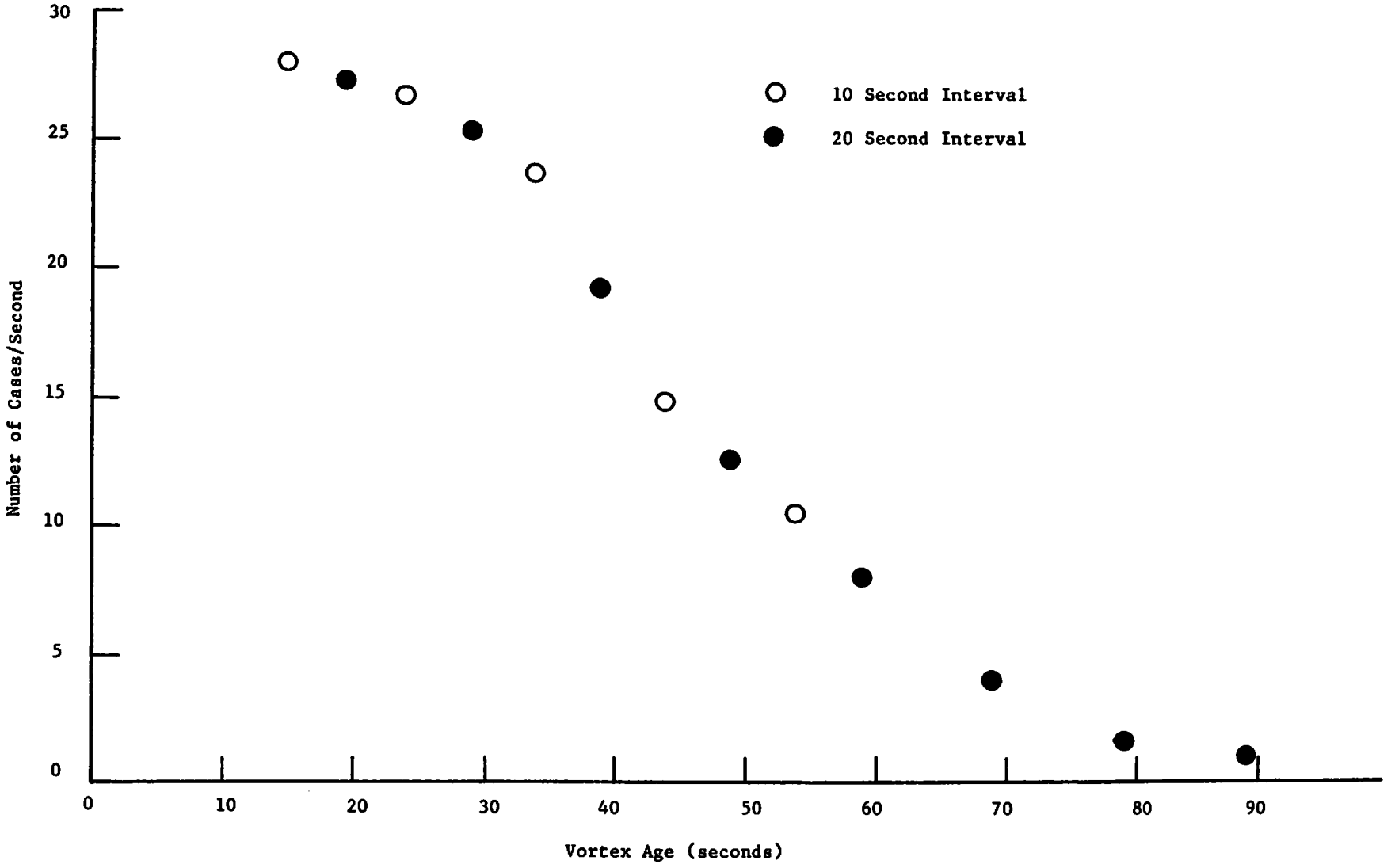

FIGURE 8. TOTAL NUMBER OF VORTEX MEASUREMENTS PER SECOND OF VORTEX AGE (B-707, 5-m, 20-second intervals)

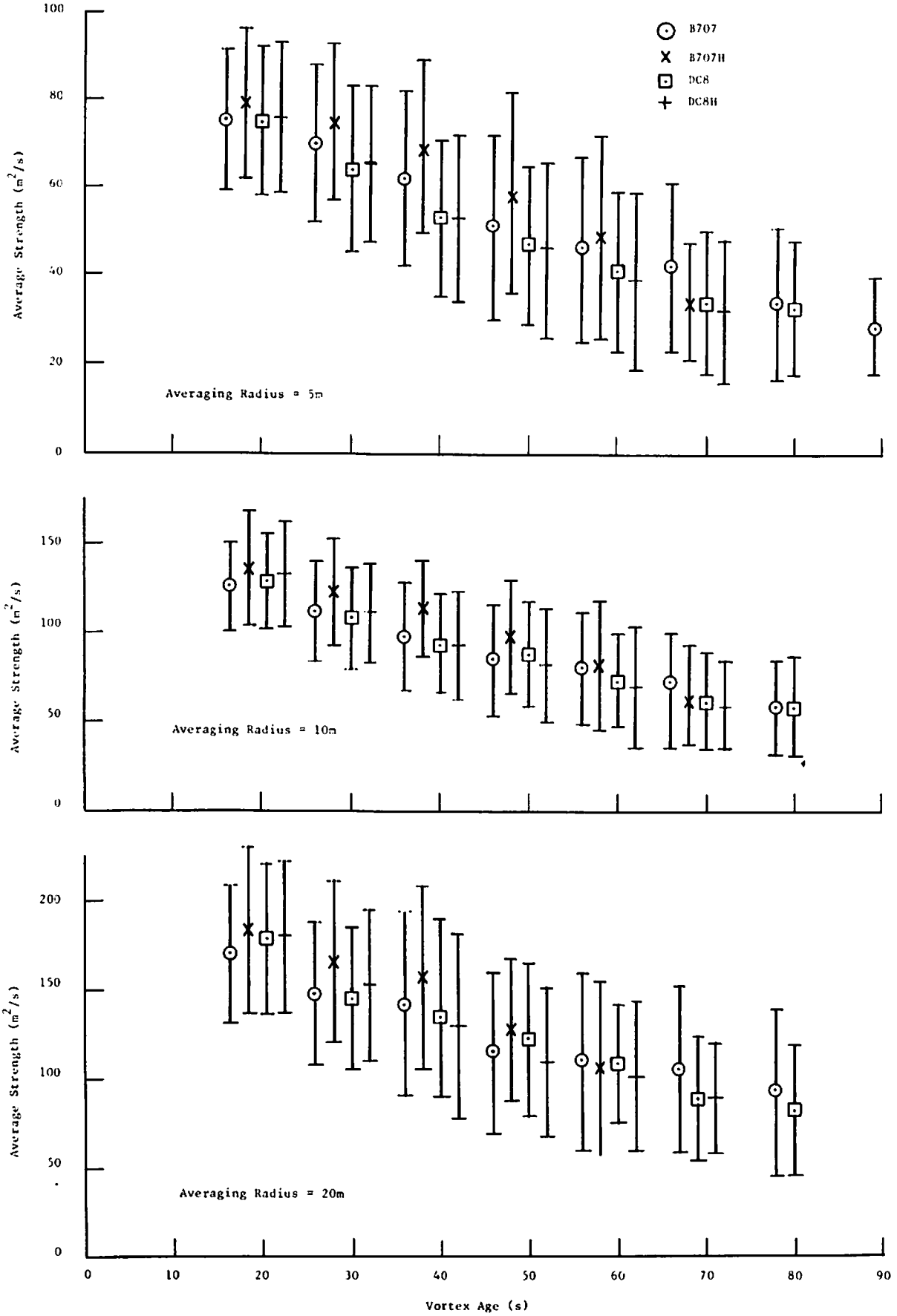

FIGURE 9. VORTEX STRENGTH VERSUS AGE

aircraft types; the plotted points are displaced laterally to avoid overlap. One should note that adjacent points at 10-second spacing are not statistically independent. When most of the vortices have decayed to below the detection threshold, one would expect the remaining vortices to exhibit a mean vortex strength about one rms deviation above the threshold. The data in fact show this effect. For times greater than 50 seconds, the lower bound of the error bars lies at the detection threshold.

The data in Figure 9 show similar decay for all three averaging radii. The four aircraft generally have similar mean strength values. At intermediate times, the B-707H shows somewhat higher strength values, particularly for the smaller averaging radii.

4.1.2 Initial Vortex Strength

The simplest approach toward verifying the applicability of Equation (2) is to make use of the average initial strength $\overline{\Gamma}$ and average weight $\overline{W}$ for each aircraft type. (The overbar indicates average value.) Table 3 presents the results on the ratio of initial vortex strength to weight ($\overline{\Gamma}/\overline{W}$) for different averaging radii. The errors are standard errors. Detections between 10 and 20 seconds are included to estimate the initial vortex strength; before 10 seconds the vortex cannot be considered to be rolled up, and the 20-second upper limit minimizes the effects of vortex decay. The values for averaging from zero radius to two non-zero radii can be combined to give a circulation average between the two non-zero radii. The values for 5 to 10 m radius and 10 to 20 m radius are computed to show the dependence of strength upon radius. The 10 to 20 m value should be outside the vortex core and therefore give the most reasonable estimate of total strength Γ_∞. The calculation of the ratio $\overline{\Gamma}/\overline{W}$ from Equation (2) requires an estimate of the average wingspan for the aircraft type as well as the airspeed and air density. The average wingspans in Table 3 were estimated from the models in Table 1. The measured ratios are somewhat less than the elliptical loading estimates. The measured values of $\overline{\Gamma}/\overline{W}$ for 10 to 20 m show the expected lower values for the

TABLE 3. RATIO OF AVERAGE INITIAL VORTEX STRENGTH TO AVERAGE AIRCRAFT WEIGHT FOR VORTEX AGES OF 10 TO 20 SECONDS

Experimental Ratio	$\overline{\Gamma}/\overline{W}$, $m^2/s/Mg$			
	B-707	B-707H	DC-8	DC-8H
5 m averaging radius	0.99 ±.01	0.95 ±.02	0.97 ±.02	0.91 ±.02
10 m averaging radius	1.71 ±.02	1.71 ±.04	1.71 ±.03	1.61 ±.03
20 m averaging radius	2.37 ±.04	2.33 ±.09	2.44 ±.05	2.24 ±.05
5 to 10 m averaging radius	2.43 ±.04	2.47 ±.08	2.45 ±.06	2.31 ±.06
10 to 20 m averaging radius	3.03 ±.08	2.95 ±.18	3.17 ±.10	2.87 ±.10
Theoretical Ratio*	3.72	3.38	3.42	3.38
Average Wingspan (m)	39.9	44.0	43.4	44.0
Value of C in Equation (2) to give measured values for 10 to 20 m averaging radius	0.81	0.87	0.93	0.85

*Elliptic Loading, 70 m/s air speed, 1.20 kg/m^3 air density.

Heavy models which have larger wingspans.

4.1.3 Correlation of Vortex Strength with Aircraft Weight

The large scatter observed in the measured strength data of Figure 6 is caused by a number of effects. Correlating the strength data with the known aircraft weights (Figure 9 and Table 3) shows that the weight dependence of the strength accounts for less than 10 percent of the variance in the data. The rest is due to measurement error, vortex decay, and the other parameters of airspeed and air density. Measurement errors dominate the scatter at early times while variations in decay dominate at later times.

One way of looking at the correlation analysis is to view it as a linear least-squares fit to the strength versus weight data for each aircraft type. The fit has the form:

$$\Gamma = \overline{\Gamma} + a(W-\overline{W}), \tag{4}$$

where Γ is the vortex strength, W is the aircraft weight, and a is the slope of the Γ versus W curve at the point $W = \overline{W}$. In view of the discussion of Section 3.1, assume a power law relationship

$$\Gamma \sim W^n \tag{5}$$

between vortex strength and aircraft weight. Differentiating Equation (5) with respect to W yields the slope of relationship (4):

$$a = n\overline{W}^{n-1} = n\overline{\Gamma}/\overline{W}. \tag{6}$$

Rearranging Equation (6) yields the value of the power n:

$$n = a/(\overline{\Gamma}/\overline{W}) \tag{7}$$

which is the ratio of the local slope to the average slope.

The results of the least-square fit to strength versus weight are shown in Figures 10 and 11. Data are shown for both 10- and 20-second intervals, the latter giving smaller errors. For each interval the points for 5 and 20 m are displaced laterally to avoid

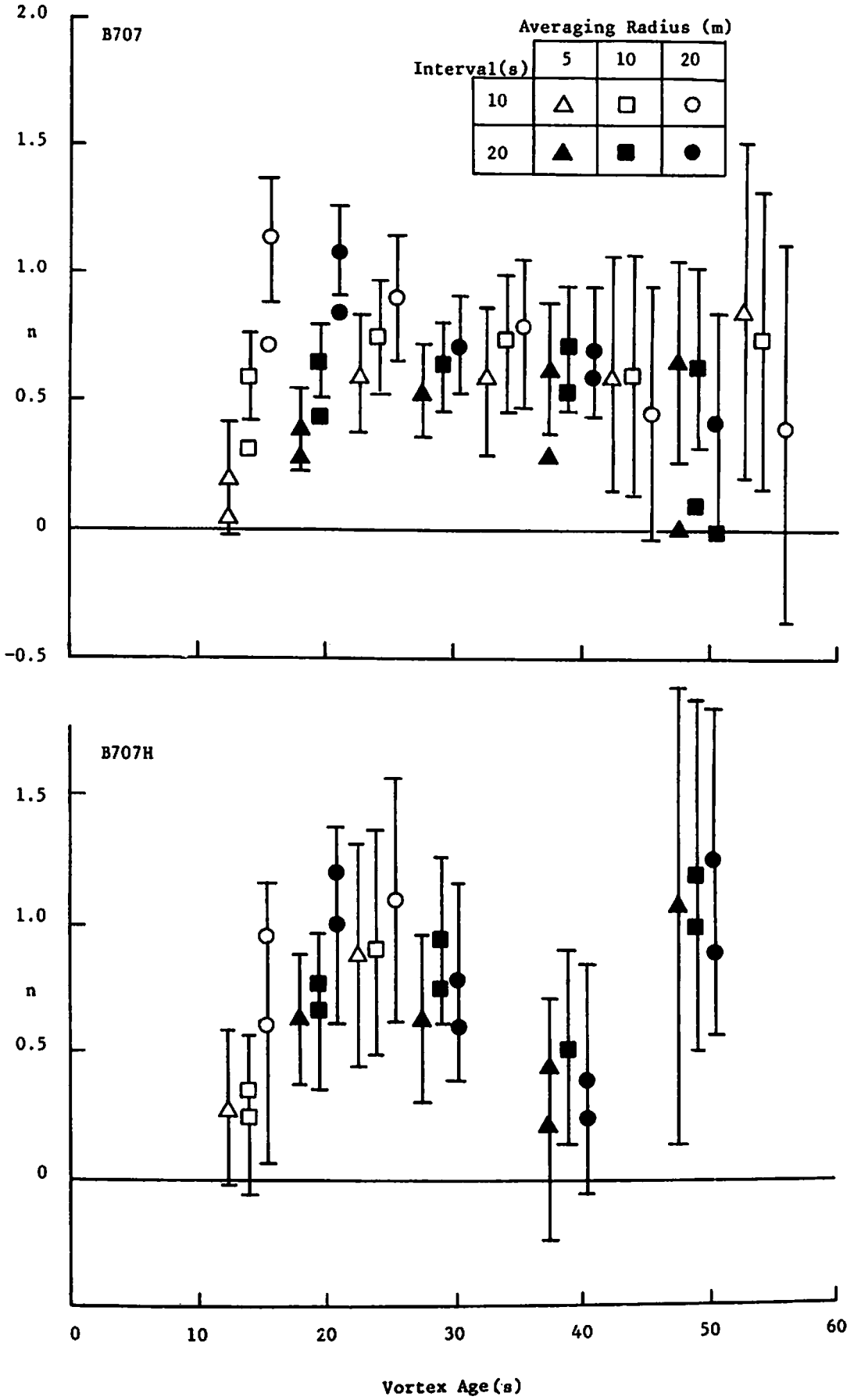

FIGURE 10. STRENGTH VERSUS WEIGHT POWER-LAW FIT AS A FUNCTION OF VORTEX AGE (B-707 AND B-707H)

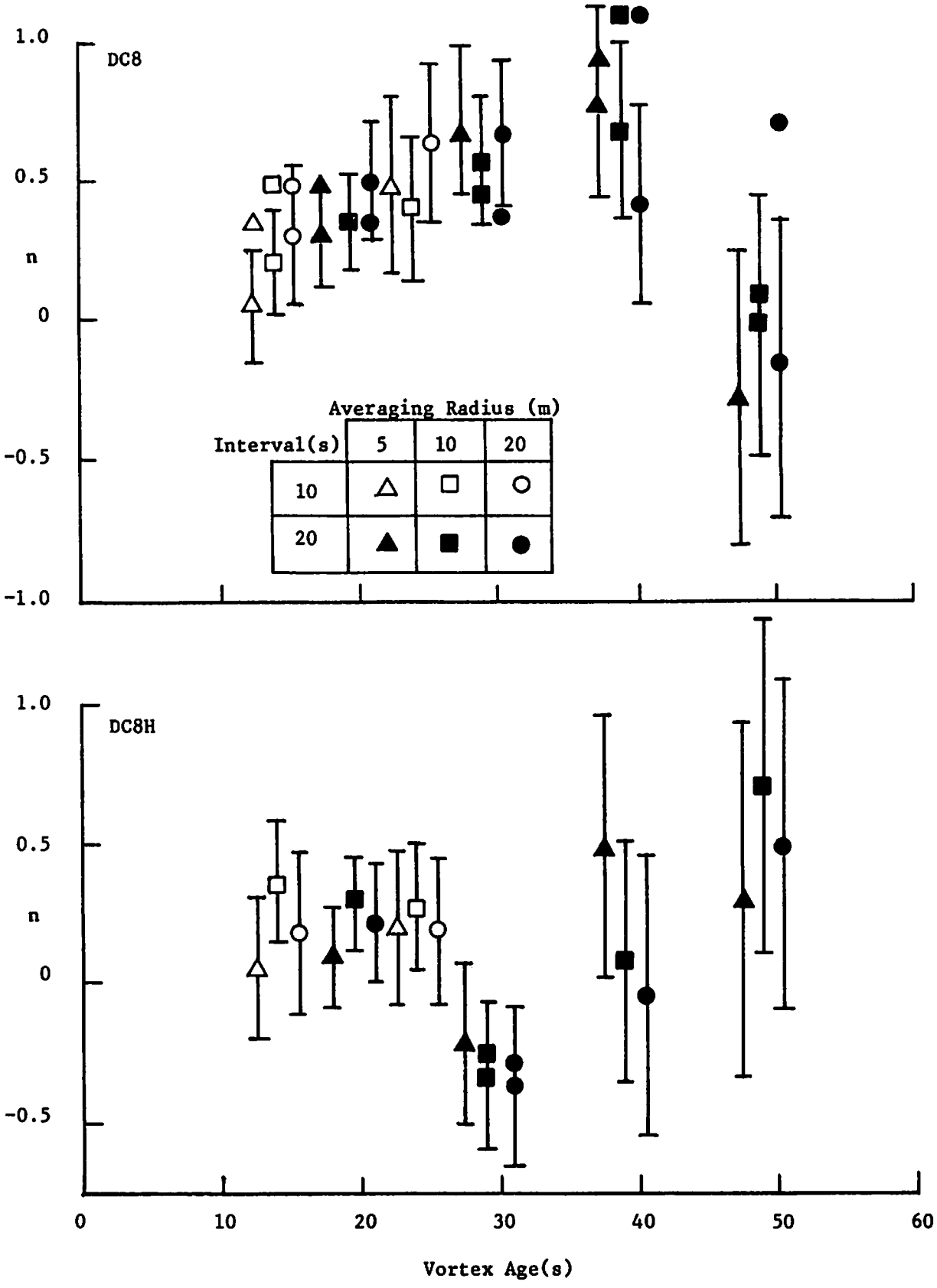

FIGURE 11. STRENGTH VERSUS WEIGHT POWER-LAW FIT AS A FUNCTION OF VORTEX AGE (DC-8 AND DC-8H)

overlap. The error bars are standard errors as discussed in Appendix B. There are extra points in Figures 10 and 11 which are not centered in the error bars. They are the results of reassigning the aircraft category according to the reported landing weight, as was discussed at the end of Section 2.2. The plots show only those points where the reassignment yielded values significantly different from the original ones.

The data in Figures 10 and 11 are reasonably consistent with the most reasonable value of n which is n = 0.5 according to the discussion of Section 3.1. One would expect that 32 percent of the measured values would be outside the standard errors, as in fact is observed. The errors in n increase rapidly with vortex age because of the decrease in the number of measurements (see Figures 7 and 8). The reassignment of aircraft categories has no major effect; some data points move closer to n = 0.5 and some move farther away.

The data in Figures 10 and 11 show no significant evidence for variation in the power n with vortex age. Thus, the data are consistent with the vortex decay hypothesis of Section 3.2, namely that the strength of a decaying vortex is proportional to the initial vortex strength when averaged over the measurement conditions. Because the errors in Figures 10 and 11 increase so rapidly with vortex age, it is not possible to use these data to set meaningful limits on the maximum variation of n with age.

4.2 HAZARD PROBABILITY ANALYSIS

This section makes use of vortex strength histories (Figure 3c, reproduced in Figure 12) to determine when the vortex strength drops below a hazard threshold. For example, with a hazard threshold of 30 m^2/s, Figure 12 shows that the first vortex decays below the threshold at 46.5 seconds while the second vortex remains a hazard until 60.5 seconds (indicated by the arrows in the figure). If the hazard threshold were 100 m^2/s, then vortex 1 would never be a hazard while vortex 2 would be a hazard for 34 seconds. The hazard model used to analyze the data is described in Section 4.2.1. Strength history data from many cases are used in Section 4.2.2 to calculate a hazard probability.

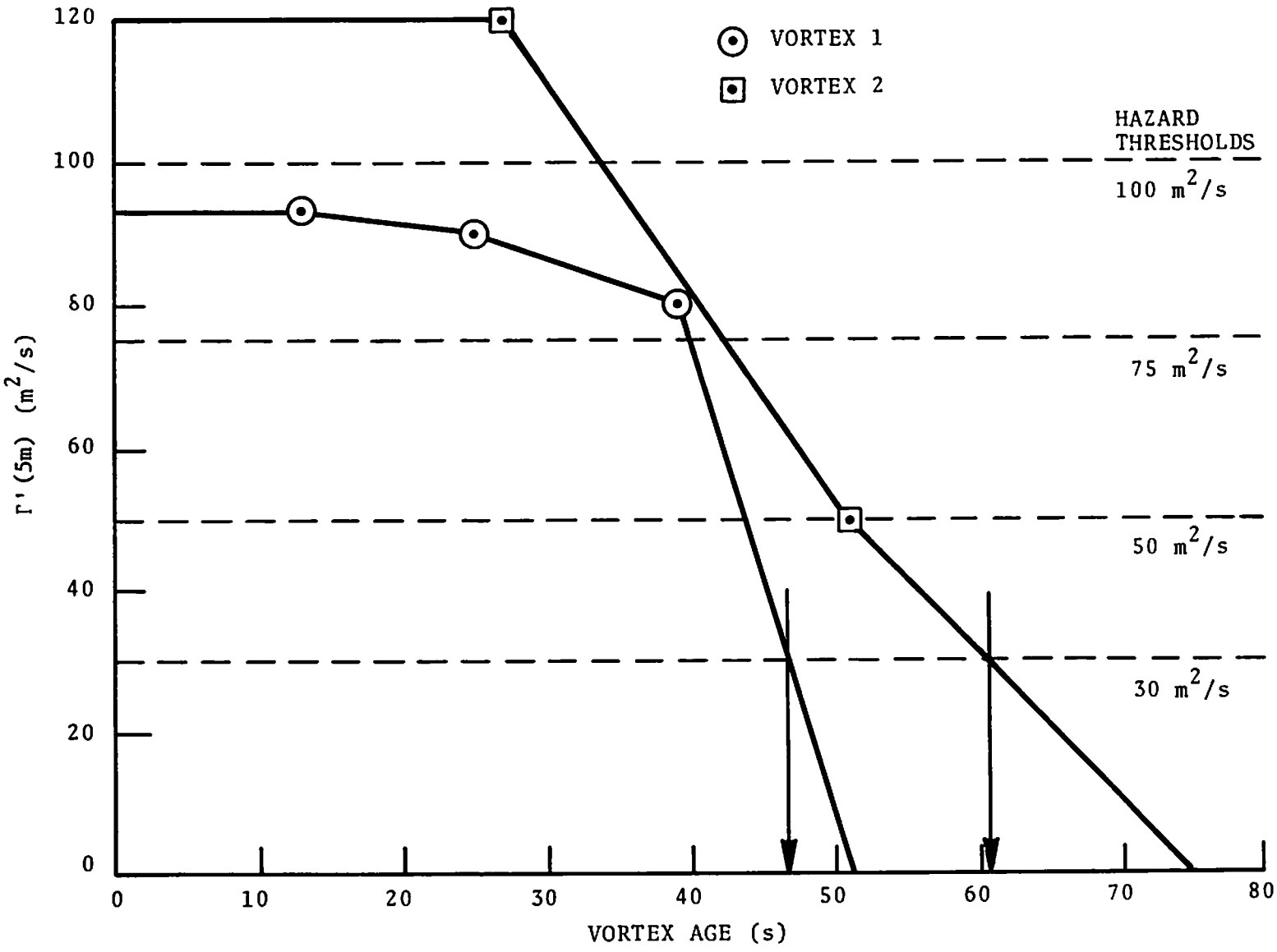

FIGURE 12. USE OF VORTEX STRENGTH HISTORIES TO DETERMINE VORTEX HAZARD DEFINITION

4.2.1 Hazard Model

The hazard model used to analyze the data is based on the capability of the following aircraft to overcome the roll rate induced by a vortex (Ref. 10). The dynamics of a wake vortex encounter are not considered. A vortex is defined to be hazardous when its maximum induced roll rate P_v is greater than a fraction f of the maximum roll control P_m of the vortex-encountering aircraft:

$$P_v > f\ P_m. \tag{8}$$

The maximum vortex-induced roll rate will occur when the wing of the following aircraft is centered in the vortex.

The torque T exerted on a wing of span b is given by the strip-theory expression

$$T = \int_{-b/2}^{b/2} r\ \ v(r)\ K(r)\ \ dr, \tag{9}$$

where K(r) is the ratio of the induced force to the vertical vortex velocity at a point r on the wing. With the assumption that K(r) is constant along the wing, one can relate the torque T to the average circulation $\Gamma'(r)$ of equation (1):

$$T = Kb\ \Gamma'(b/2)/2\pi. \tag{10}$$

The torque depends only on Γ' and not upon the particular velocity distribution v(r). The errors introduced by this assumption have not been examined; for similar wing planforms and similar velocity profiles the error is probably a simple correction factor.

The vortex-induced rolling rate P_v in this approximation can be obtained by selecting a velocity profile corresponding to solid body rotation at the rate P_v:

$$v(r) = r\ P_v. \tag{11}$$

There are no forces on a wing rotating at rate P_v in such a profile. The value of $\Gamma'(b/2)$ for this velocity profile can be obtained from equation (1):

$$\Gamma'(b/2) = \frac{\pi}{6} P_v b^2. \quad (12)$$

Now relate P_v to the maximum roll control P_m of the aircraft, which is often expressed in the nondimensional form

$$\hat{p} = P_m b/2V, \quad (13)$$

where V is the flight speed. Equation (8) leads to the following expression for the hazard threshold on vortex strength Γ':

$$\Gamma'(b/2) > \frac{\pi}{3} fbV\hat{p}. \quad (14)$$

The nondimensional roll rate $\hat{p}$ is typically 0.06 for commercial aircraft and 0.08 for general aviation aircraft. The hazard threshold value used to analyze the data is given by

$$\Gamma'(b/2) \sim 5b \quad (m^2/s) \quad (15)$$

in metric units. This expression is consistent with the values f = 1, V = 130 knots (68 m/s), and $\hat{p}$ = 0.07. Thus, the hazard threshold values in Table 4 will be used.

4.2.2 Probability Analysis

Figure 12 showed the way in which the duration of the hazard for a particular vortex is determined. If the results for many similar vortices are combined, the probability of a vortex hazard can be derived. The probability of the vortex strength being above the hazard threshold at a given time t is defined as the ratio of the number of vortices with strength above the threshold to the total number of vortices with valid strength measurements at that time. The number of vortices with valid measurements decreases as the time t increases because of the restrictions on extrapolating beyond the last vortex detection (Section 2.1).

The probabilities were calculated for six hazard threshold values (30, 50, 75, 100, 150, and 200 m^2/s) to illustrate the sensitivity of the results to the selected hazard thresholds (see

TABLE 4. VORTEX STRENGTH HAZARD THRESHOLDS

AIRCRAFT TYPE	SEMISPAN	STRENGTH THRESHOLD
SMALL GA	5 m	50 m^2/s
LARGE GA	10 m	100 m^2/s
DC-9	15 m	150 m^2/s
B-707	20 m	200 m^2/s

Figure 12). The probabilities decrease as the threshold increases. Figures 13 and 14 show these probabilities for the B-707 aircraft and two strength averaging radii: 5 and 20 m. "All cases" are included; that is, all the B-707 vortices regardless of the wind conditions or vortex number are included in the plots. The Heavy and Large B-707s are segregated into separate plots. An X is plotted for each evaluation time t (10, 20, 30, etc. seconds) at the probability corresponding to one vortex above threshold. The rise of the X's with time shows how many vortices are lost from the statistics because of extrapolation restrictions. If the probability drops to zero at a particular time, a dashed line is drawn to the value for one case (zero cannot be plotted on a logarithmic scale). The probabilities are plotted against the square of the vortex age (t^2) since this dependence on time corresponds to the tail of a Gaussian distribution (exp $(-\alpha t^2)$) of vortex decay times; this model will be developed in Volume III. [Note: It is indeed fortunate that the hazard probability decays so quickly. If the probability decayed as exp $(-t/\tau)$ with τ the decay time, one would have to wait many times τ before the vortex hazard probability would decay to a satisfactory value.]

In addition to the probability plots for all cases, various disaggregated plots were generated and are included in Appendix C. The strongest observed systematic effect was that first vortices (vortex 1) decay more rapidly than second vortices (vortex 2) as shown in Figures 15 and 16). The difference is more pronounced for the DC-8 than for the B-707. In addition, the vortices decay more rapidly in higher ambient winds. The reasons for these effects will be discussed in Volume III.

The vortex safety implications of these effects are significant. The second, longer-lasting vortex (vortex 2) is the one which tends to linger near the extended runway centerline. Thus, only measurements on second vortices are directly relevant to aircraft spacing on approach for single runway operations. The slower decay for lower ambient winds indicates that the relative hazards from different aircraft are better compared at low wind speeds,

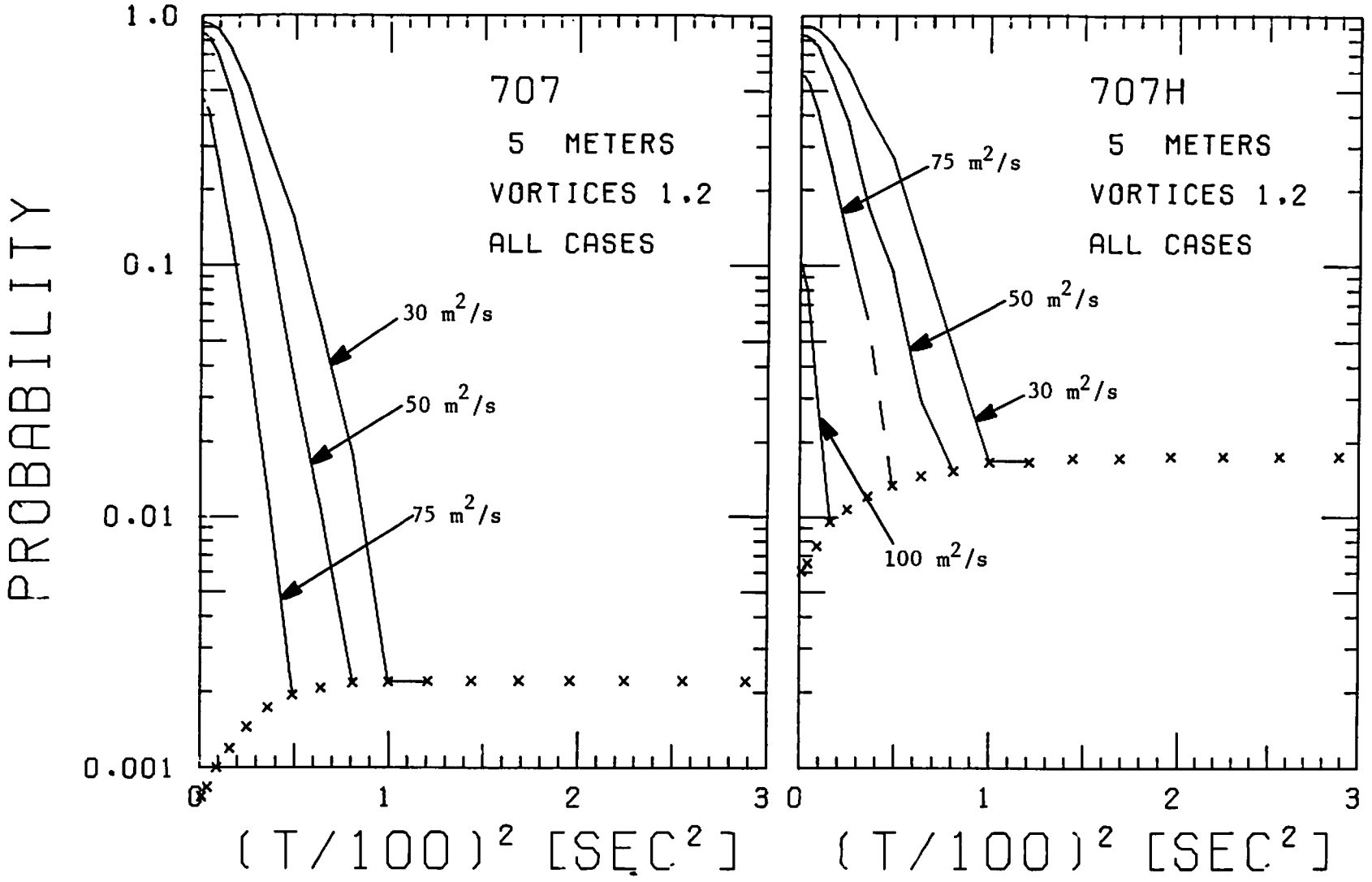

FIGURE 13. PROBABILITY OF DECAY, B-707, 5-m AVERAGEING RADIUS

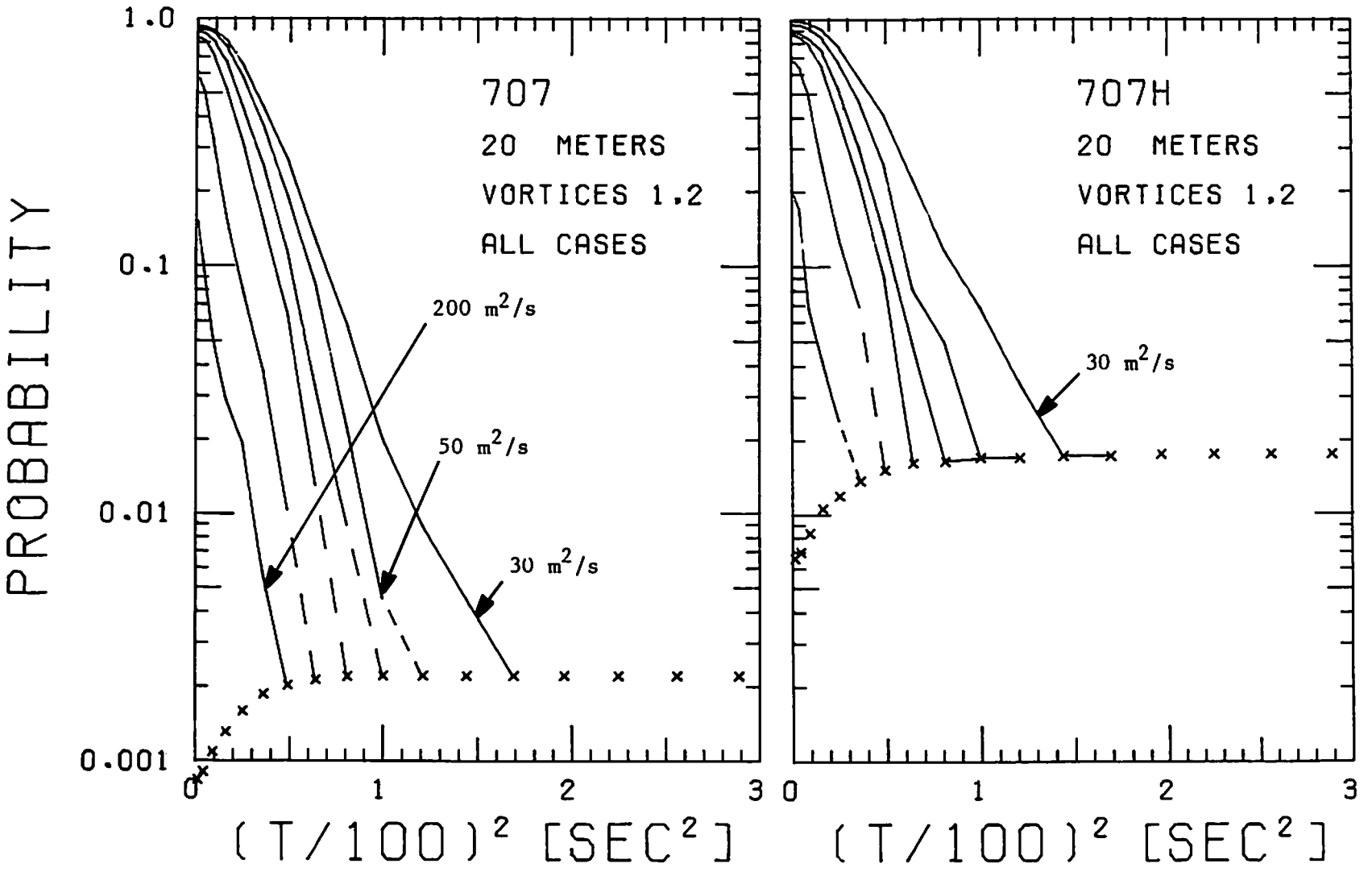

FIGURE 14. PROBABILITY OF DECAY, B-707, 20-m AVERAGING RADIUS

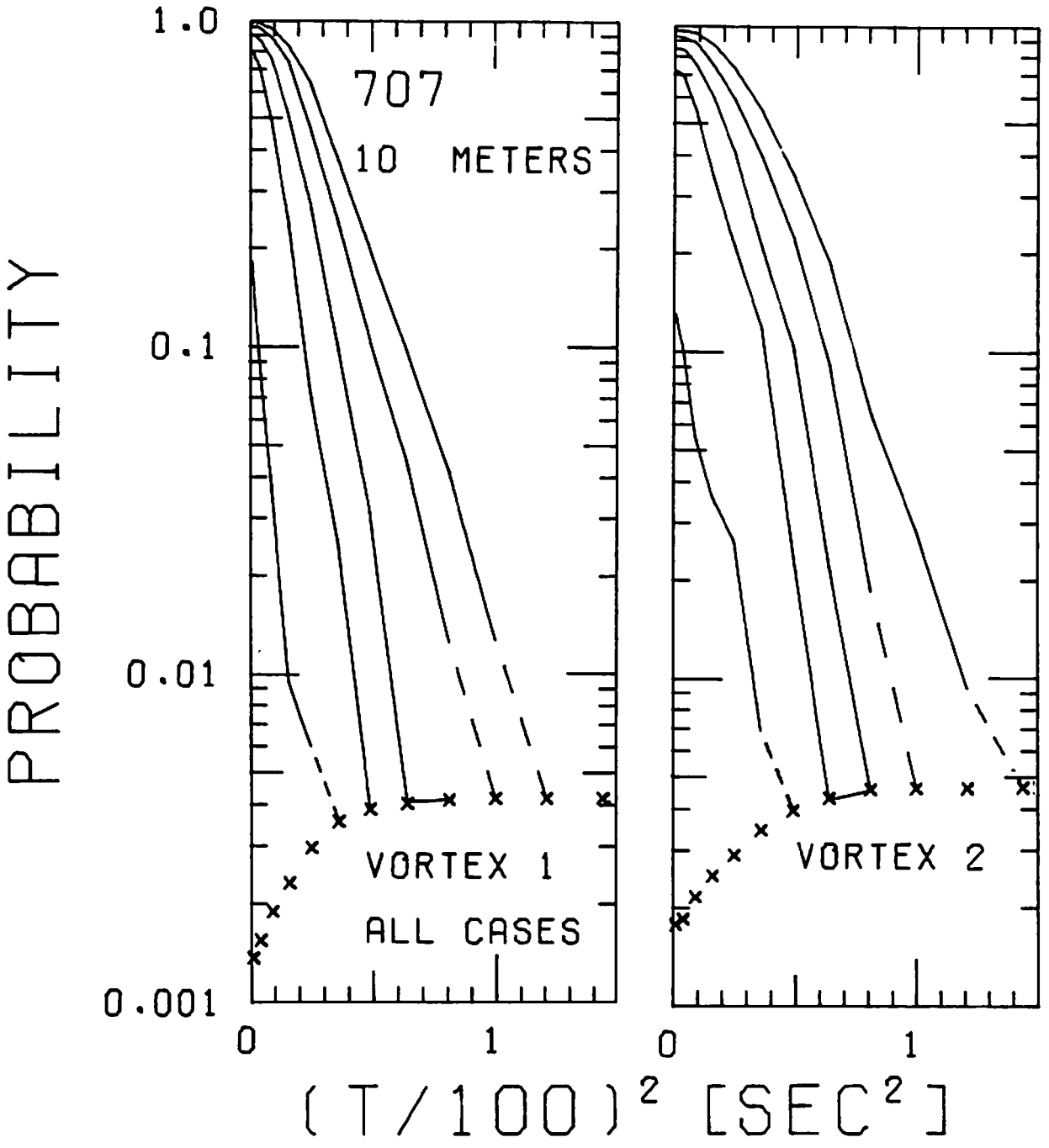

FIGURE 15. COMPARISON OF VORTEX DECAY FOR VORTEX 1 AND VORTEX 2; B-707 AIRCRAFT, 10-m AVERAGING RADIUS

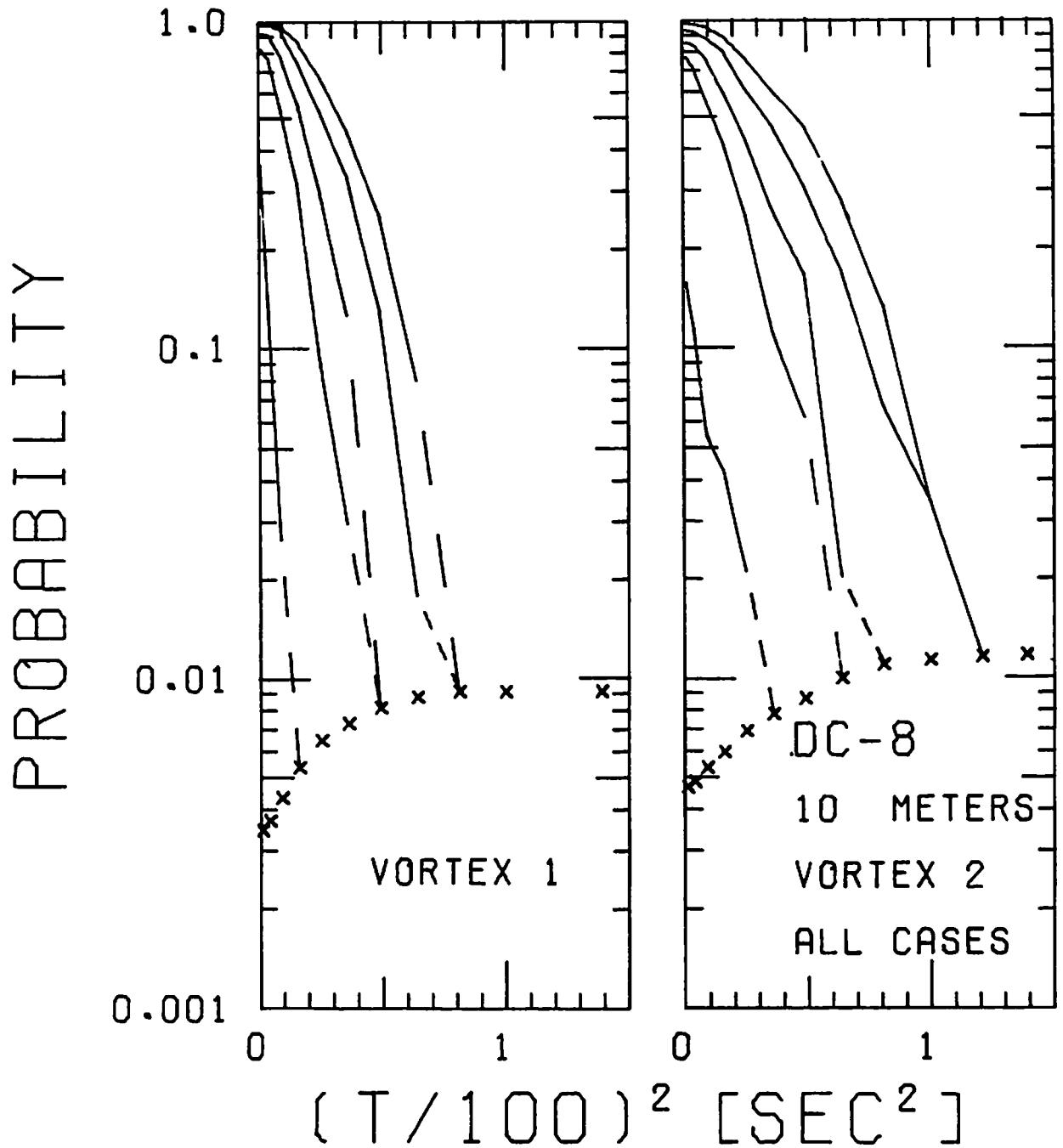

FIGURE 16. COMPARISON OF VORTEX DECAY FOR VORTEX 1 AND 2; DC-8 AIRCRAFT, 10-m AVERAGING RADIUS

if enough cases are included to allow reasonable statistical accuracy.

4.2.3 Decay Comparisons Between Aircraft Types

Many questions concerning the accuracy of the strength measurements and the validity of the strength history extrapolation can be avoided if the analysis deals only with comparisons between different types of aircraft. Possible sources of error should similarly affect the results for all aircraft types and therefore should introduce no relative biases into the analysis.

The decay of hazard probability is compared for different aircraft in Figures 17 to 20 for second vortices (vortex 2) and with ambient winds less than 8 knots. The f = 1.0 hazard strengths defined in Section 4.2.1 are used. Two types of plots are included. The first compares data for all of the jet transport aircraft studied. These plots allow the B-707/DC-8 data to be studied in the context of the current fleet of aircraft. For convenience, the shaded portion of the plot indicates the extent of the B-707/DC-8 data. The second plot includes only B-707/DC-8 data so that detailed comparisons of the Large and Heavy versions can be made. Because there are few cases with winds less than 8 knots for many aircraft types, the probability curves for second vortices under all wind conditions are plotted in Figures 21 to 24. Table 5 shows the percentage of second and first vortices (at long times) measured under various wind conditions for the different aircraft. The distributions of ambient winds are generally similar for all aircraft, so that one can rule out large systematic biases in the all-winds data.

Some guidelines to interpreting Figures 17 to 24 should prove useful. As in Figures 13 to 16, the last point plotted for each aircraft corresponds to one case above threshold. The total number of cases at that time is simply the inverse of the probability at that point. The data can be strongly affected by statistical fluctuations where only a few cases are involved. Appendix D contains an error analysis for these data which was used to compute

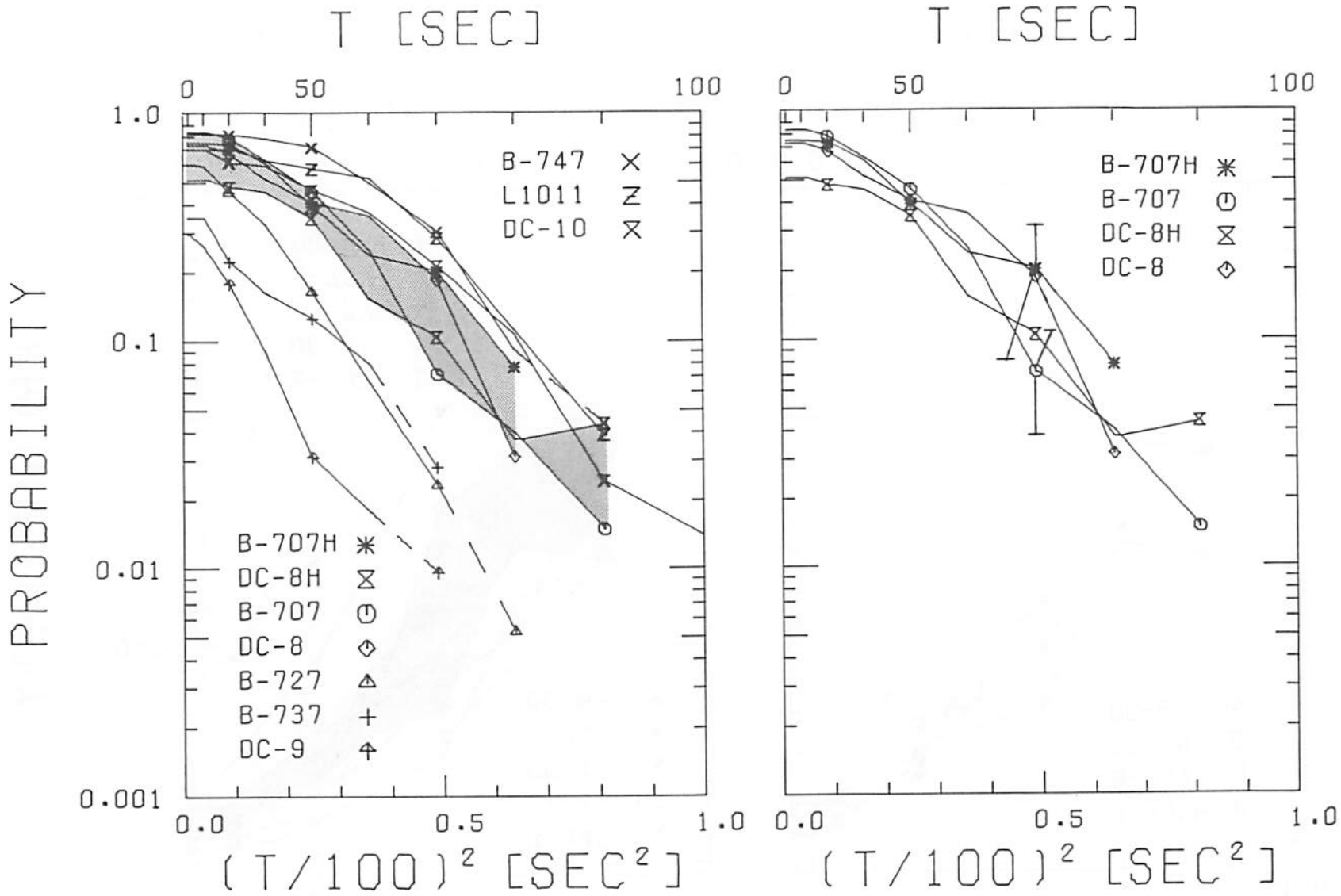

FIGURE 17. DEPENDENCE OF VORTEX DECAY ON AIRCRAFT TYPE: 5 METERS, 50 m^2/s, VORTEX 2, 0-8 KNOTS

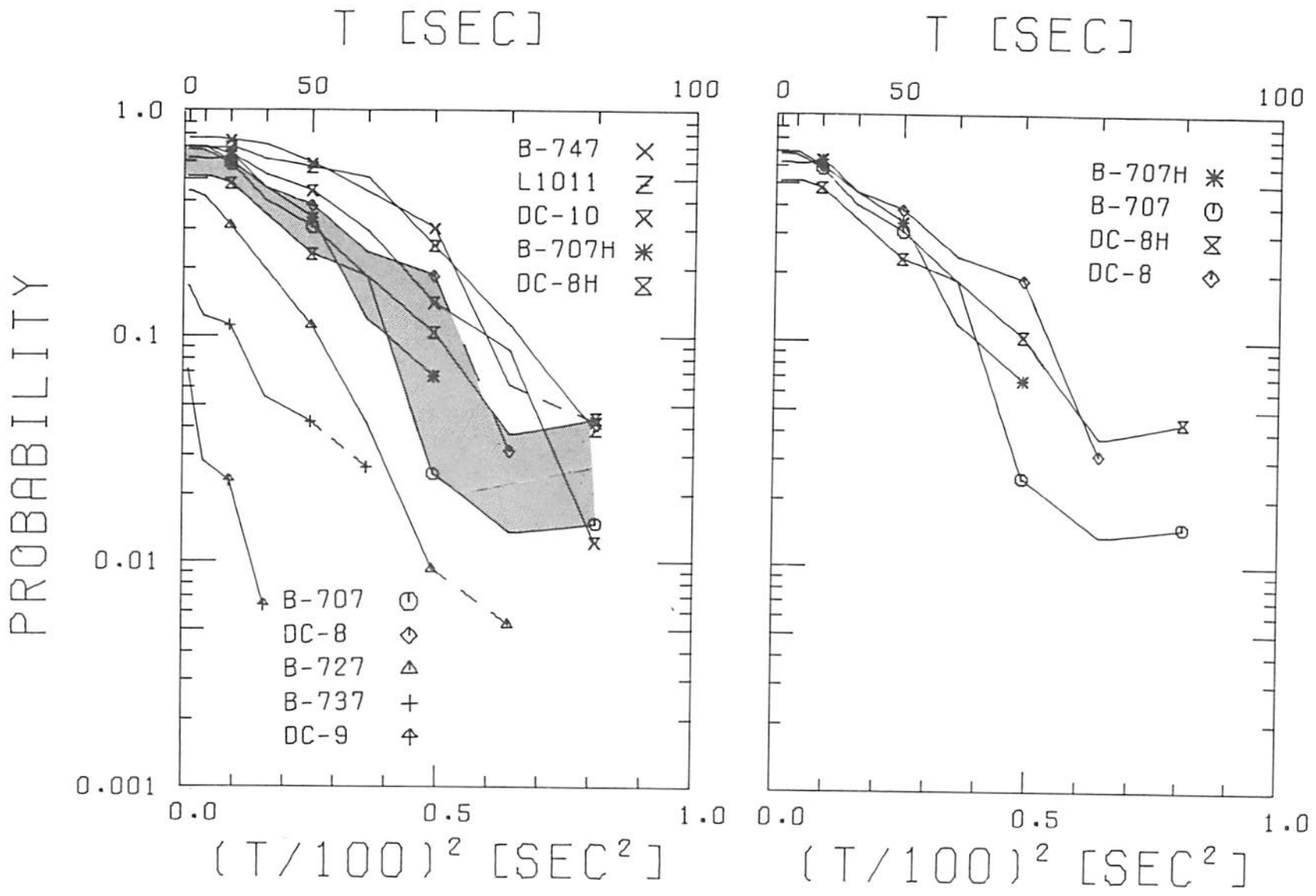

FIGURE 18. DEPENDENCE OF VORTEX DECAY ON AIRCRAFT TYPE; 10 METERS, 100 m^2/s, VORTEX 2, 0-8 KNOTS

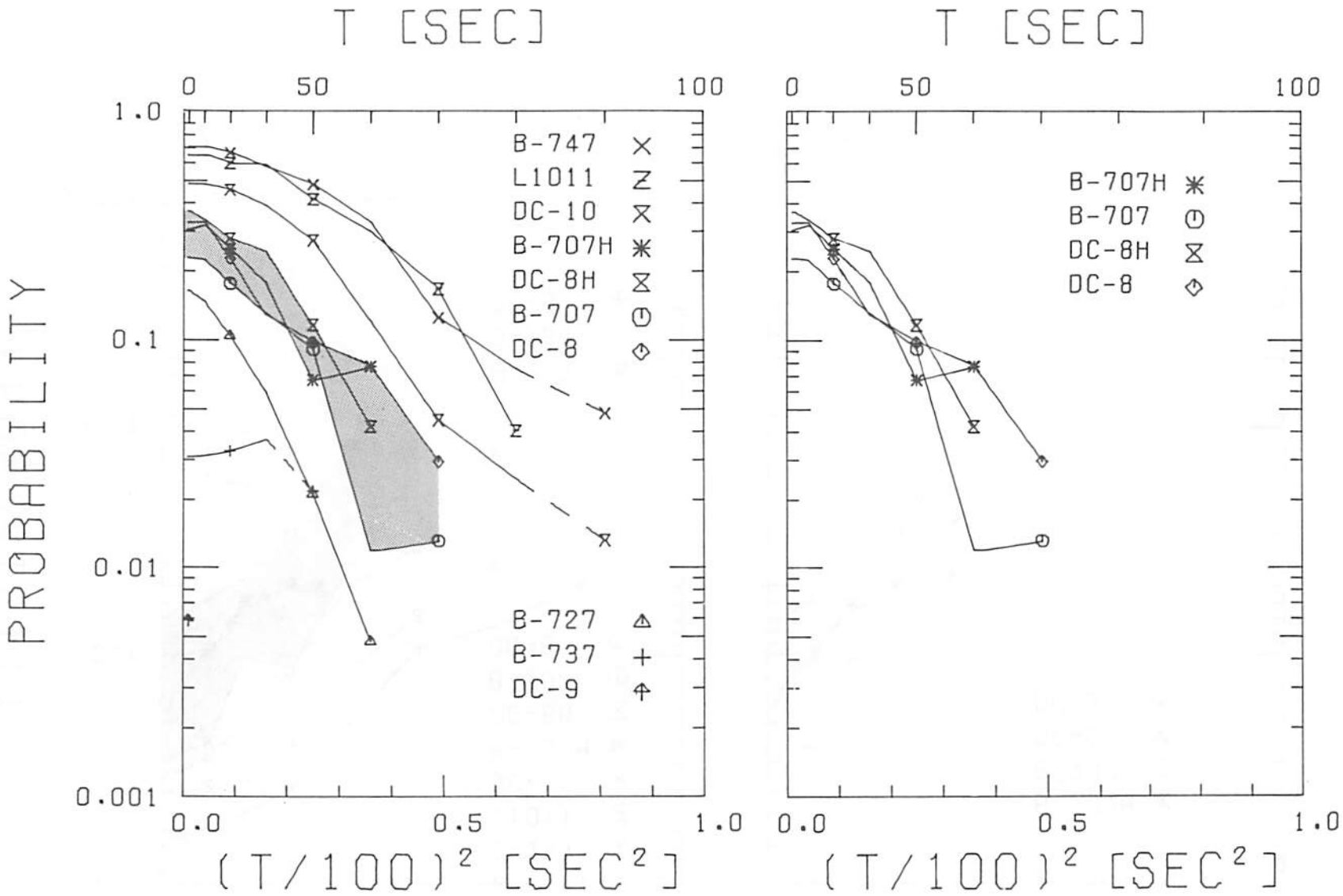

FIGURE 19. DEPENDENCE OF VORTEX DECAY ON AIRCRAFT TYPE; 15 METERS, 150 m^2/s, VORTEX 2, 0-8 KNOTS

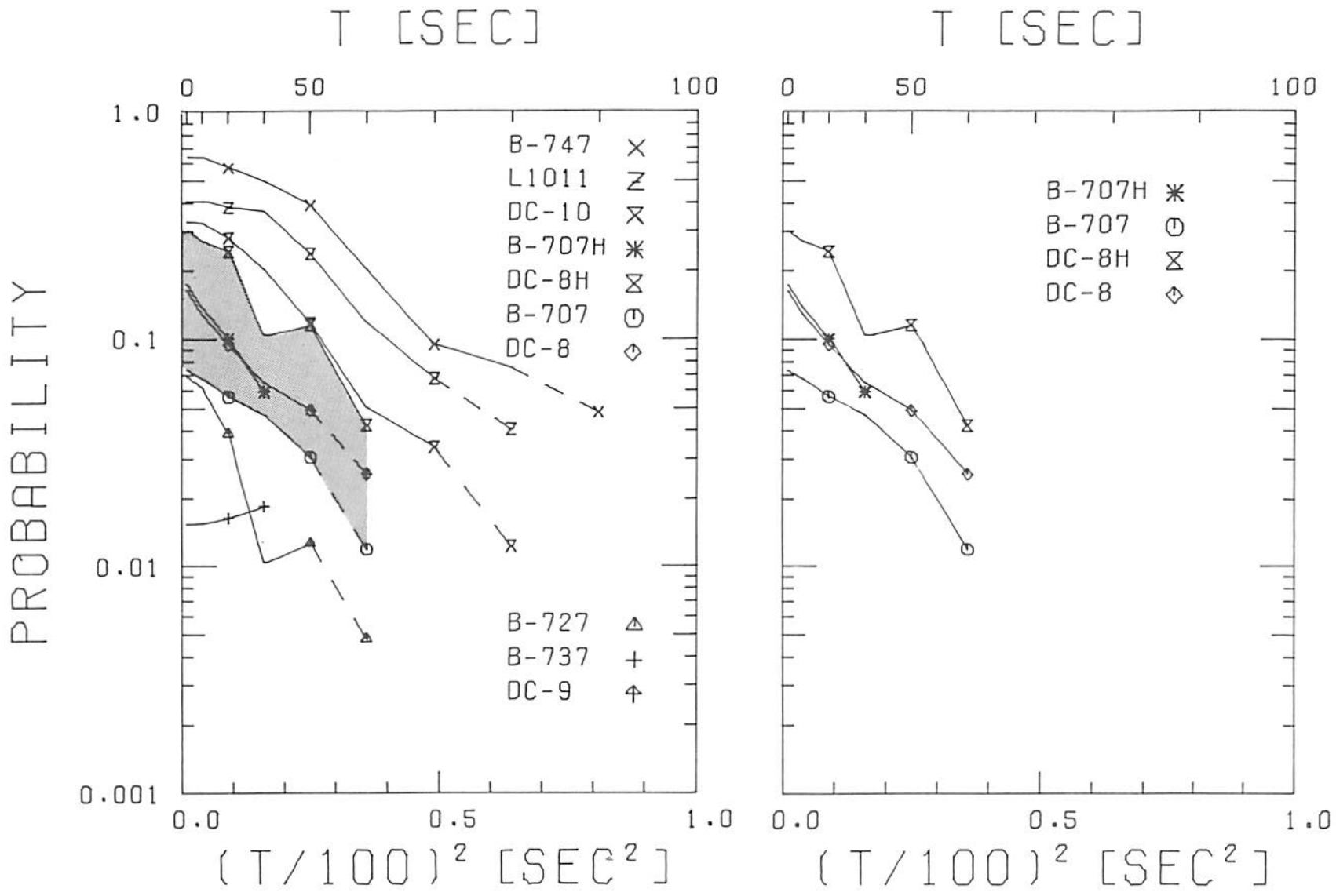

FIGURE 20. DEPENDENCE OF VORTEX DECAY ON AIRCRAFT TYPE; 20 METERS, 200 m^2/s, VORTEX 2, 0-8 KNOTS

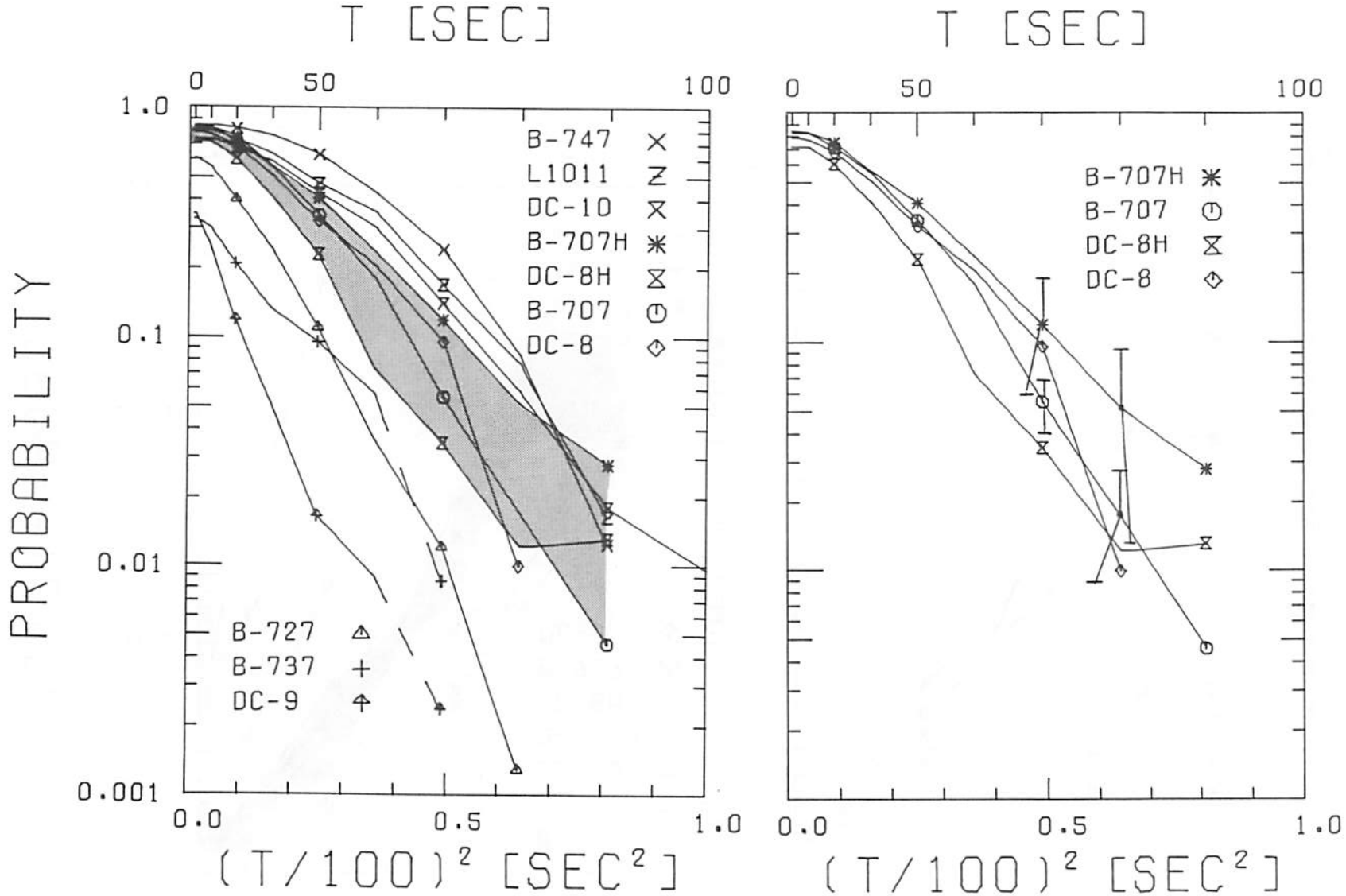

FIGURE 21. DEPENDENCE ON VORTEX DECAY ON AIRCRAFT TYPE; 5 METERS, 50 m^2/s, VORTEX 2, ALL WINDS

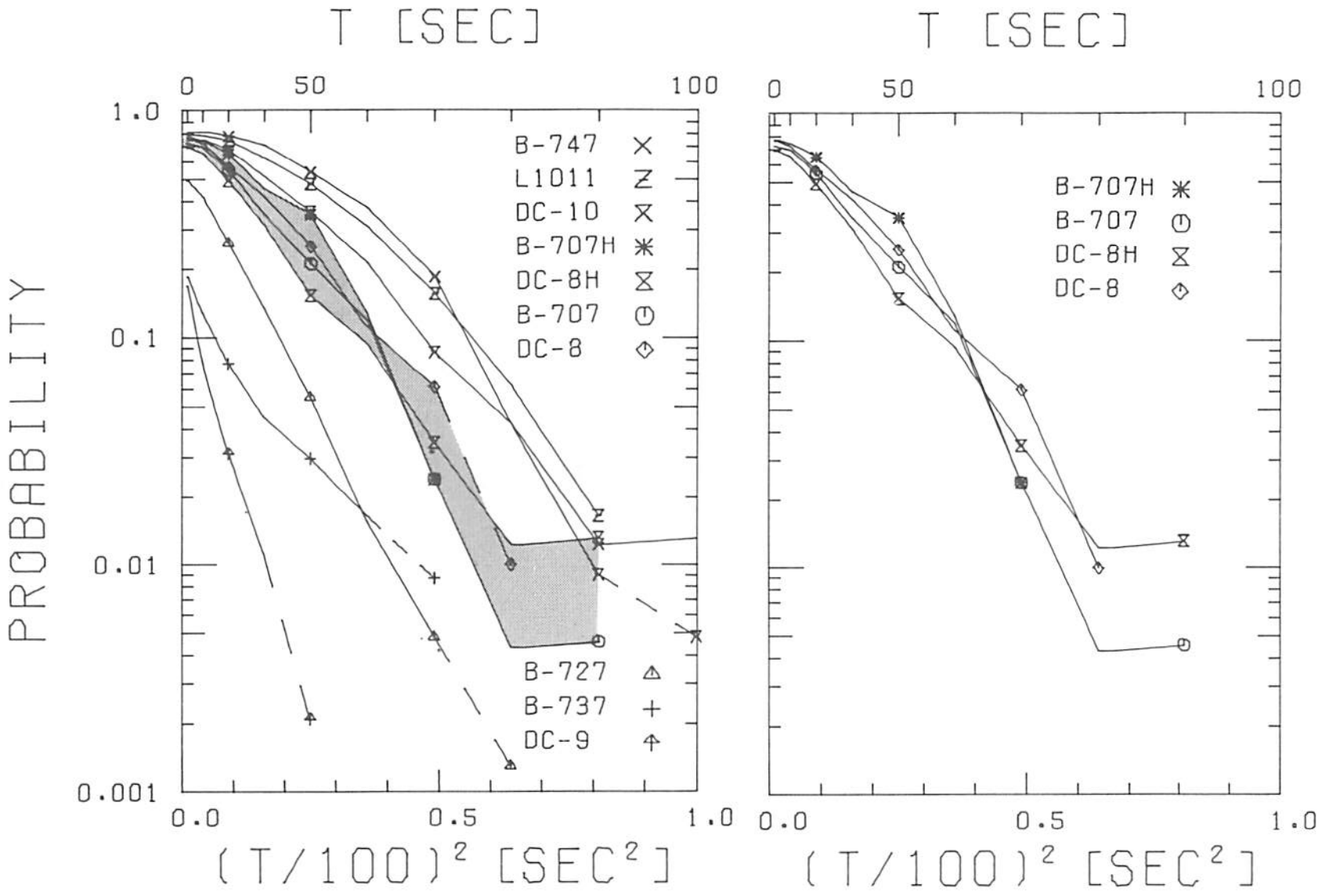

FIGURE 22. DEPENDENCE ON VORTEX DECAY ON AIRCRAFT TYPE; 10 METERS, 100 m^2/s, VORTEX 2, ALL WINDS

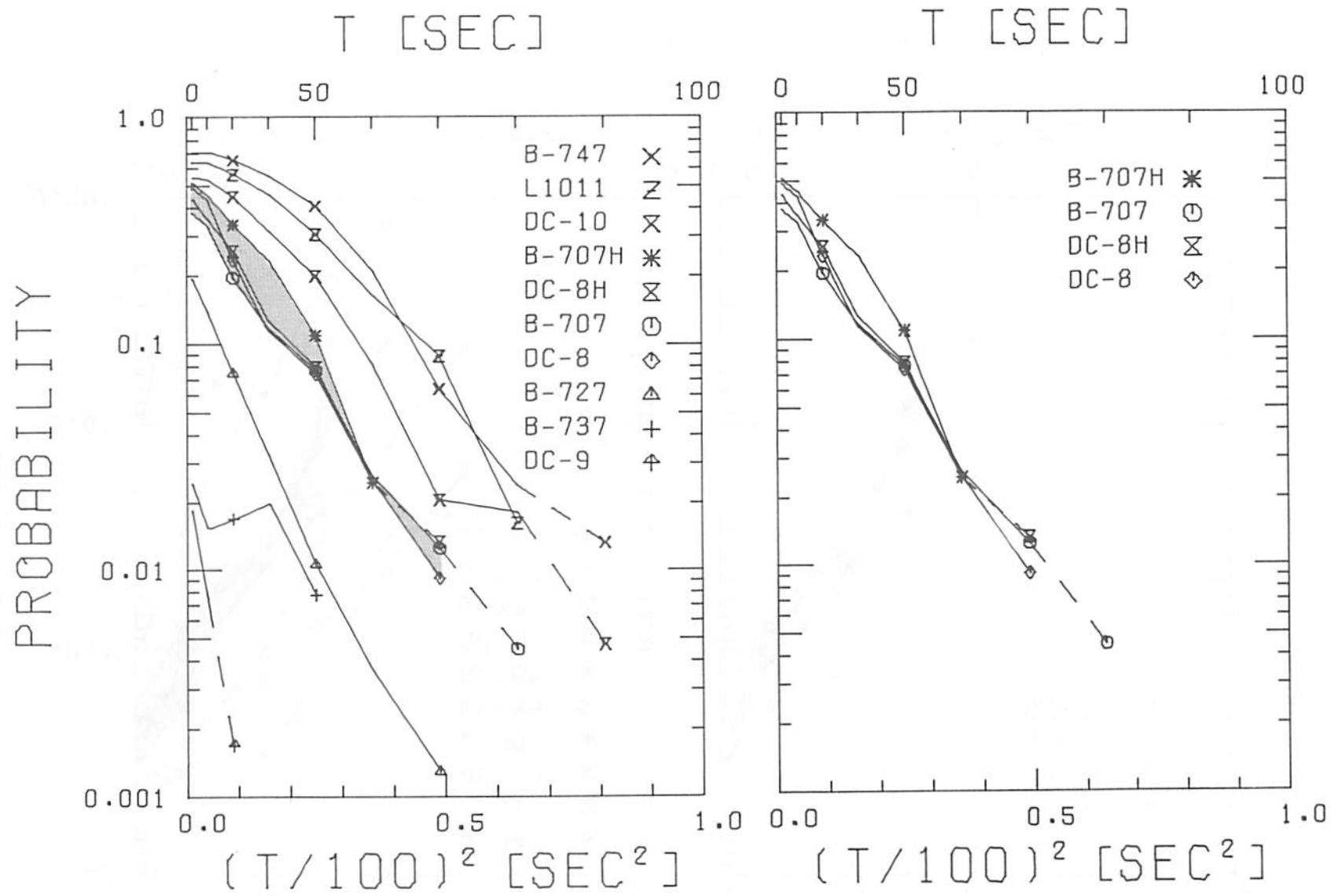

FIGURE 23. DEPENDENCE OF VORTEX DECAY ON AIRCRAFT TYPE; 15 METERS, 150 m^2/s, VORTEX 2, ALL WINDS

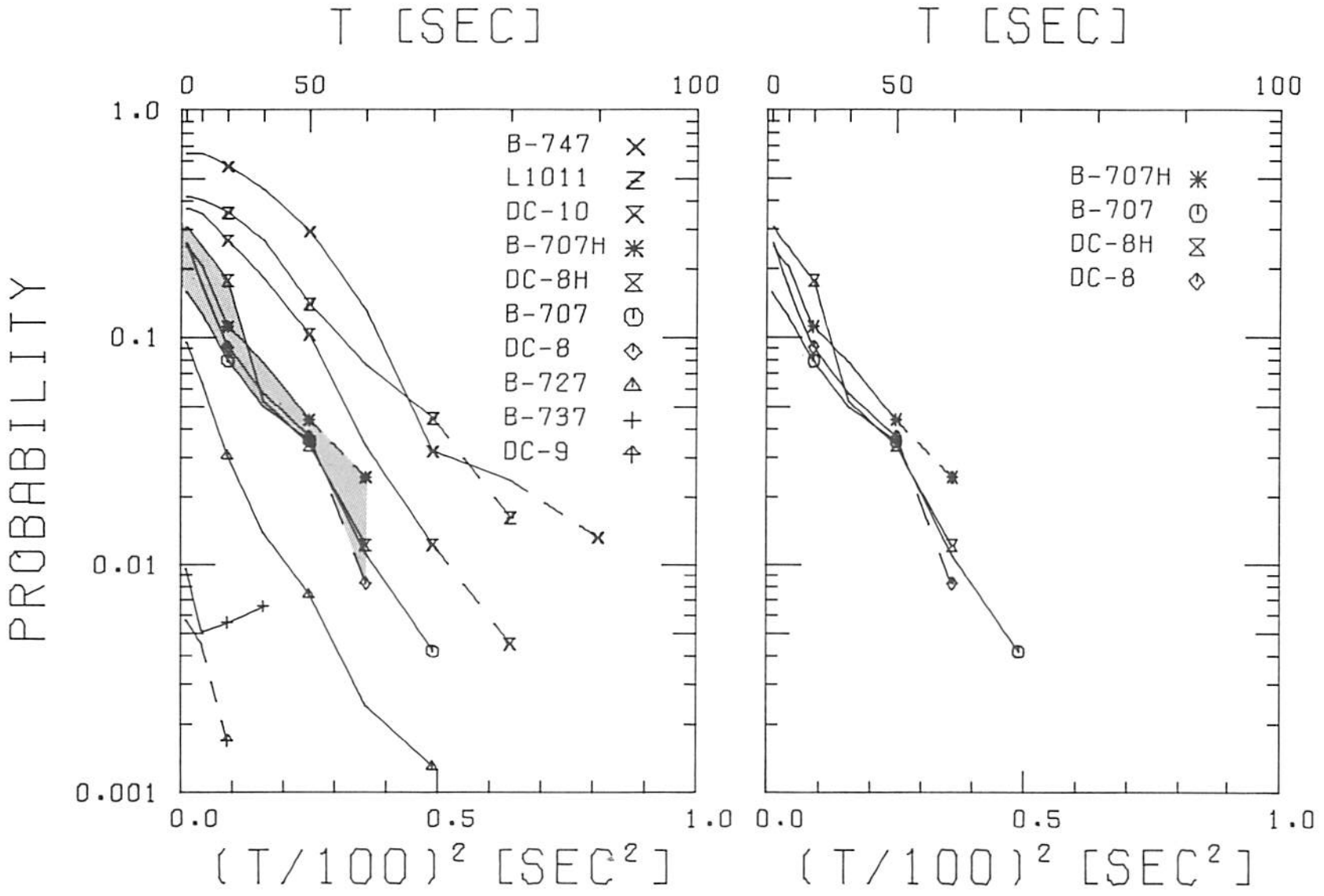

FIGURE 24. DEPENDENCE OF VORTEX DECAY ON AIRCRAFT TYPE; 20 METERS, 200 m^2/s, VORTEX 2, ALL WINDS

TABLE 5. DISTRIBUTION OF AMBIENT WINDS*

AIRCRAFT TYPE	WIND MAGNITUDE CONDITIONS (KNOTS)					
	0-8	>8	0-5.5	5.5-8.0	8-10	>10
VORTEX 2						
B-707	30%	69%	11%	18%	26%	43%
B-727	22	77	8	14	19	57
B-737	30	69	7	22	19	50
B-747	26	73	8	18	33	39
DC-8	27	72	7	20	28	44
DC-9	23	76	7	16	24	52
DC-10	32	67	12	20	24	42
L-1011	40	60	6	34	22	38
B-707H	22	77	9	12	25	51
DC-8H	22	77	13	8	34	43
VORTEX 1						
B-707	29	70	13	16	20	50
B-727	22	77	10	12	16	61
B-737	22	77	7	14	21	56
B-747	40	59	29	10	19	40
DC-8	31	68	11	20	21	47
DC-9	24	75	9	14	19	56
DC-10	38	61	20	17	19	42
L-1011	34	65	14	19	23	42
B-707H	38	61	23	15	19	42
DC-8H	45	54	23	21	20	34

*Roundoff errors may lead to total percentage not summing to 100 percent.

the error bars added to some of the figures. The error bars correspond to one standard deviation.

The vortex hazard decay data in Figures 17 to 24 are generally consistent with the expectation that larger, heavier aircraft produce a more persistent vortex hazard. The widebody aircraft (B-747, L-1011, and DC-10) show the most persistent vortex harzard. The B-707/DC-8 classes are next in persistence and form the middle of the plots. The B-727 has the next lower persistence, followed finally by the B-737 and DC-9. The distinctions between the different sized aircraft are greater for the larger averaging radii (15 and 20 m).

4.2.4 Sensitivity Analysis

The results shown in Section 4.2.3 were based on a hazard model with f = 1.0, i.e., the vortex hazard disappears when the vortex-induced roll rate is less than the roll control of the encountering aircraft. In this section the results for other more conservative values of f are compared for the B-707/DC-8 groups (Figures 25 to 32). (An f of 0.6, for example, means that the vortex hazard disappears when the vortex-induced roll rate is less than 60 percent of the roll control of the vortex-encountering aircraft.) Decreasing the value of f increases the persistence of the vortex hazard but generally has only small effects on the relative hazard for different aircraft categories.

The plots in Figures 33 to 36 show the sensitivity of the results to the apparent anomalies in aircraft landing weights discussed in Section 2.2. The plots for f = 1.0, vortex 2, and all winds are compared for (a) all cases, (b) only cases with weight data, and (c) cases with weights and aircraft category sorted by the reassignment procedure of Section 2.2. Only minor variations in hazard decay are introduced by these changes in the data analysis.

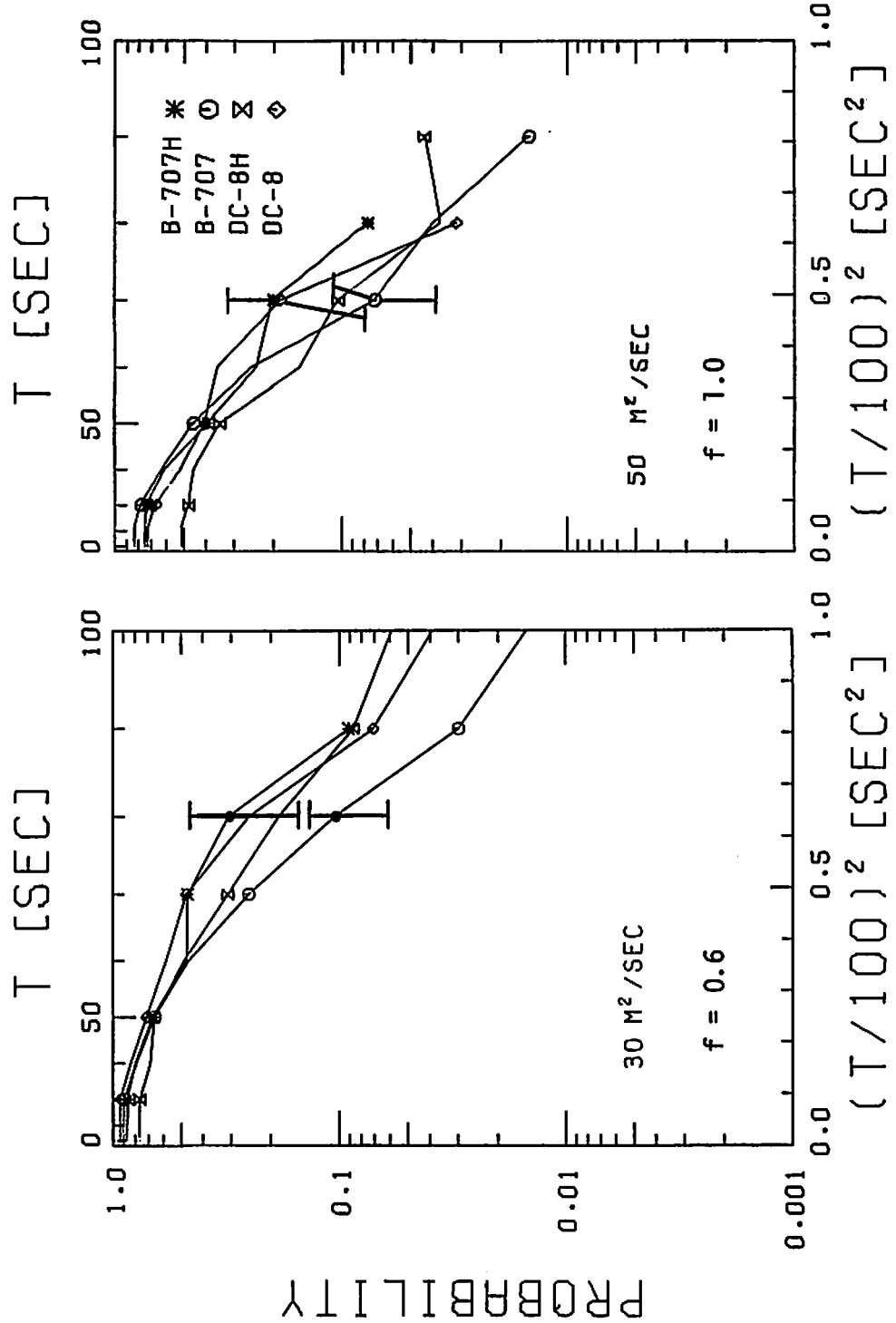

FIGURE 25. DEPENDENCE OF VORTEX DECAY ON FRACTION OF ROLL CONTROL CAPABILITY OF AIRCRAFT; 5 METERS, VORTEX 2, 0-8 KNOTS

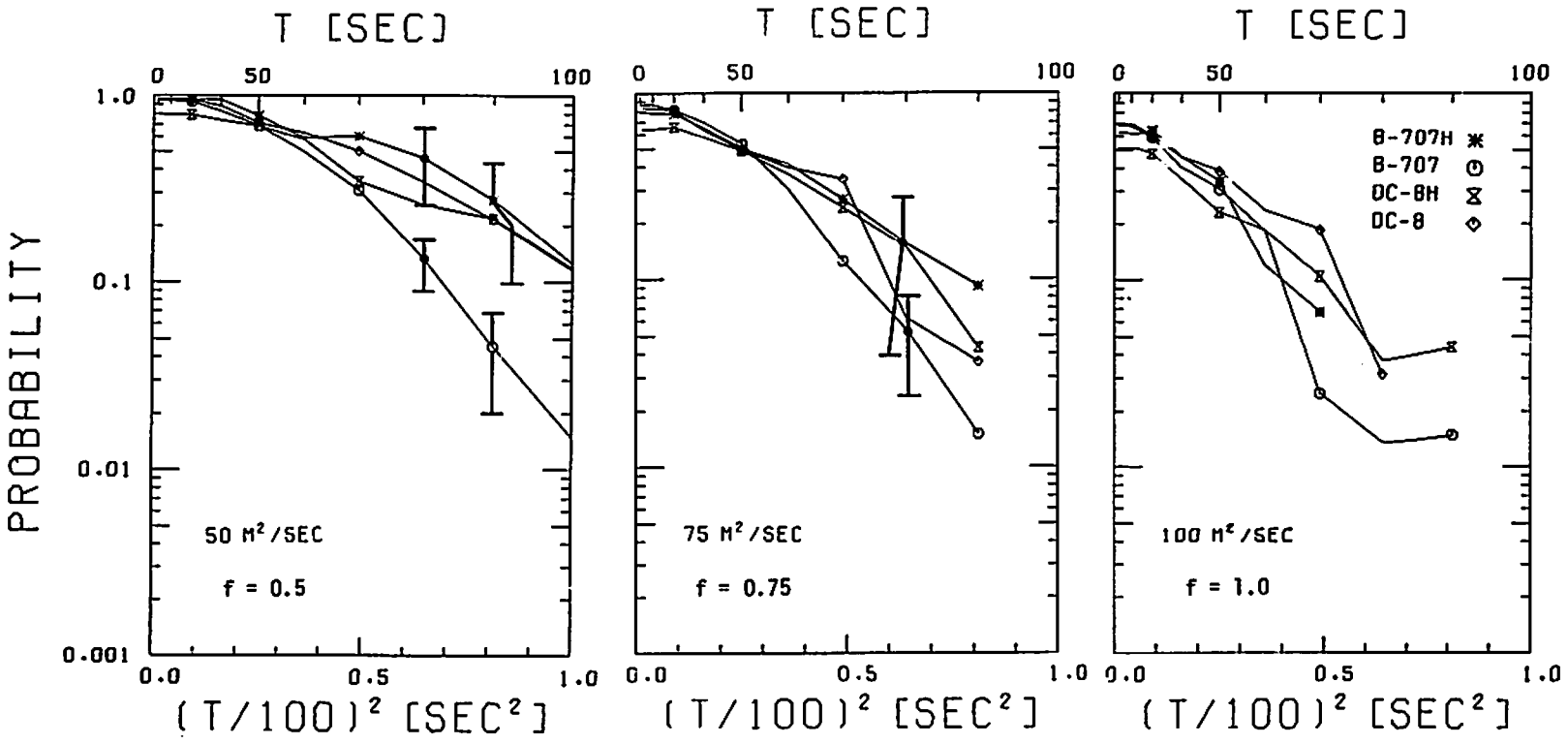

FIGURE 26. DEPENDENCE OF VORTEX DECAY ON FRACTION OF ROLL CONTROL CAPABILITY OF AIRCRAFT; 10 METERS, VORTEX 2, 0-8 KNOTS

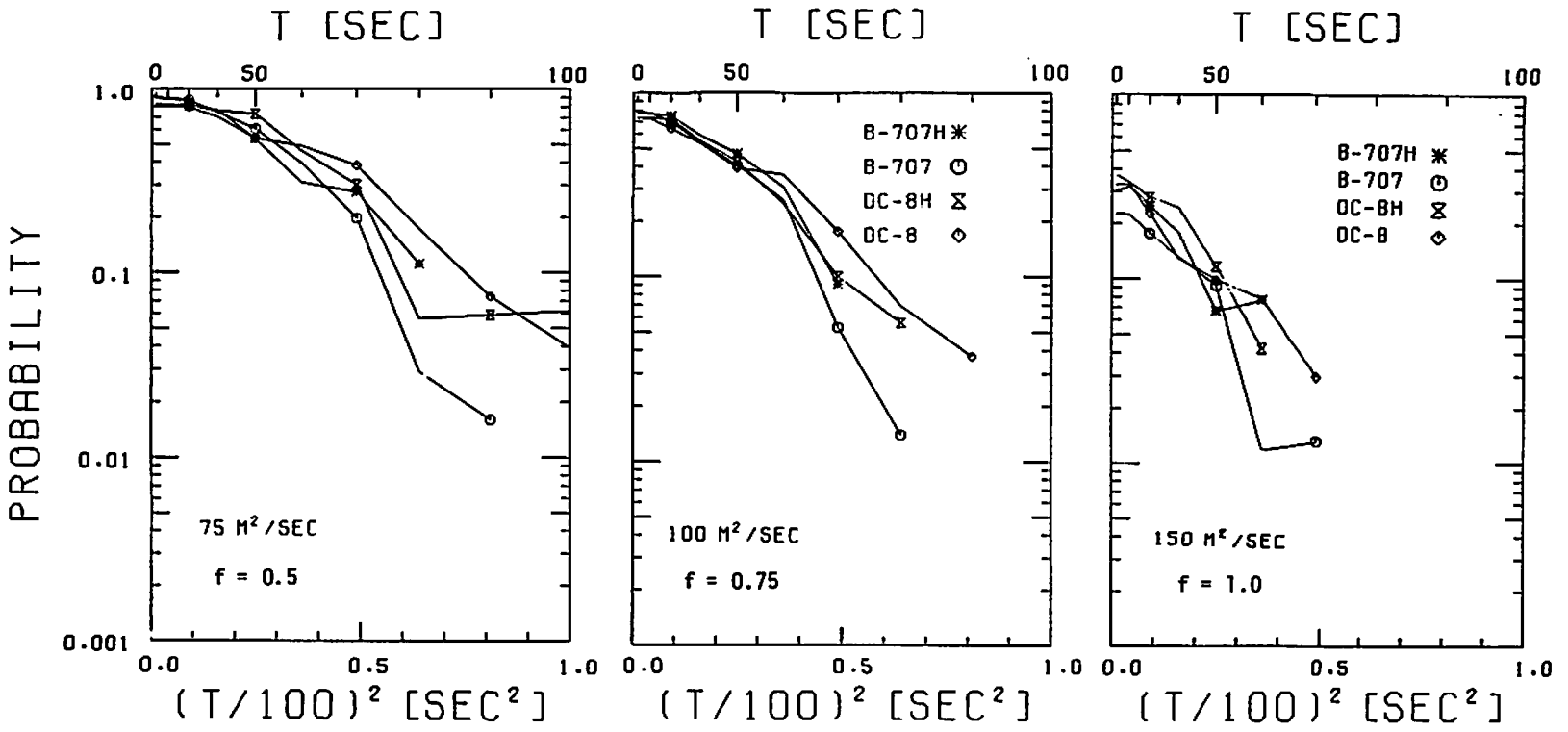

FIGURE 27. DEPENDENCE OF VORTEX DECAY ON FRACTION OF ROLL CONTROL CAPABILITY OF AIRCRAFT; 15 METERS, VORTEX 2, 0-8 KNOTS

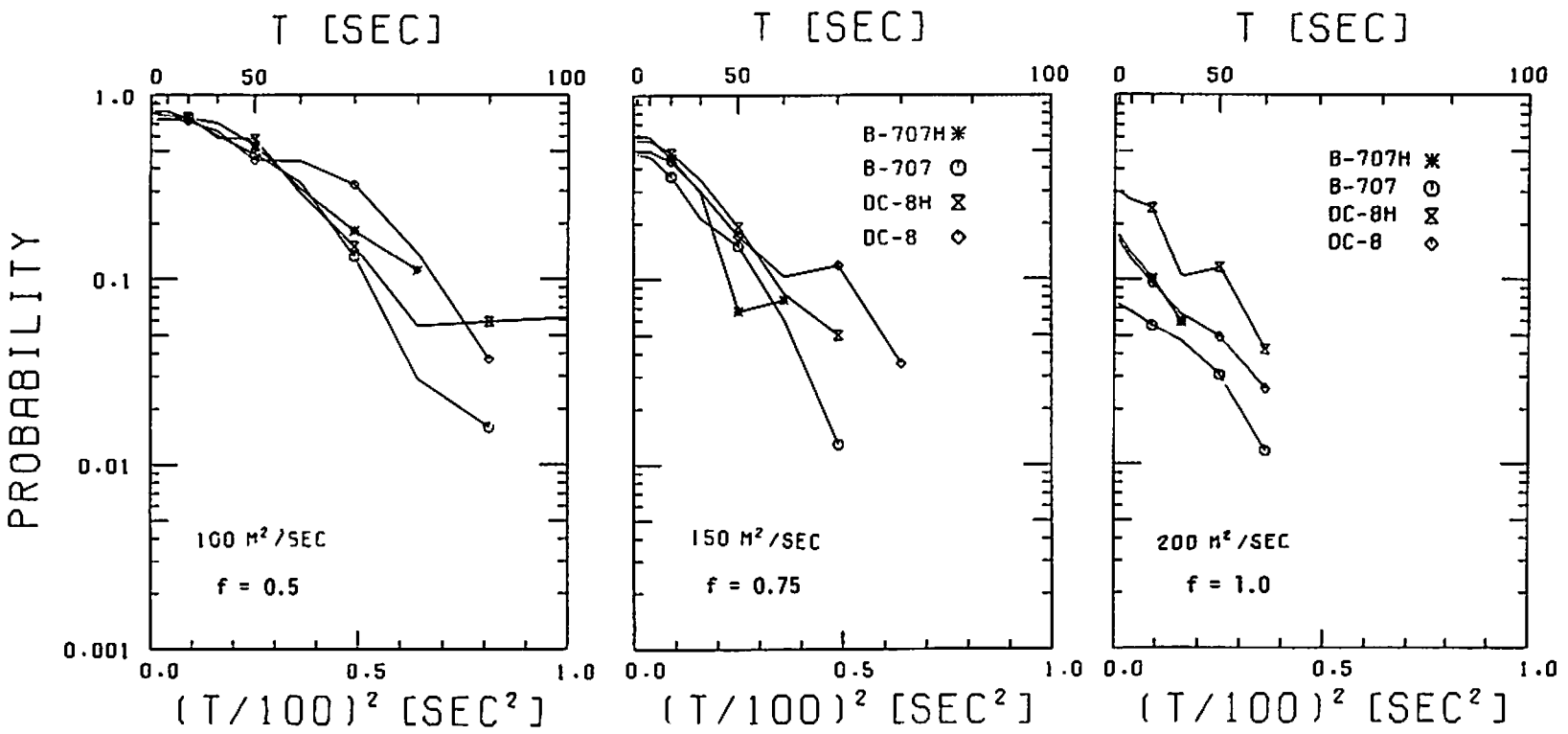

FIGURE 28. DEPENDENCE OF VORTEX DECAY ON FRACTION OF ROLL CONTROL CAPABILITY OF AIRCRAFT; 20 METERS, VORTEX 2, 0-8 KNOTS

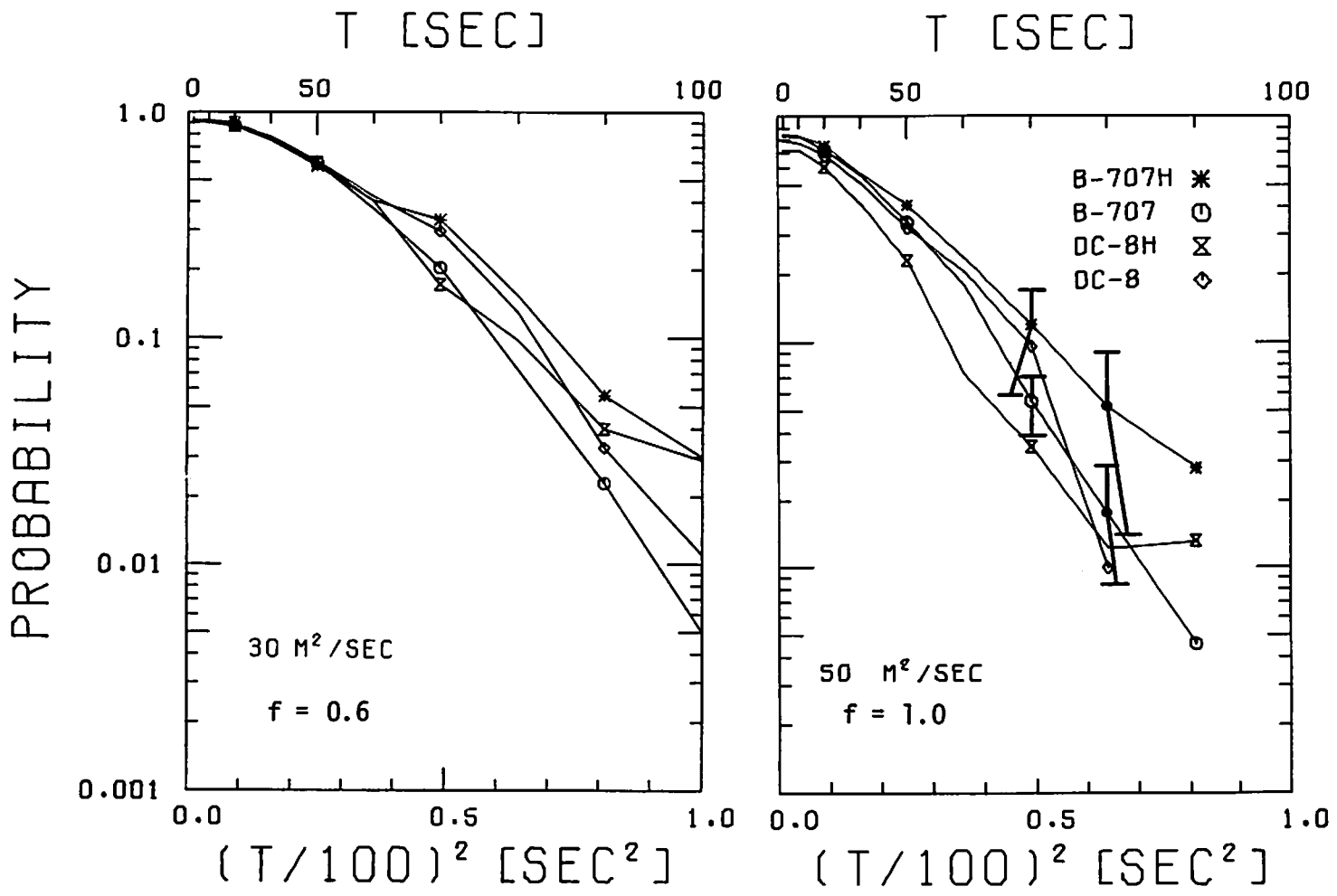

FIGURE 29. DEPENDENCE OF VORTEX DECAY ON FRACTION OF ROLL CONTROL CAPABILITY OF AIRCRAFT; 5 METERS, VORTEX 2, ALL WINDS

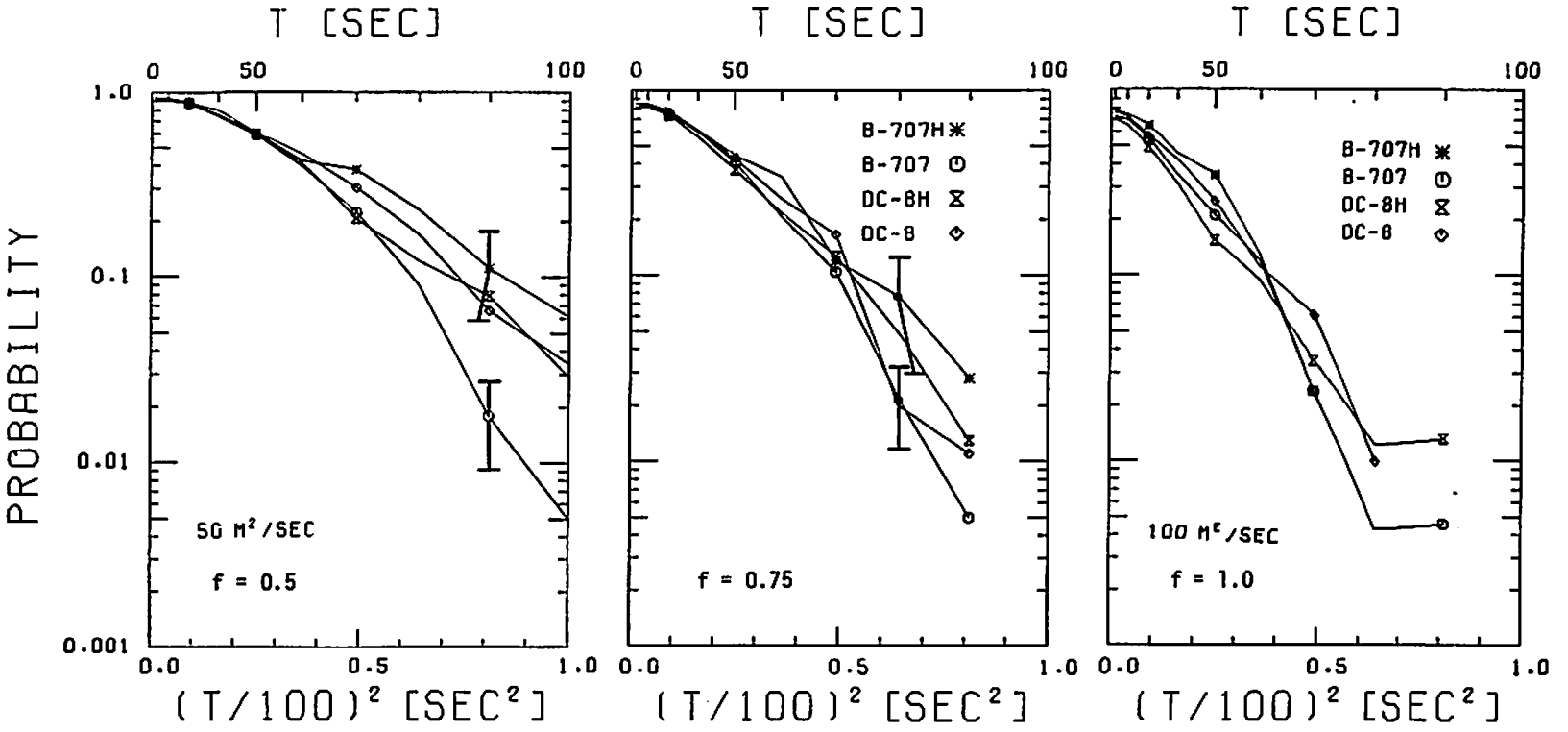

FIGURE 30. DEPENDENCE OF VORTEX DECAY ON FRACTION OF ROLL CONTROL CAPABILITY OF AIRCRAFT; 10 METERS, VORTEX 2, ALL WINDS

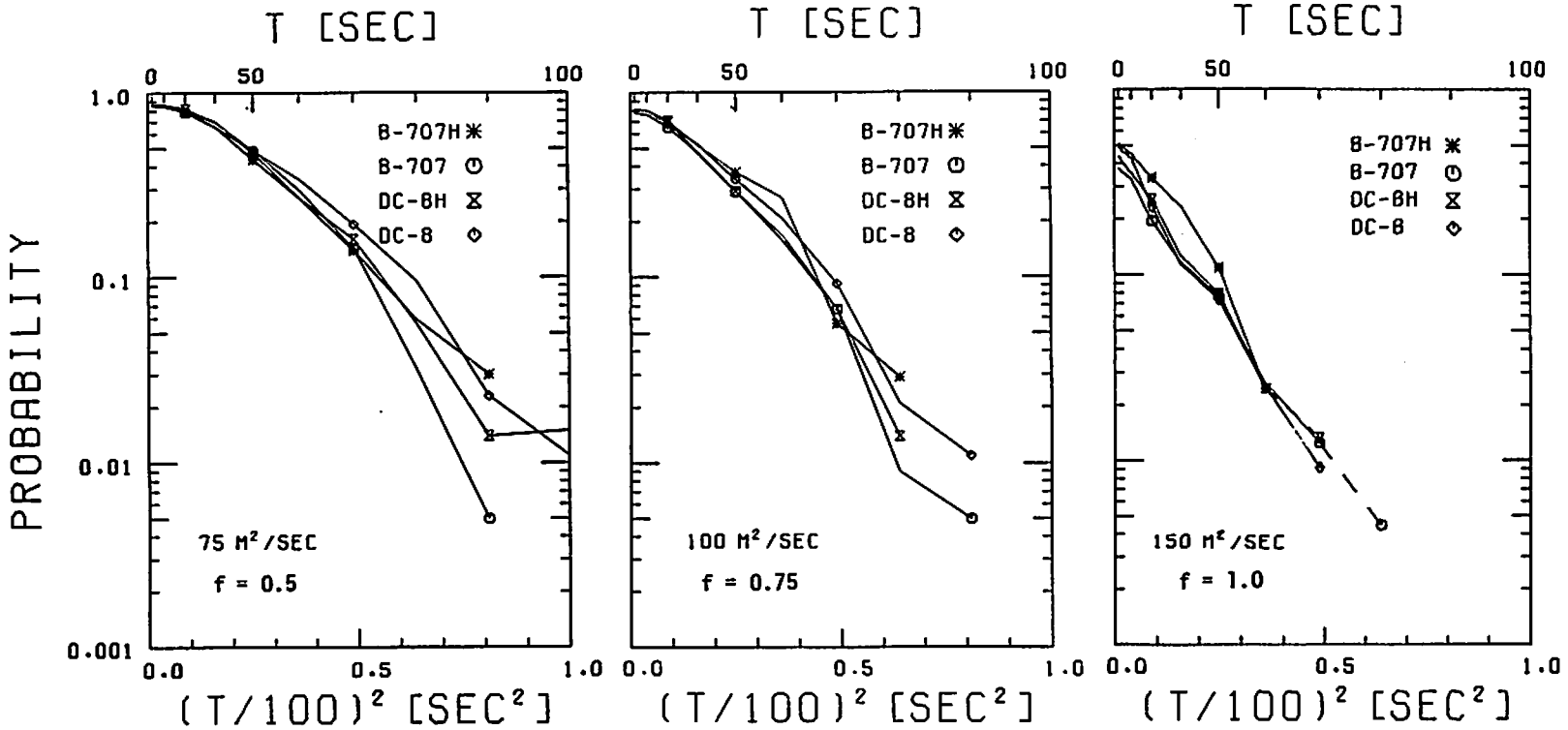

FIGURE 31. DEPENDENCE OF VORTEX DECAY ON FRACTION OF ROLL CONTROL CAPABILITY OF AIRCRAFT; 15 METERS, VORTEX 2, ALL WINDS

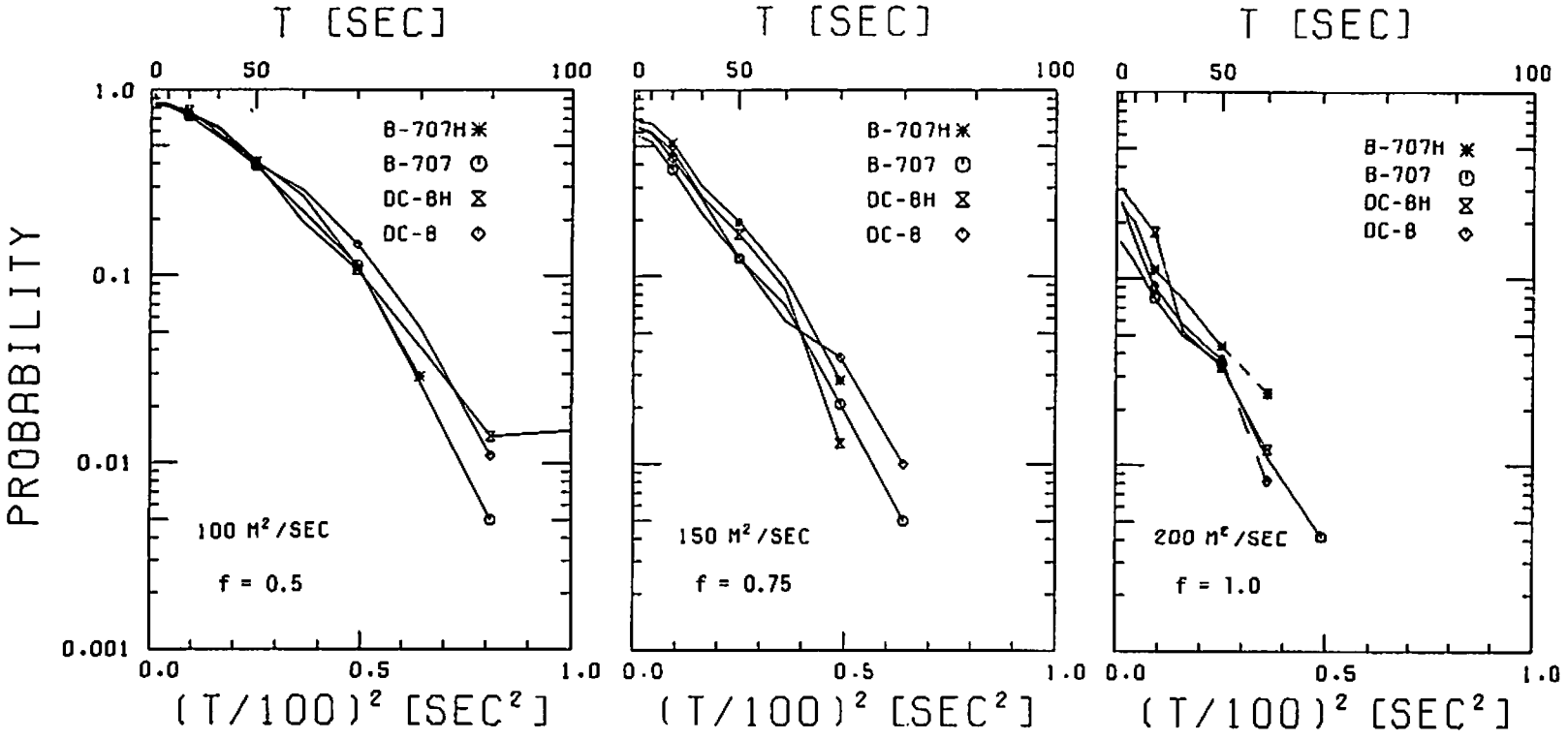

FIGURE 32. DEPENDENCE OF VORTEX DECAY ON FRACTION OF ROLL CONTROL CAPABILITY OF AIRCRAFT; 20 METERS, VORTEX 2, ALL WINDS

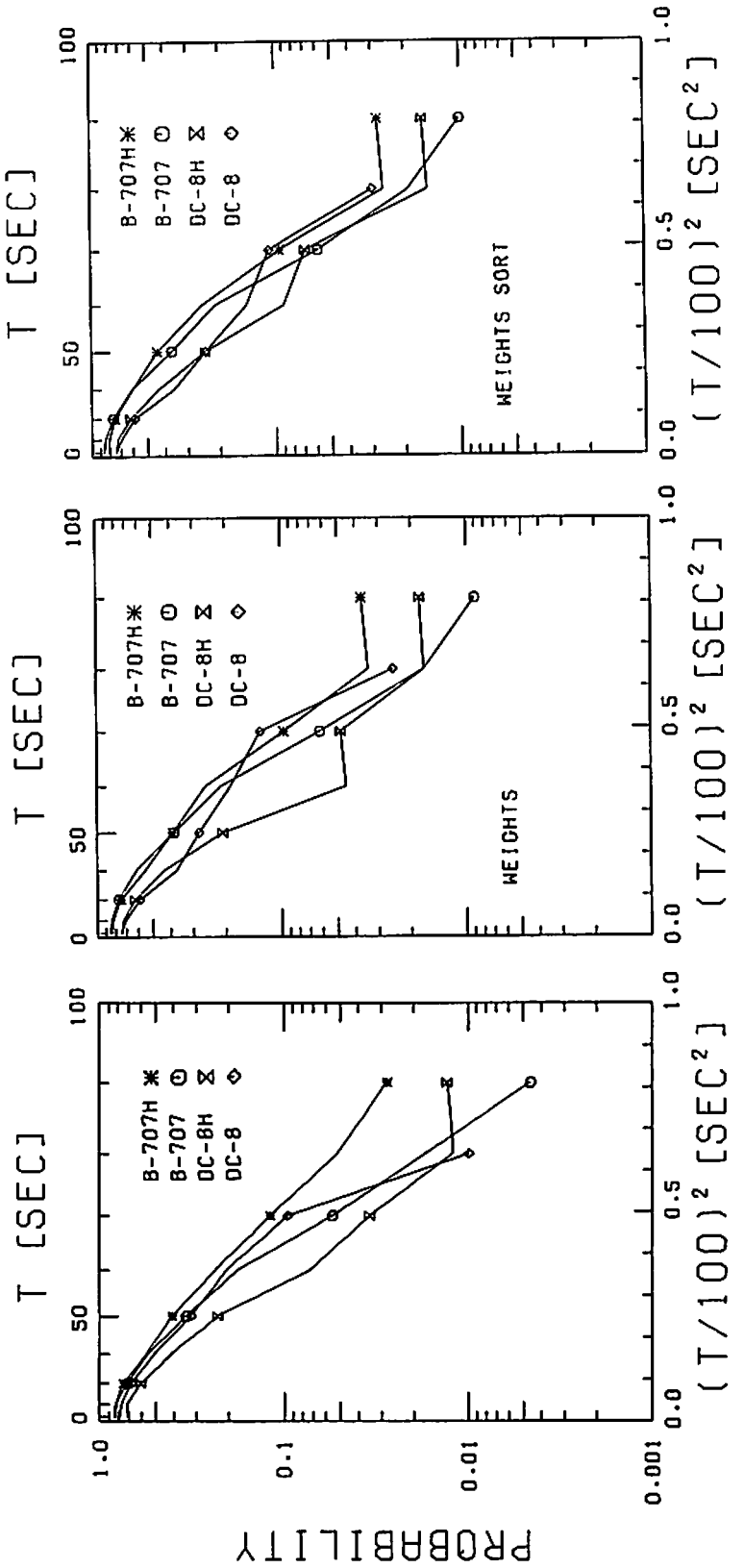

FIGURE 33. DEPENDENCE OF VORTEX DECAY ON WEIGHT SORT; 5 METERS, 50 m2/s, VORTEX 2, ALL WINDS

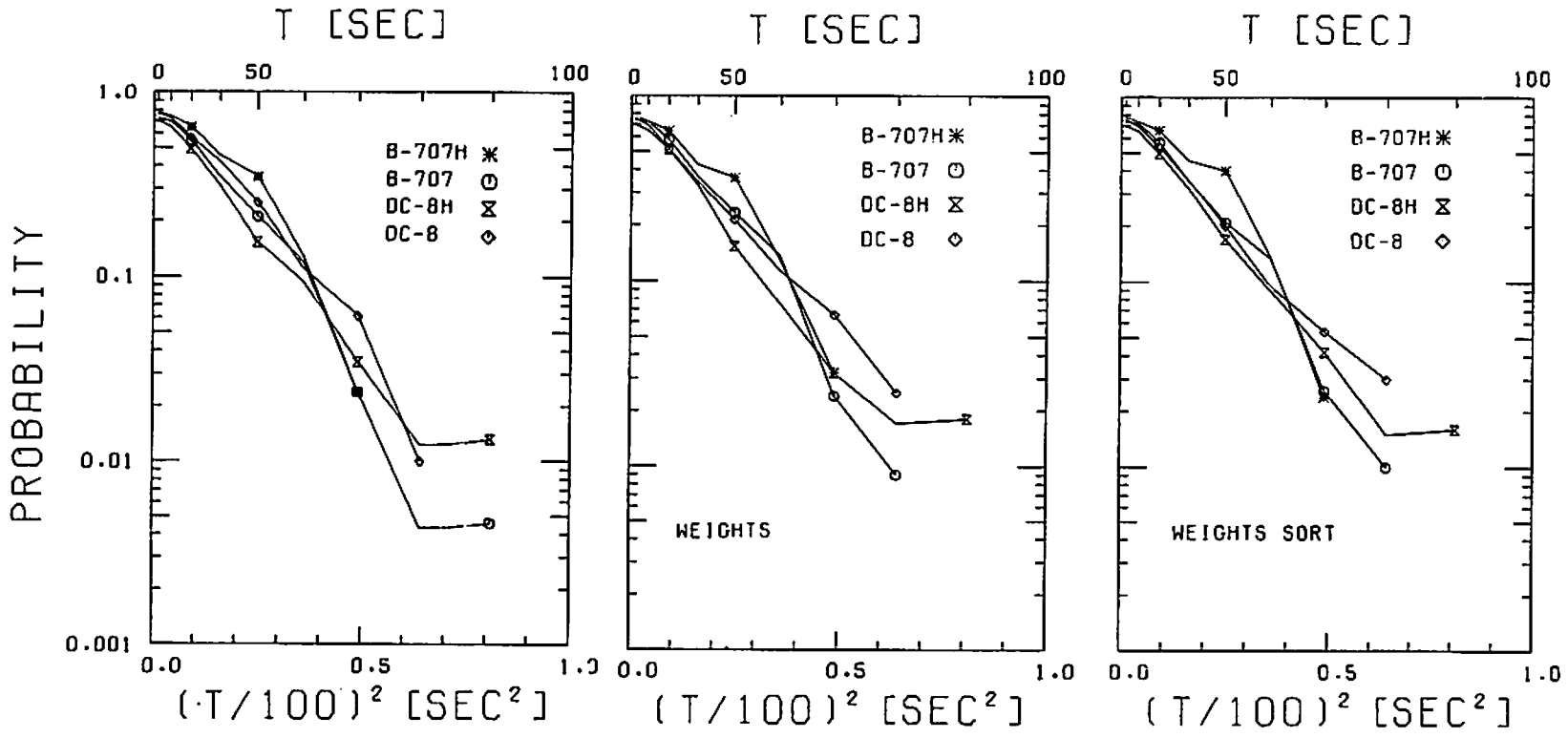

FIGURE 34. DEPENDENCE OF VORTEX DECAY ON WEIGHT SORT; 10 METERS 100 m^2/s, VORTEX 2, ALL WINDS

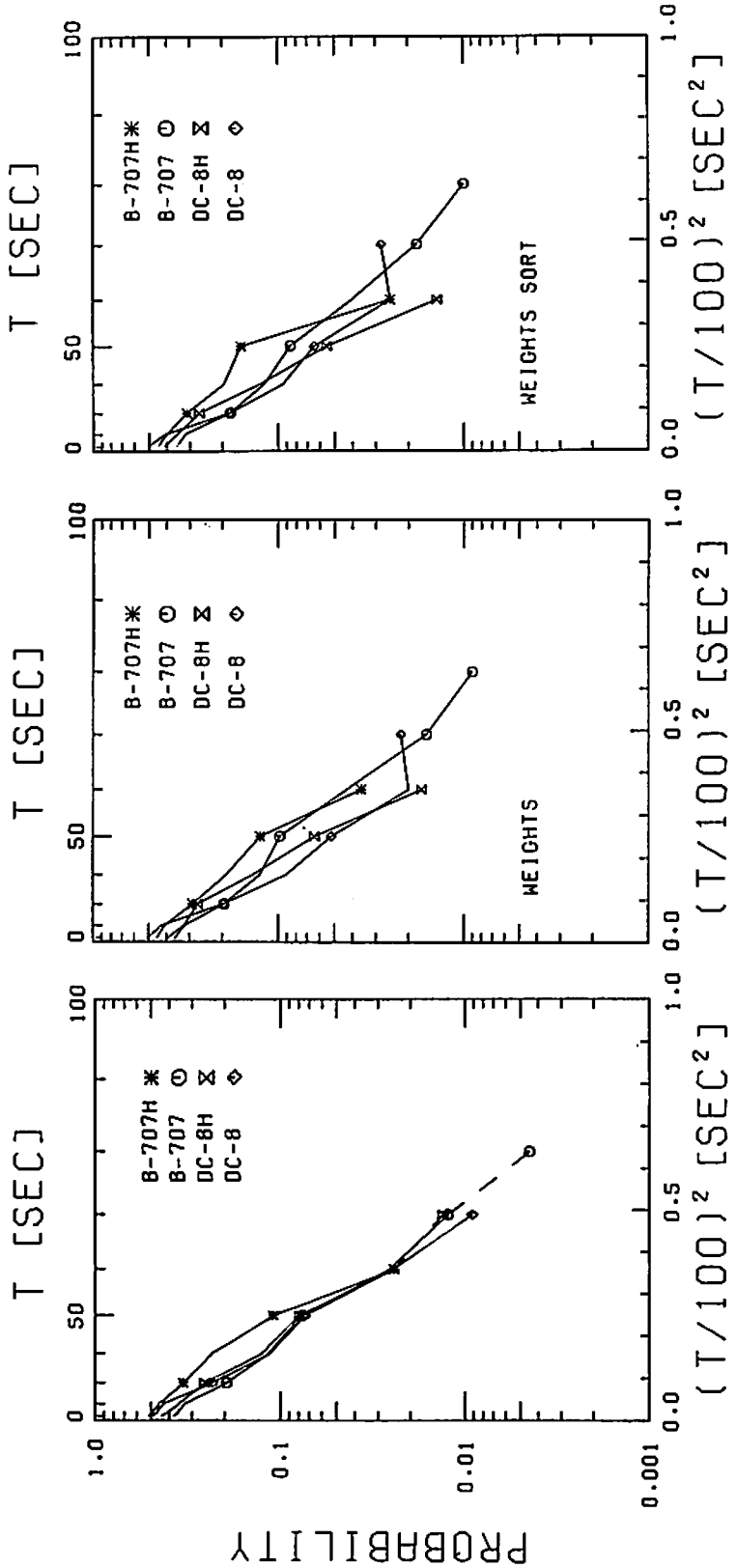

FIGURE 35. DEPENDENCE OF VORTEX DECAY ON WEIGHT SORT; 15 METERS, 150 m^2/s, VORTEX 2, ALL WINDS

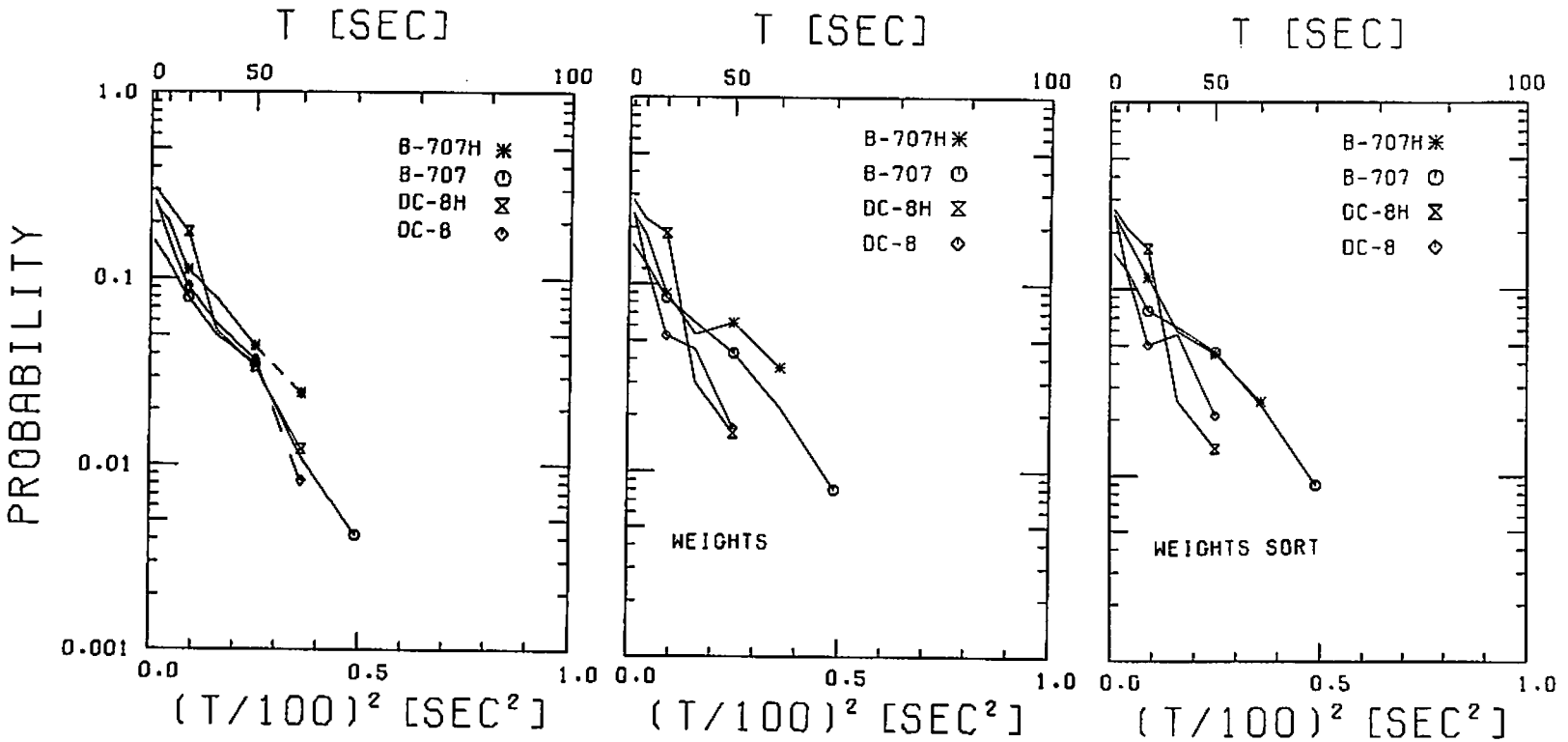

FIGURE 36. DEPENDENCE OF VORTEX DECAY ON WEIGHT SORT; 20 METERS, 200 m^2/s, VORTEX 2, ALL WINDS

4.2.5 Decay Comparisons Between Heavy and Large Versions of the Same Aircraft Type

This section examines the question of whether there are any statistically significant differences in the decay of the wake vortex hazard between Heavy and Large B-707s and DC-8s. In view of the small difference in average aircraft weights (about 10 percent) between the Large and Heavy classes, one would not expect to see much difference in the decay of the wake vortex hazard. In fact, the DC-8 data in Figures 17 to 36 show no significant difference between the two categories. With one exception, the vortices from the Large DC-8s may even be slightly more persistent than the vortices from Heavy DC-8s. The exception occurs for winds 0 to 8 knots for 20-m averaging radius, f = 1.0 (Figure 28). This exception occurs when the strength threshold is near the average initial vortex strength, so that the slightly higher initial strengths of the Heavy cases lead to longer persistence. Since it is unconfirmed at lower values of f and for the all-winds data in Figures 29 and 32, this exception has no practical significance.

The B-707 strength decay data do show a significantly greater hazard persistence for the Heavy category in one situation. The situation has possible operational significance. The vortex hazard tends to be more persistent for Heavy B-707 vortices than for Large B-707 vortices for small averaging radii (5 and 10 m) and reduced values of f. The standard error bars do not overlap for (1) winds 0 to 8 knots for the f = 0.6, 5-m data (Figure 25) and the f = 0.5, 10-m data (Figure 26); and (2) all winds for the f = 0.5, 10-m data (Figure 30). The non-overlapping of the error bars implies a disagreement greater than two standard errors, which should occur statistically in 4.4 percent of a set of identical measurements. Thus, the observed difference could be due to statistical fluctuations. A smaller one standard error disagreement is observed for the f = 1.0, 5-m data in Figures 25 and 29. However, since all the various plots use at least some of the same vortices, they are not statistically independent. The data in Figures 25 through 32 actually use only two different

ensembles, the all-winds ensemble and the 0 to 8 knots winds ensemble. Figures 33 to 36 use two additional ensembles, those cases with weights and the reassignment of cases with weights. The variation of the decay curves for the different ensembles are an indication of the effects of statistical fluctuations. For example, the one standard error disagreement for the all winds, f = 1.0, 5-m data disappears for the weights ensembles in Figure 33.

The apparent difference in persistence between Heavy and Large B-707 vortices prompted a more complete study of the available data. The decay curves for vortex 1 shown in Figure 37 for f = 1.0 and 5-m averaging radius indicate a greater persistence for the Heavy class, but not by a statistically significant amount. The raw data for the two longest-lived vortices, both vortex 1 and 2, were examined in detail (see Appendix E) and were found to have no anomalies. The landing weights for these long-lived cases are not particularly high; the three cases having weight data show weights less than half the rms variation above the mean B-707H weight.

The observed difference in decay between Heavy and Large B-707 vortices appears to be mostly accounted for by a reduced persistence for the Large category rather than an increased persistence for the Heavy category. The Heavy B-707 category shows good agreement with the two DC-8 categories.

The question can be raised about the usefulness of additional data collection on the strength and decay of B-707 and DC-8 wake vortices. It would require increasing the size of the data base by a factor of 4 to reduce the errors by a factor of 2. Such an effort may not be cost effective. Additional data collection would be warranted if a way could be found to increase the number of light and heavy landing weights, along with more careful identification of aircraft by model. Such data could quickly refine the estimates of the weight dependence of strength and persistence.

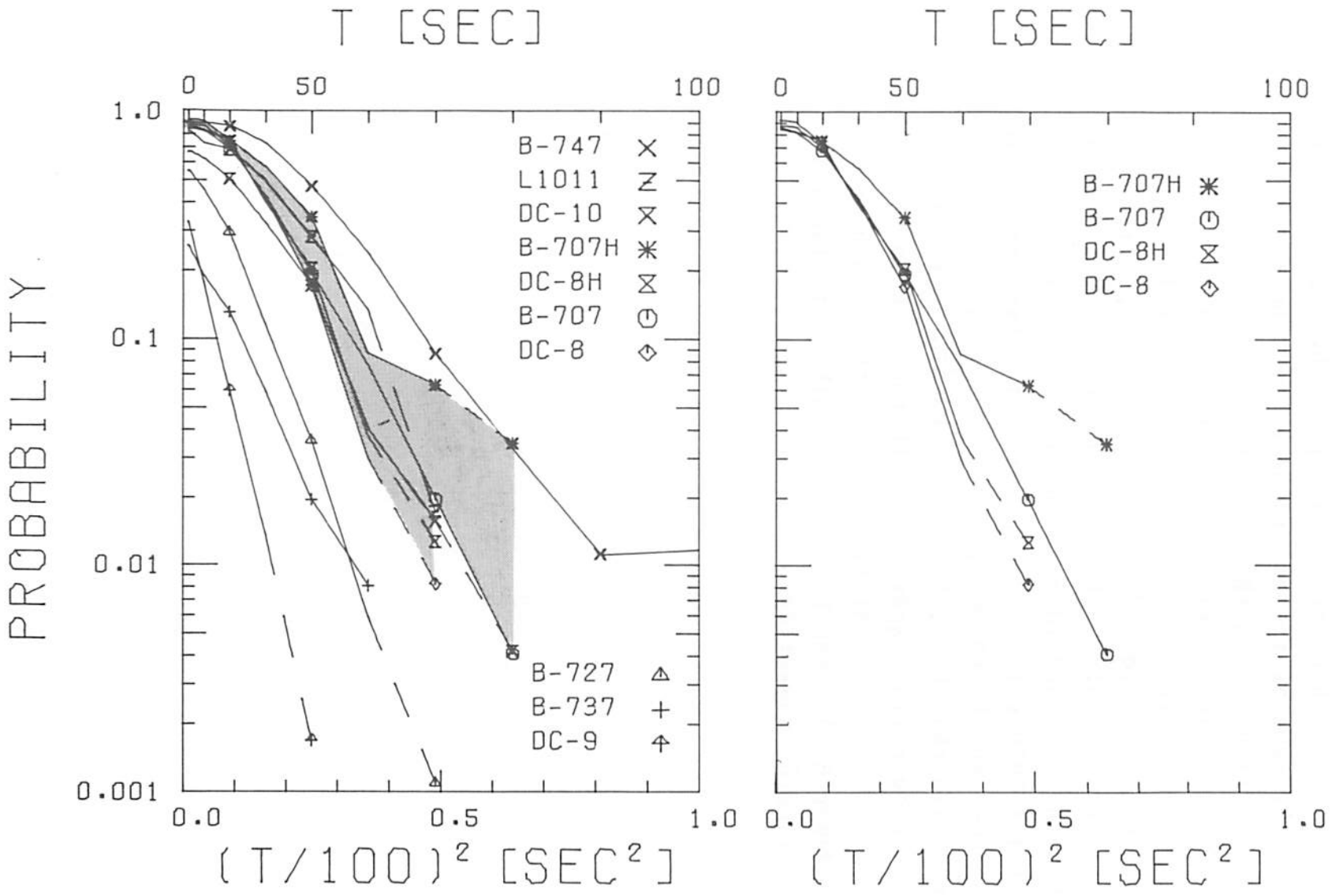

FIGURE 37. DEPENDENCE OF VORTEX DECAY ON AIRCRAFT TYPE; 5 METERS, 50 m^2/s, VORTEX 1, ALL WINDS

In summary, it was found that landing DC-8 and DC-8H vortices cannot be distinguished; the hazard posed by a DC-8H vortex is apparently the same as the hazard posed by a DC-8 vortex. Since operating experience with the DC-8 in the Large category has not led to safety problems (Ref. 11), the data herein suggest that the DC-8H could be reclassified as a Large for landing operations. The B-707H vortices did indicate an increased persistence compared to B-707 vortices. Although the hazard posed by a B-707H vortex is greater than the hazard posed by a B-707 vortex, the level of hazard of a B-707H vortex is apparently the same as the level of hazard of DC-8 and DC-8H vortices. B-707 vortices pose, in general, a lesser hazard than DC-8, DC-8H, and B-707H vortices. As noted above, since operating experience with the DC-8 in the Large category has not led to safety problems, the data herein suggest that the Heavy B-707s and DC-8s could both be reclassified as Large for landing operations.

5. ISSUES IN WAKE VORTEX CATEGORIZATION OF AIRCRAFT

The basic operational question addressed by this report is the safety impact of reclassifying all B-707H and DC-8H aircraft in the Large category. Section 4 approached this question in the conventional way by asking whether there is any significant difference between the vortices generated by the Large and Heavy classes of the same aircraft type. In the case of the B-707, a statistically significant difference was in fact observed within the accuracy of the measurements. A more important question concerns the safety implication of any difference between the Large and Heavy categories. This section will examine the latter question by first establishing the wake vortex hazard characteristics of the Large and Heavy categories, and then examining the effect of aircraft weight on the wake vortex hazard.

5.1 WAKE VORTEX CHARACTERISTICS FOR LARGE AND HEAVY AIRCRAFT

The assigning of aircraft into particular wake vortex categories is somewhat arbitrary. Since the persistence of the wake vortex hazard increases continuously with aircraft size (see Figures 17 to 24), the dividing line between two categories falls into a continuum of hazards. This section examines the vortex hazard on the current boundary between the Large and Heavy categories.

The data in Figures 17 to 24 show that DC-8 and B-707 aircraft generate the most persistent vortices of all aircraft in the Large category. The DC-8H and B-707H vortices were found to be similar to DC-8 vortices, but in some cases more persistent than B-707 vortices. Since the DC-8 is an accepted member of the Large category, one can use the common DC-8/DC-8H/B-707H vortex decay data to characterize the upper boundary of the Large category.

The characteristic vortex decay for the Heavy category can be obtained from the data in Figures 17 to 24 for the B-747 and the L-1011 which show similar persistence. The other widebody aircraft studied, the DC-10, shows somewhat less persistent vortices.

To evaluate the wake vortex hazard for aircraft assigned to the Large category, one must evaluate the hazard at the current separation standards of 3 nautical miles for Large and 4 nautical miles for Small following aircraft. These distances translate to times of 80 and 107 seconds for a typical approach speed of 135 knots (70 m/s). Table 6 lists the hazard probabilities at these two times for the plots in Figures 17 to 32. The data are indicated as approximate when there was a large spread in values for different aircraft categories or when extrapolation beyond the range of the data was required. At 80 seconds the difference between the DC-8/B-707H/DC-8H group and the Heavy category is large for semispans or averaging radii of 15 and 20 m (e.g., a following DC-9 and B-707, respectively), about a factor of 10 in hazard probability for f = 1.0. This difference decreases to about a factor of 5 for 10-m averaging radius (e.g., a following Gulfstream) and to about 3 for 5-m averaging radius (e.g., a following Learjet). At 107 seconds the ratios appear to be somewhat less, although the results are uncertain because of extrapolation errors.

The results in Table 6 show one remarkable consistency. The DC-8/B-707H/DC-8H hazard probabilities for f = 0.75 are approximately the same as the B-747/L-1011 probabilities for f = 1.0. Under the vortex decay hypothesis of Section 3.2, this similarity in decay can be interpreted as meaning that the effective vortex strength for the B-747/L-1011 group is a factor of 1.33 (1.0/0.75) greater than that for the DC-8/B-707H/DC-8H group. Thus, a simple numerical factor can be used to characterize the difference in vortex hazard between the upper edge of the Large category and the middle of the Heavy category.

5.2 SHOULD LANDING WEIGHT PLAY A ROLE IN CATEGORIZATION?

The strength of the wake vortex generated by a landing aircraft depends upon the actual landing weight according to Equation (2). An aircraft landing at the maximum certificated landing weight could conceivably produce a significantly more hazardous wake than one landing at the average weight. This section makes use of the

TABLE 6. VORTEX 2 HAZARD PROBABILITIES

Averaging Radius (m)	B-747/L-1011		DC-8/B-707H/DC-8H	
	All Winds	Winds 0-8 Knots	All Winds	Winds 0-8 Knots
Age = 80 seconds, f = 1.0				
5	0.08	0.11	∿0.025	∿0.05
10	0.05	0.10	0.01	∿0.035
15	0.02	0.06	0.0025	∿0.005
20	0.02	0.06	0.002	∿0.004
Age = 107 seconds, f = 1.0				
5	∿0.002	∿0.005	∿0.001	∿0.003
10	∿0.001	∿0.003	∿0.0002	∿0.001
Averaging Radius (m)	f = 0.75		f = 0.5	
	All Winds	Winds 0-8 Knots	All Winds	Winds 0-8 knots
B-707/DC-8, Age = 80 seconds				
5	0.10*	∿0.2*	-	-
10	∿0.04	∿0.1	∿0.11	∿0.3
15	0.02	∿0.06	0.05	∿0.09
20	0.008	∿0.015	0.04	∿0.08
B-707/DC-8, Age = 107 seconds				
5	∿0.005*	∿0.02*	-	-
10	∿0.001	∿0.01	∿0.02	∿0.07

*$\overline{f = 0.6}$

concepts and data of Sections 3 and 4 to estimate the increase of hazard from a fully loaded aircraft compared to an aircraft at average weight.

Table 7 evaluates the estimated strength of a vortex generated at the maximum allowed landing weight (B-707H at 247,000 lb, DC-8H at 245,000 lb). The data from Table 3 and a power-law relationship between strength and weight (Equation (5)) are used to relate the maximum strength to the average strength. The power 0.5 was justified on theoretical grounds in Section 3.1 and was consistent with the data in Section 4.1.2. The results in Table 7 show a 14 percent increase in vortex strength for the B-707H and an 11 percent increase for the DC-8H at their maximum allowed landing weight. Table 7 also references these strengths to the average strength of the strongest vortex in the Large category, namely the DC-8. These results indicate that the heaviest B-707H could generate a 19 percent stronger vortex than a typical DC-8. The DC-8H, however, shows a possible increase of only 13 percent.

At the end of Section 5.1 the vortex hazard from the widebody aircraft was characterized by an effective strength 33 percent greater than that of the DC-8. From Table 7 one can see that the heaviest DC-8H produces a vortex only 13 percent stronger than an average weight Large DC-8. The heaviest DC-8H is therefore closer to the Large category than to the B-747/L-1011 group. The heaviest B-707H could have a strength 19 percent larger than the average Large DC-8 and thus would fall about half way between the B-747/L-1011 group and the Large category. The resulting increase in vortex hazard probability would be about a factor of 2 or 3 at 80 seconds according to Table 6. Since the B-707H and DC-8H apparently land at weights less than the permitted maximum landing weight (see Figures 4 and 5 and Table 8 in Appendix A), the B-707H and DC-8H are closer to the Large category (i.e., the DC-8) than to the B-747/L-1011 or Heavy group. This observation is underscored when the strength ratios are compared to the heaviest DC-8 (maximum landing weight, 199,500 lb; average landing weight, 183,000 lb). The ratios of Γ_{ave} for the B-707H and DC-8H to Γ_{max} for the Large

TABLE 7. LANDING WEIGHTS AND MAXIMUM INITIAL VORTEX STRENGTHS FOR THE B-707H AND DC-8H

Landing Weights and Maximum Initial Vortex Strengths	B-707H	DC-8H
Maximum Landing Weight (lb)	247,000	245,000
Average Landing Weight (lb)	190,000	199,000
Ratio Max./Ave. Landing Weight	1.30	1.23
Power of Γ versus W, Equation (5)	0.5	0.5
$\Gamma_{max}/\Gamma_{ave}$	1.14	1.11
$\Gamma_{max}(5m)/\Gamma_{ave}^{DC-8}$ (5 m)	1.20	1.12
$\Gamma_{max}(10m)/\Gamma_{ave}^{DC-8}$ (10 m)	1.20	1.14
$\Gamma_{max}(20m)/\Gamma_{ave}^{DC-8}$ (20 m)	1.18	1.13

DC-8 are 0.97 and 0.93, respectively. Thus, the strength of a vortex from the heaviest DC-8 is greater than the strengths of the average B-707H and DC-8H. As argued before, since the DC-8 is an accepted member of the Large category, the analysis herein further supports recategorizing the B-707H and DC-8H from the Heavy category to the Large category.

6. BRITISH OBSERVATIONS IN THE INCIDENT REPORTING SYSTEM

Prior to August 1978, the United Kingdom (UK) included the B-707H and DC-8H in the Large weight category for the purpose of wake vortex separation on the approach. Subsequently, the UK adopted the US/ICAO division of the B-707 and DC-8 aircraft into both the Heavy and Large categories; the dividing line between Heavy and Large aircraft was lowered by the UK from 375,000 lb to 300,000 lb.

The UK has an active and successful program for reporting apparent wake vortex incidents (Ref. 12), particularly for operations at Heathrow airport. Prior to the rule change the incident probability behind Heavy aircraft (in this case, more than 375,000 lb certificated maximum gross takeoff weight) was comparable to the incident probability for Large aircraft behind aircraft with certificated maximum gross takeoff weights between 300,000 and 375,000 lb. Thus, the separation standard which grouped all B-707 and DC-8 aircraft into the same category (Large) gave a well-balanced system in which the incident probability was approximately the same for various aircraft pairs. Subsequent to the rule change, the incident risk to aircraft following a B-707H or DC-8H has been virtually eliminated (the minimum separation was increased from 3 to 6 nautical miles for most following aircraft); however, the incident risk to B-707H/DC-8H aircraft following widebody aircraft has increased at least fourfold (the minimum separation was decreased from 6 to 4 nautical miles) and is now the highest risk of any category.

In a related situation, the UK have experienced some complications with the categorization of the A-300B. When introduced into service, the A-300B was classed as Large along with the B-707H (recall that the UK dividing line was at 375,000 lb). However, an unacceptably high vortex incident rate led to reclassifying the A-300B as a Heavy when landing, although this special situation became redundant when the UK accepted the ICAO criteria promulgated

in August 1978. The point is that, perhaps maximum certificated gross takeoff weight may not be the best discriminant of vortex hazard.

Including the B-707H and DC-8H in the Heavy category has brought about a reduction in capacity in the UK without any apparent overall increase in safety. The evidence collected both prior to and since August 1978 through the incident reporting system appears to support the unification of all B-707/DC-8 aircraft into the Large category.

APPENDIX A

LANDING WEIGHTS OF HEAVY DC-8 AIRCRAFT

To determine whether the landing weights of Heavy aircraft at O'Hare airport were characteristic of landing weights at other airports, data were obtained for other airports from the United Airlines Area Operations Manager. The results for Heavy DC-8 aircraft are shown in Table 8. The calculated mean and standard deviation of the landing weights are 205,900 and 11,500 lb, respectively. The lowest landing weight was 178,100 lb. Comparing these results with those in Figures 4 and 5 and in Table 2, it appears that the only difference between the two distributions occurs at the low weight end where the O'Hare data show a number of landings below 175,000 lb. The O'Hare mean value is about 2 percent lower and the standard deviation about 30 percent larger than the data in Table 8. These small differences are most likely due to the misidentified non-Heavy DC-8s which have a peak in weight distribution at 175,000 lb.

TABLE 8. LANDING WEIGHTS OF UNITED AIRLINES HEAVY DC-8 AIRCRAFT

ORIGIN	DEST	FLITE NO.	1/14/80	1/15/80	1/16/80
DEN	JFK	378	207,400 lb	192,200 lb	192,600 lb
SFO	JFK	2872	192,500 lb	199,900 lb	197,600 lb
LAX	JFK	2856	209,000 lb	213,800 lb	216,400 lb
ORD	JFK	2822	226,400 lb	217,100 lb	208,200 lb
ORD	EWR	616	202,300 lb	202,400 lb	205,900 lb
DEN	PHL	644	199,300 lb	200,600 lb	194,400 lb
DEN	PHL	694	197,300 lb	197,100 lb	178,100 lb
SFO	PHL	32	205,400 lb	191,500 lb	199,600 lb
ORD	PHL	10	214,500 lb	209,500 lb	
ORD	BAL	2844	216,700 lb		206,300 lb
SFO	IAD	58	213,000 lb	198,900 lb	202,600 lb
DEN	IAD	372	206,100 lb	212,300 lb	200,600 lb
ORD	BOS	156	223,800 lb	216,400 lb	214,900 lb
ORD	BOS	366	213,200 lb	201,800 lb	200,700 lb
DEN	BOS	154	221,200 lb	210,200 lb	209,800 lb
DEN	BOS	368	207,200 lb	198,700 lb	193,200 lb
ORD	BDL	142	222,900 lb	224,700 lb	233,800 lb
ORD	BDL	2826	180,500 lb	204,000 lb	194,100 lb

APPENDIX B

ERROR ANALYSIS

This appendix presents the error analysis for the least-square fit to the strength Γ versus weight W data described in Section 4.1.3. The statistical analysis can be found in any standard statistics book (e.g., Ref. 13). The fitted slope of the linear fit is given by

$$a = \frac{\sum_{i=1}^{N} \Gamma_i W_i}{\sum_{i=1}^{N} W_i^2} \qquad \text{(B1)}$$

where N is the number of measurements. The variance of the strength is estimated by

$$s^2 = [\Sigma \Gamma_i^2 - a^2 \Sigma W_i^2]/(N-2). \qquad \text{(B2)}$$

The standard error of the average strength measurement is $s/N^{1/2}$. The standard error s_n in the power n is given by

$$s_n = \left(\frac{\overline{W}}{\overline{\Gamma}}\right)[(\Sigma \Gamma_i^2/\Sigma W_i^2 - a^2)/(N-2)]^{1/2}. \qquad \text{(B3)}$$

APPENDIX C

HAZARD PROBABILITY PLOTS

This appendix contains the disaggregated plots of hazard probability versus time for B-707/B-707H and DC-8/DC-8H aircraft. Figures 38 to 43 compare the curves for all vortices and all winds for the Large and Heavy cases. (Two plots in this set are included as Figures 13 and 14 in the main body of the report.) These results are disaggregated into vortices 1 and 2 and winds less than 8 knots in Figures 44 to 59. There were enough Large B-707 cases to plot the curves for winds less than 5.5 knots and they are shown in Figure 60.

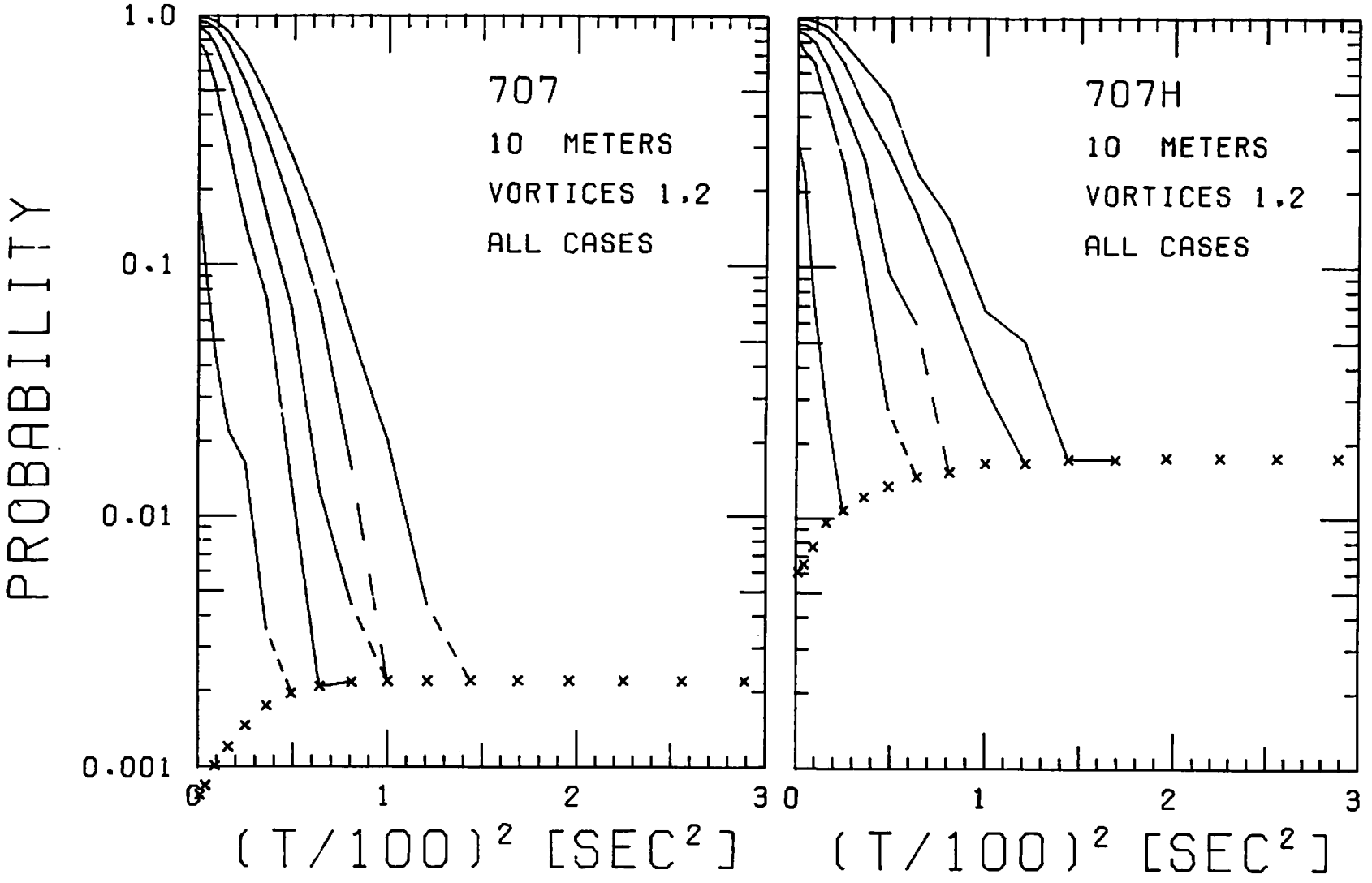

FIGURE 38. PROBABILITY OF DECAY, B-707 AND B-707H, 10-m AVERAGING RADIUS

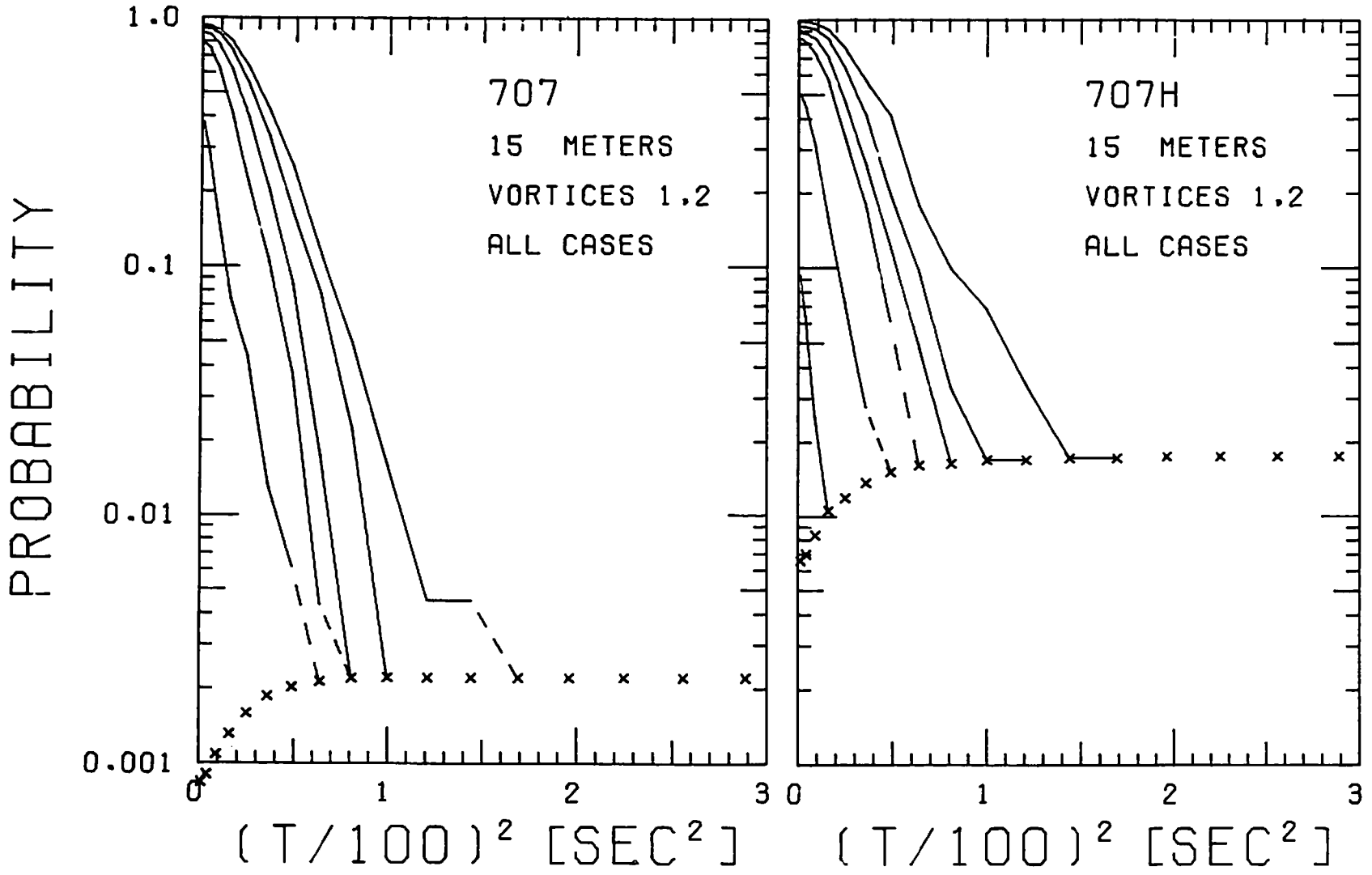

FIGURE 39. PROBABILITY OF DECAY, B-707 AND B-707H, 15-m AVERAGING RADIUS

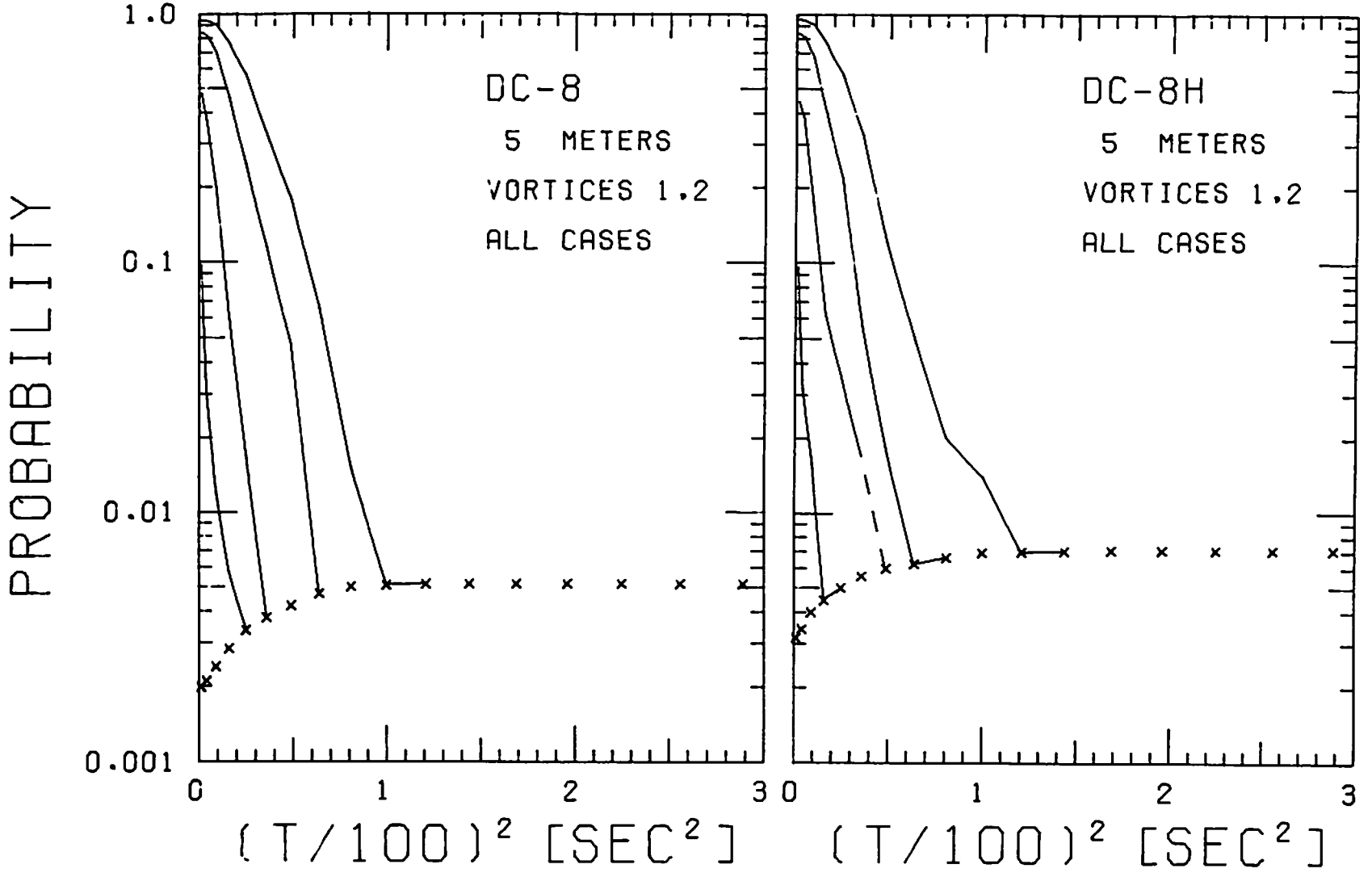

FIGURE 40. PROBABILITY OF DECAY, DC-8 AND DC-8H, 5-m AVERAGING RADIUS

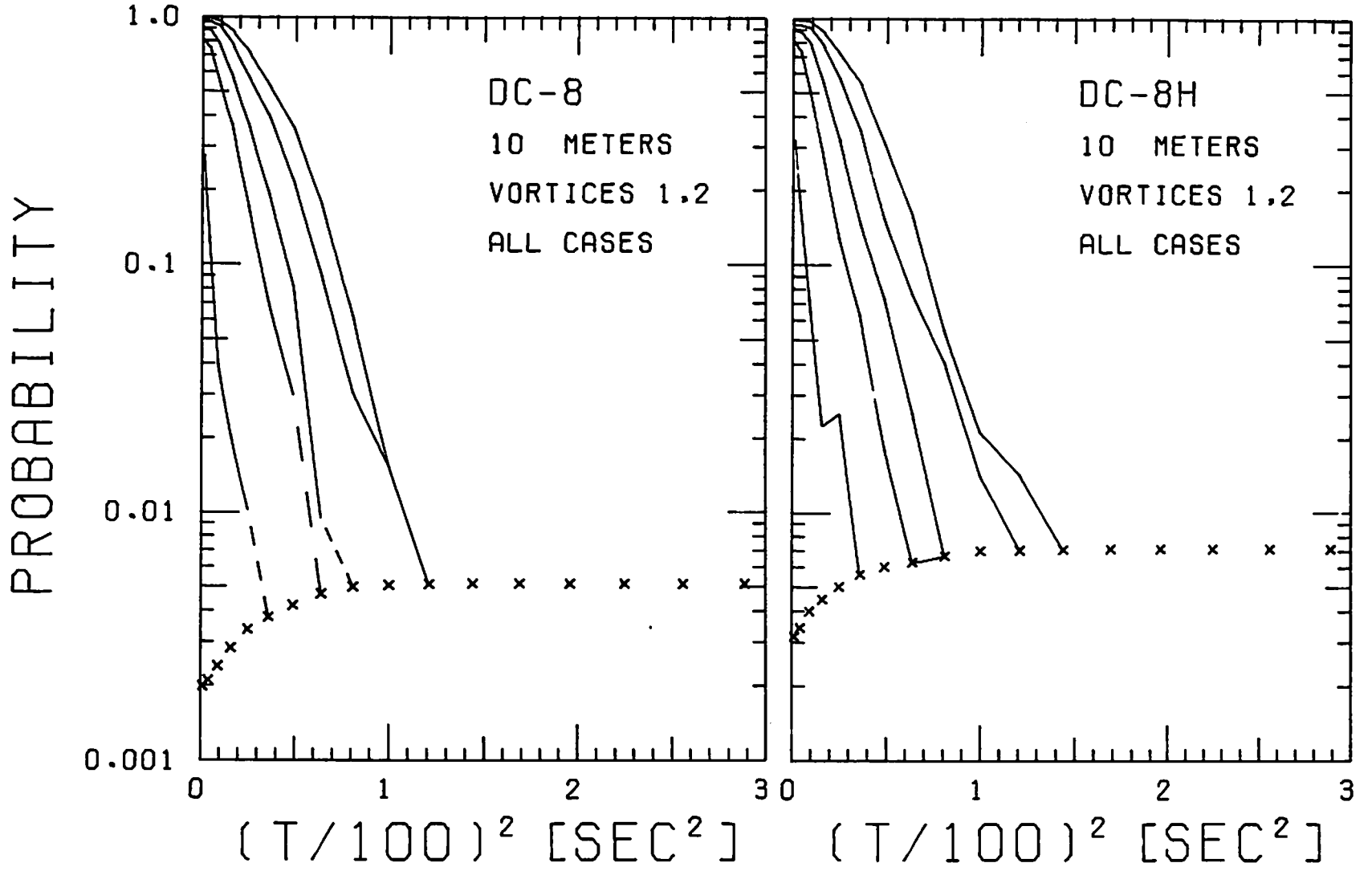

FIGURE 41. PROBABILITY OF DECAY, DC-8 AND DC-8H, 10-m AVERAGING RADIUS

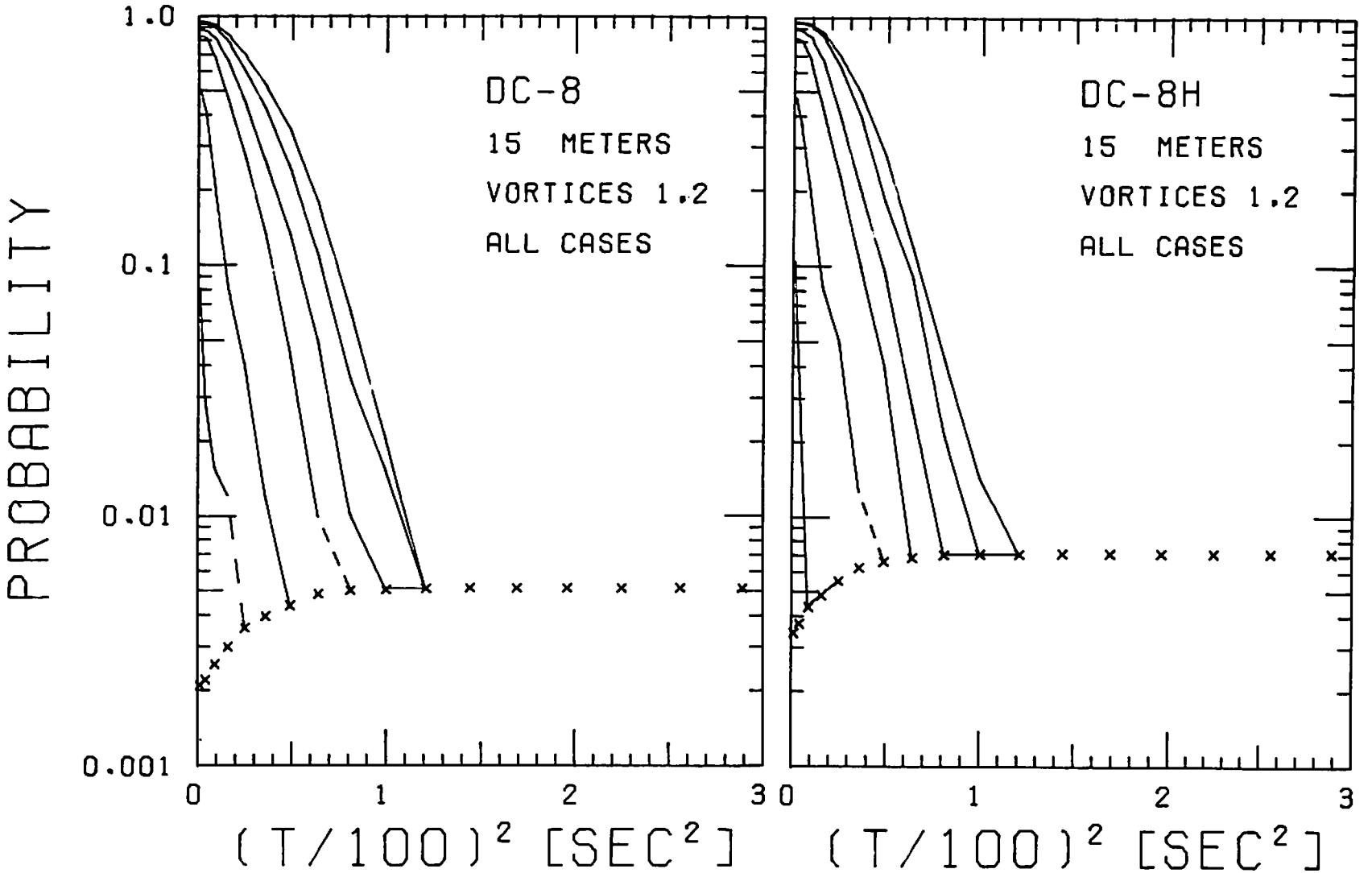

FIGURE 42. PROBABILITY OF DECAY, DC-8 AND DC-8H, 15-m AVERAGING RADIUS

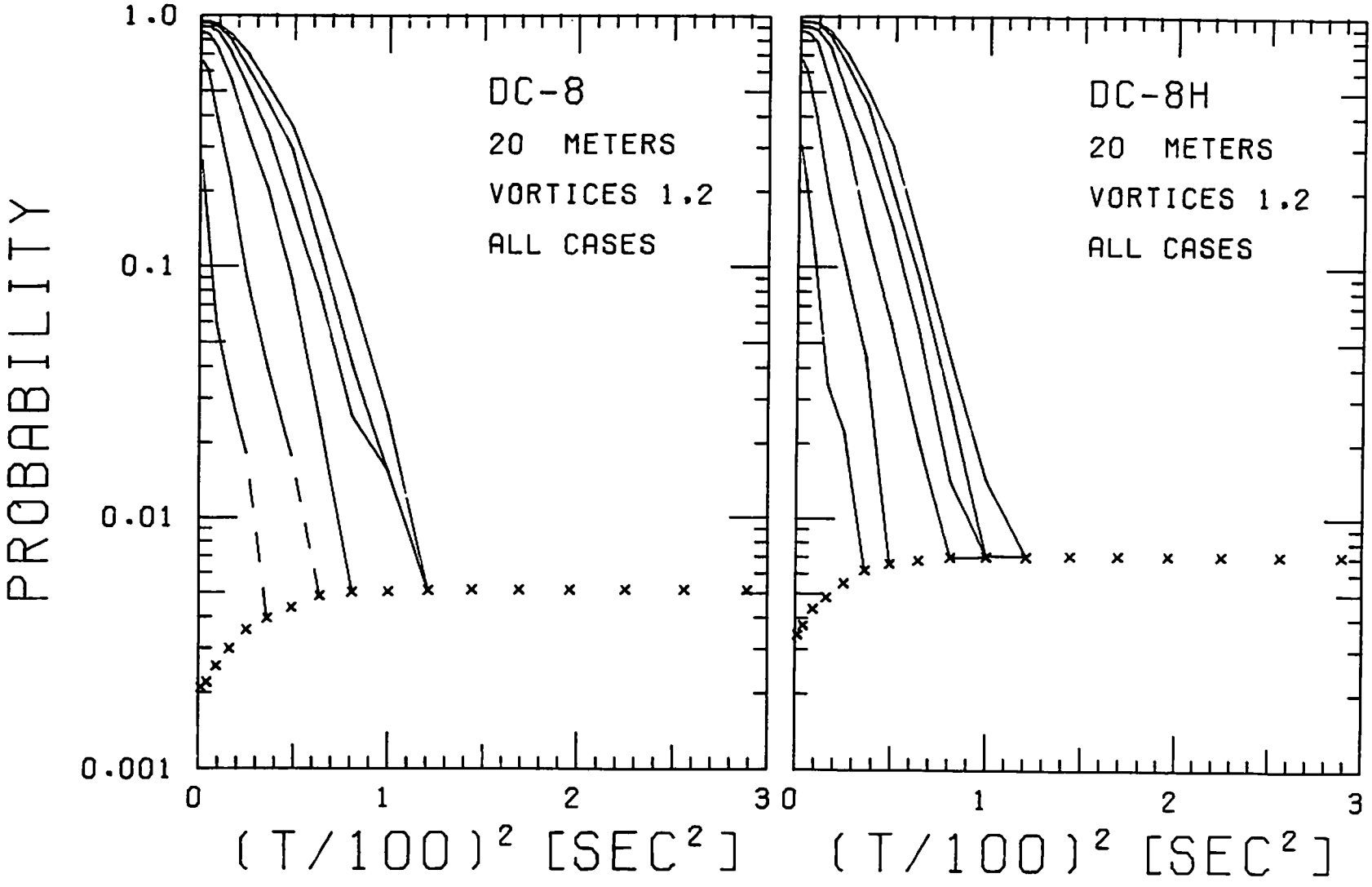

FIGURE 43. PROBABILITY OF DECAY, DC-8 AND DC-8H, 20-m AVERAGING RADIUS

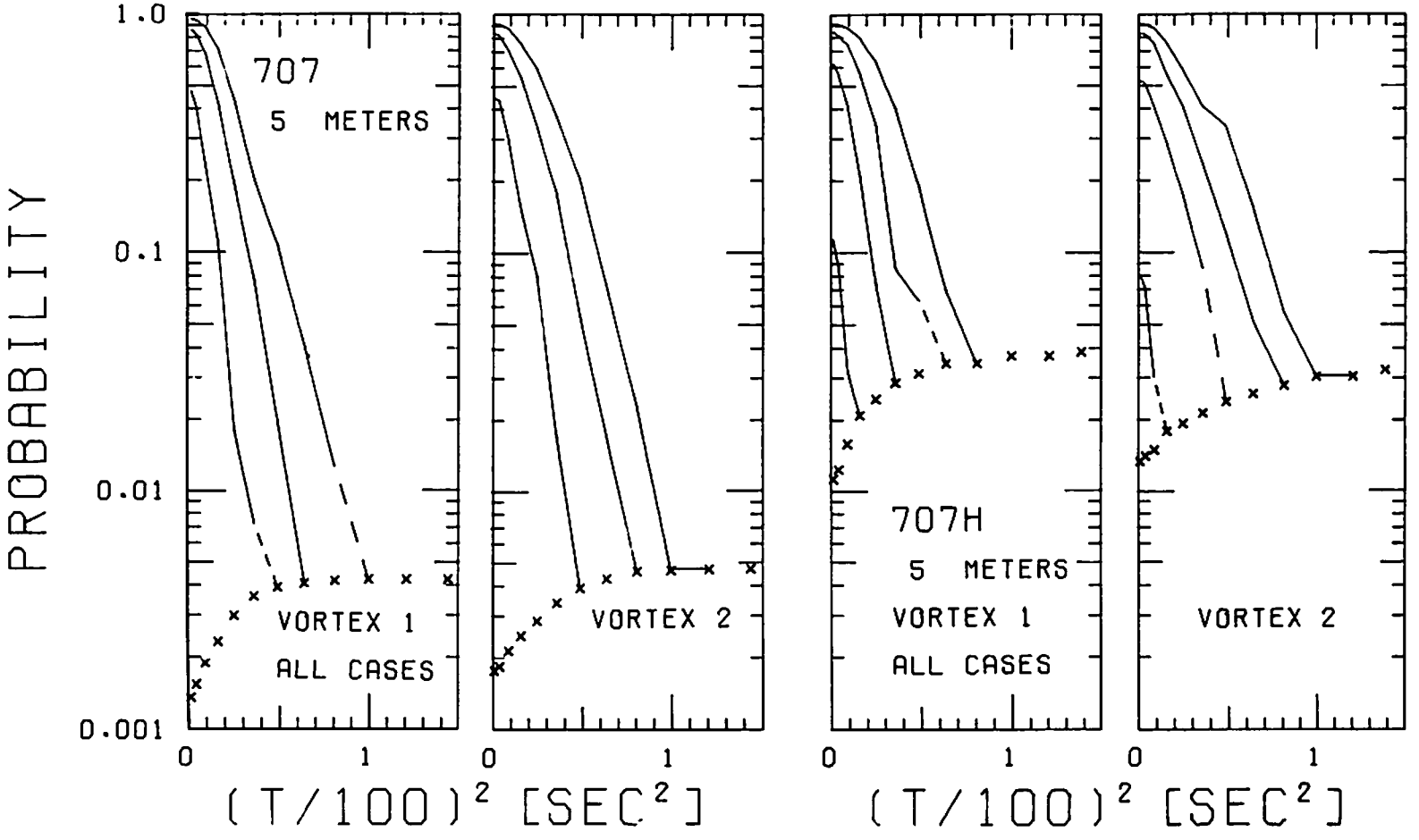

FIGURE 44. PROBABILITY OF DECAY, B-707 AND B-707H, VORTEX 1 AND 2, 5-m AVERAGING RADIUS

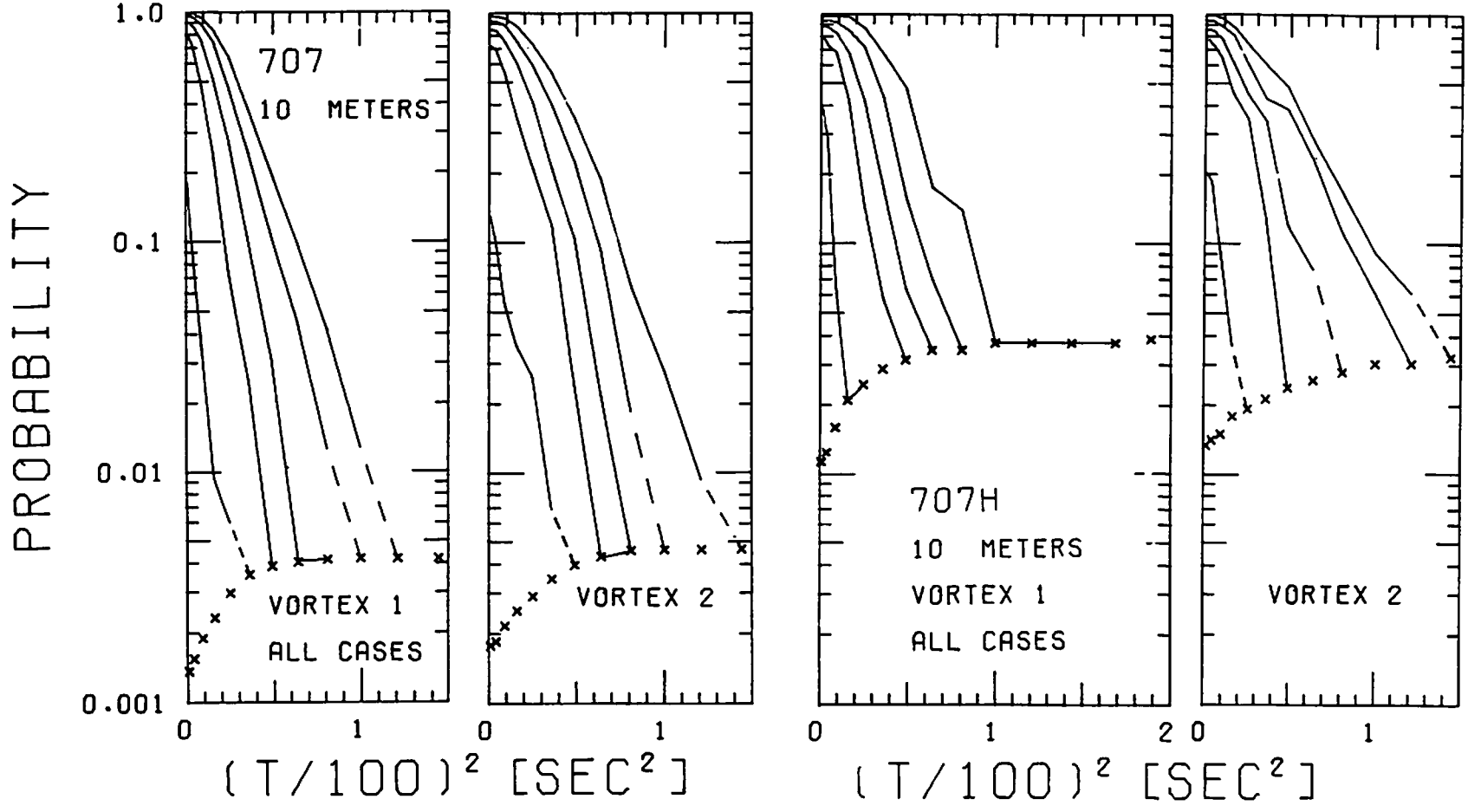

FIGURE 45. PROBABILITY OF DECAY, B-707 AND B-707H, VORTEX 1 AND 2, 10-m AVERAGING RADIUS

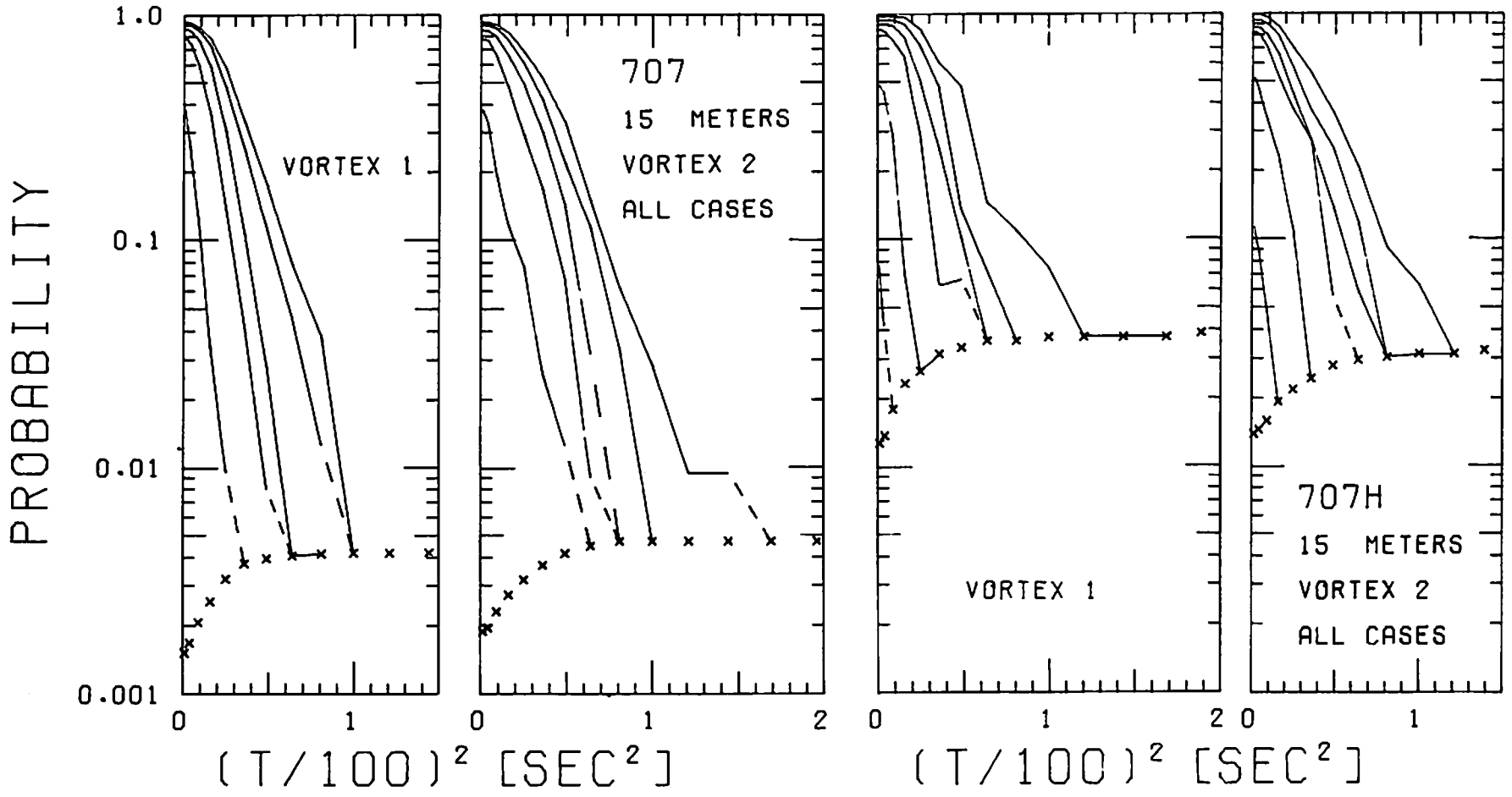

FIGURE 46. PROBABILITY OF DECAY, B-707 AND B-707H, VORTEX 1 AND 2, 15-m AVERAGING RADIUS

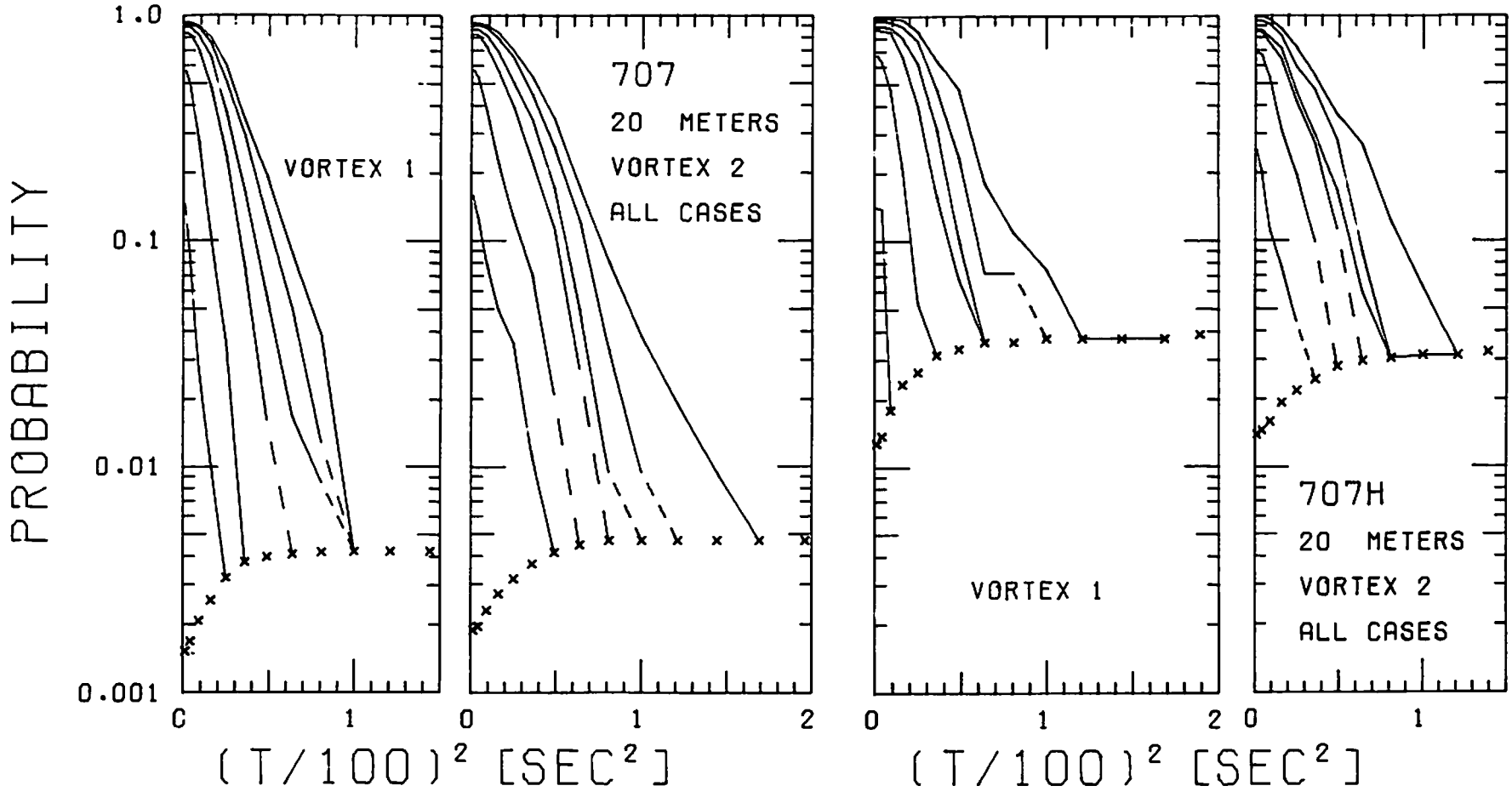

FIGURE 47. PROBABILITY OF DECAY, B-707 AND B-707H, VORTEX 1 AND 2, 20-m AVERAGING RADIUS

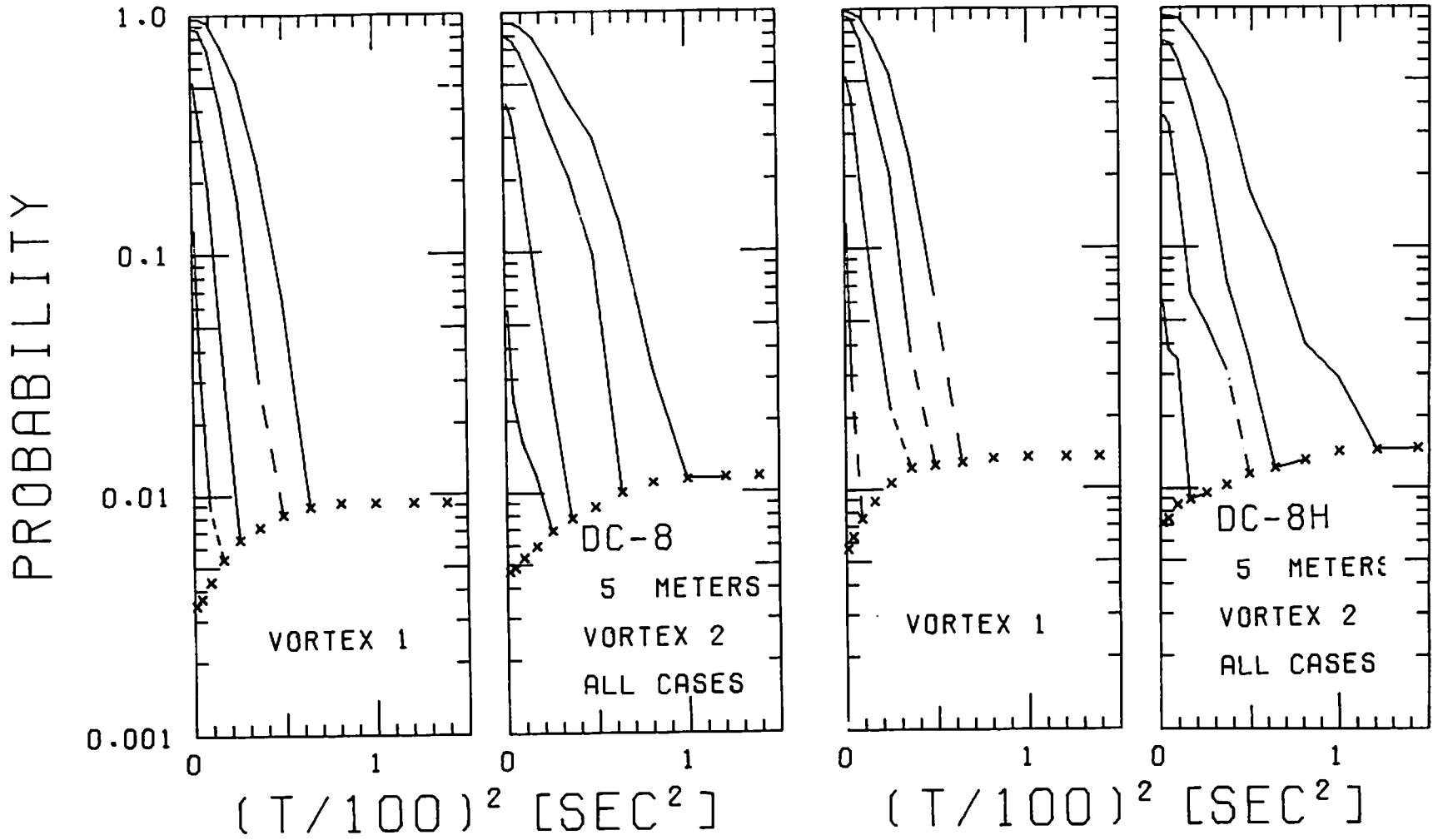

FIGURE 48. PROBABILITY OF DECAY, DC-8 AND DC-8H, VORTEX 1 AND 2, 5-m AVERAGING RADIUS

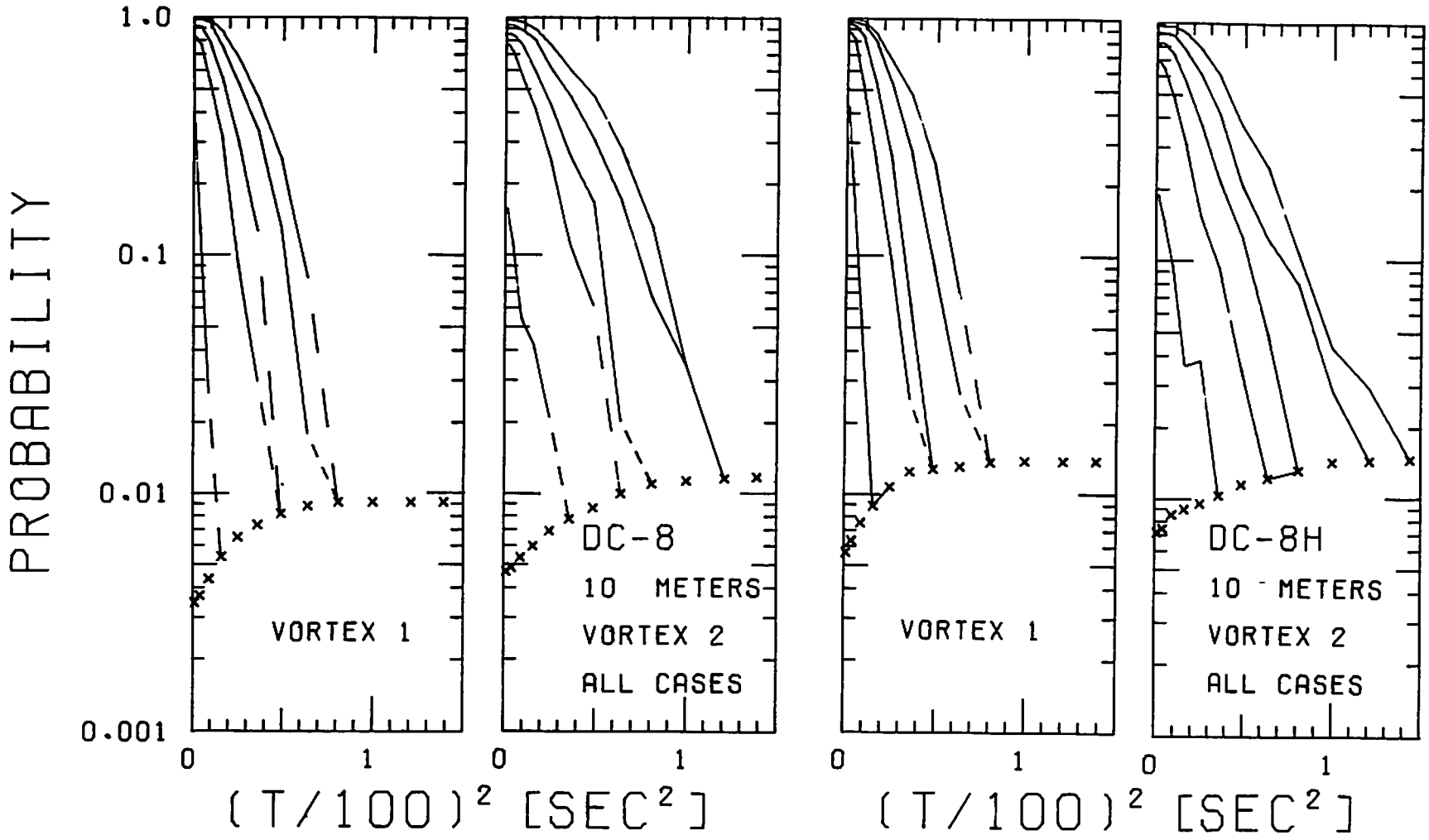

FIGURE 49. PROBABILITY OF DECAY, DC-8 AND DC-8H, VORTEX 1 AND 2, 10-m AVERAGING RADIUS

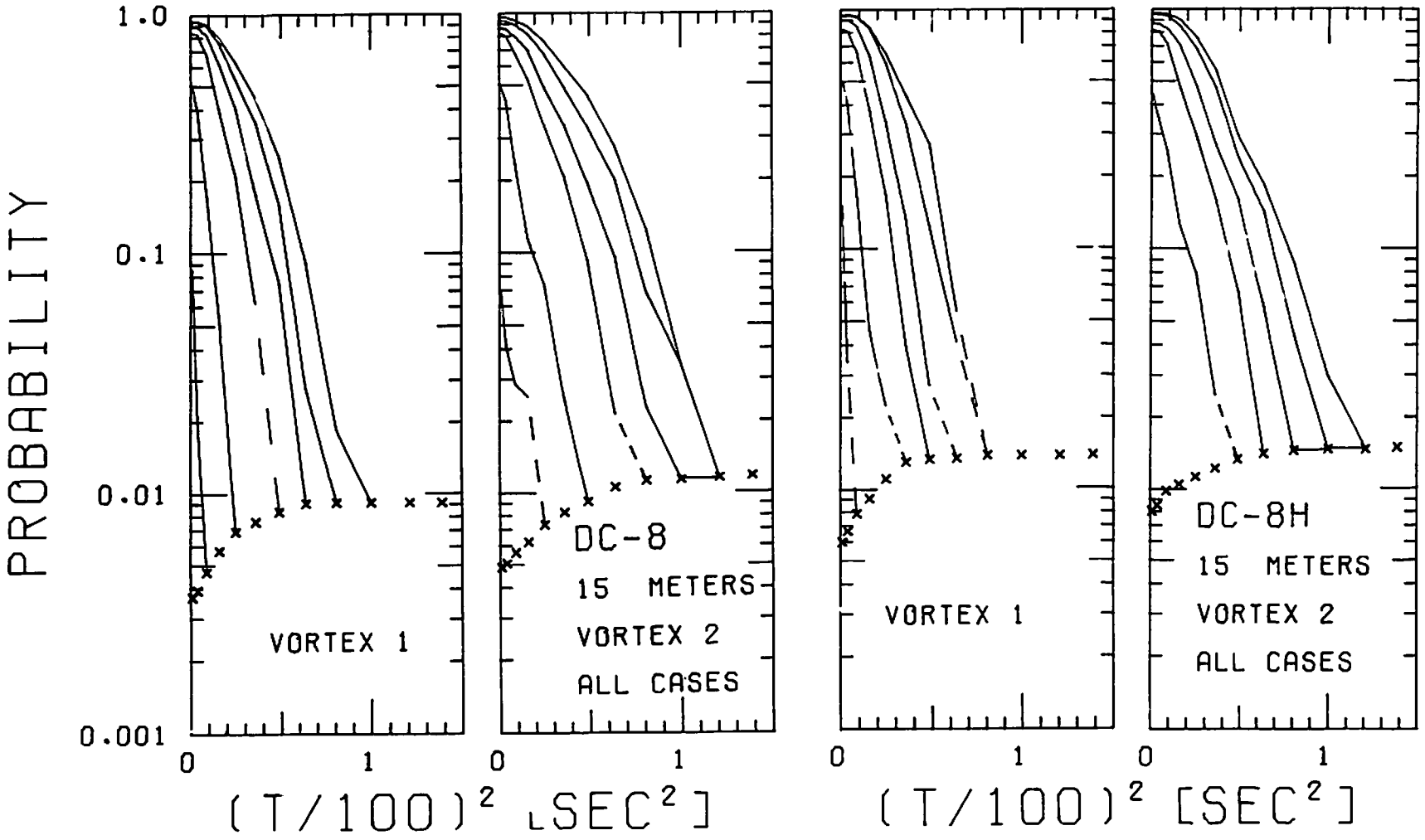

FIGURE 50. PROBABILITY OF DECAY, DC-8 AND DC-8H, VORTEX 1 AND 2, 15-m AVERAGING RADIUS

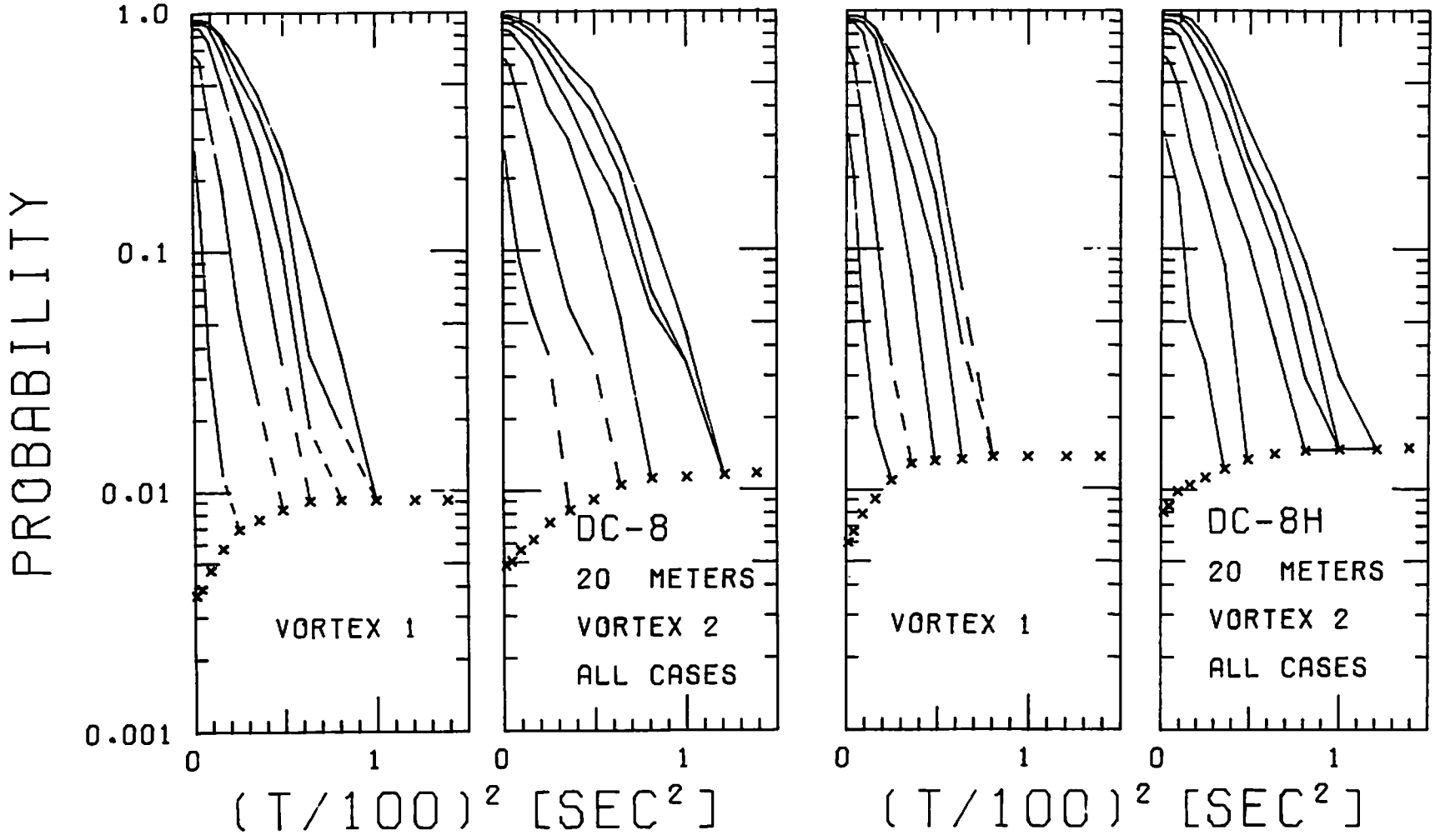

FIGURE 51. PROBABILITY OF DECAY, DC-8 AND DC-8H, VORTEX 1 AND 2, 20-m AVERAGING RADIUS

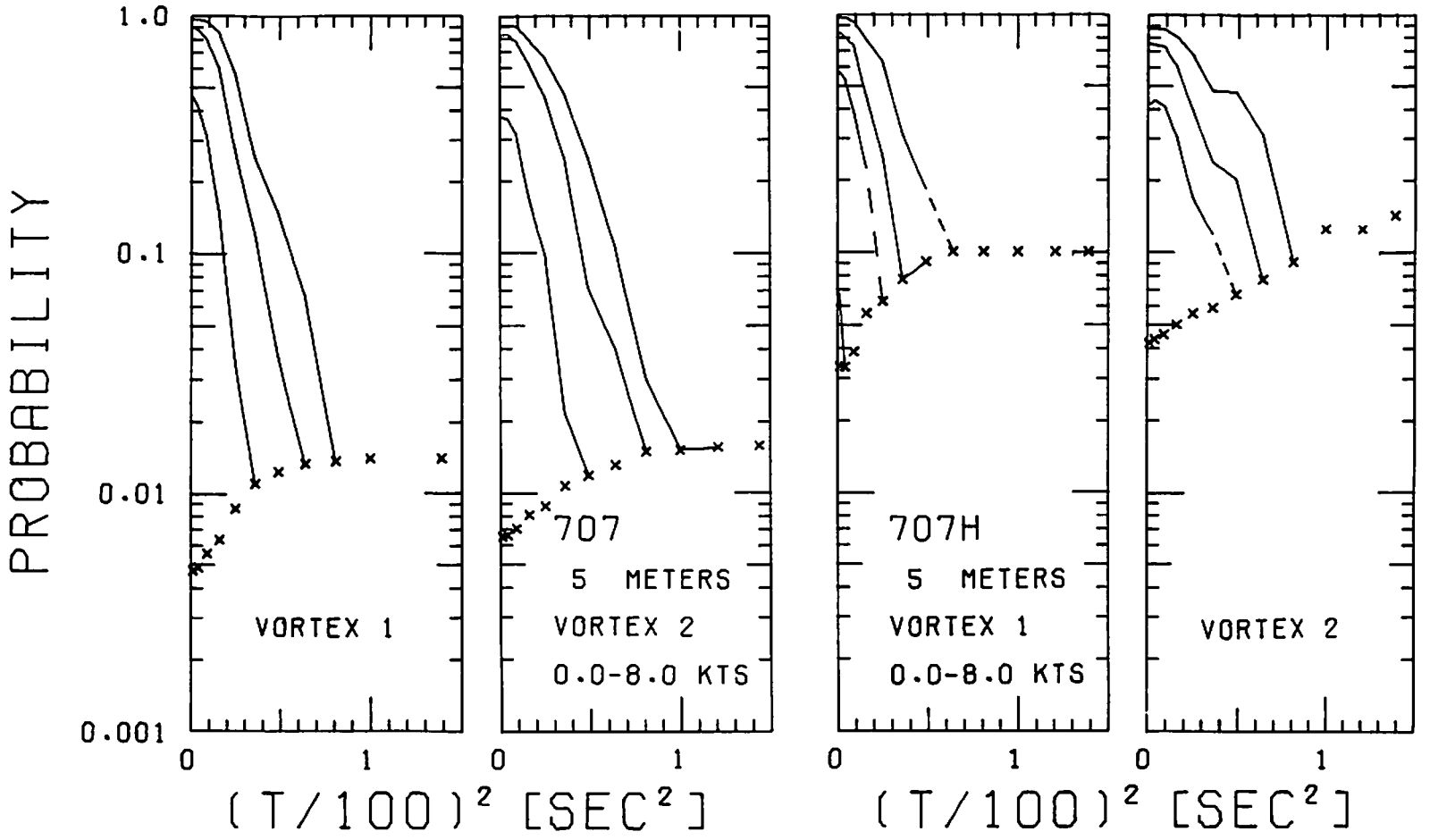

FIGURE 52. PROBABILITY OF DECAY, B-707 AND B-707H, WINDS LESS THAN 8 KNOTS, 5-m AVERAGING RADIUS

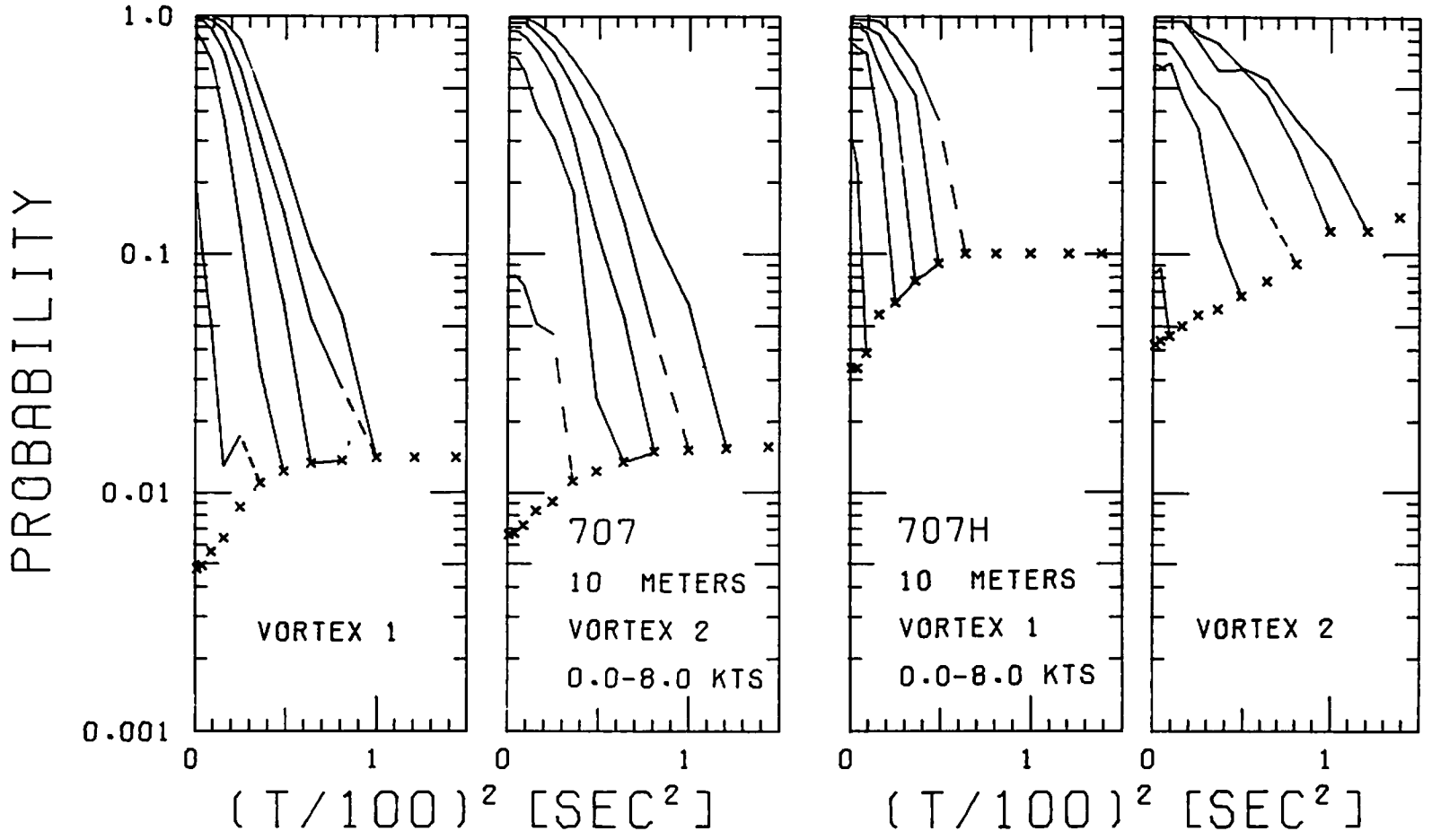

FIGURE 53. PROBABILITY OF DECAY, B-707 AND B-707H, WINDS LESS THAN 8 KNOTS, 10-m AVERAGING RADIUS

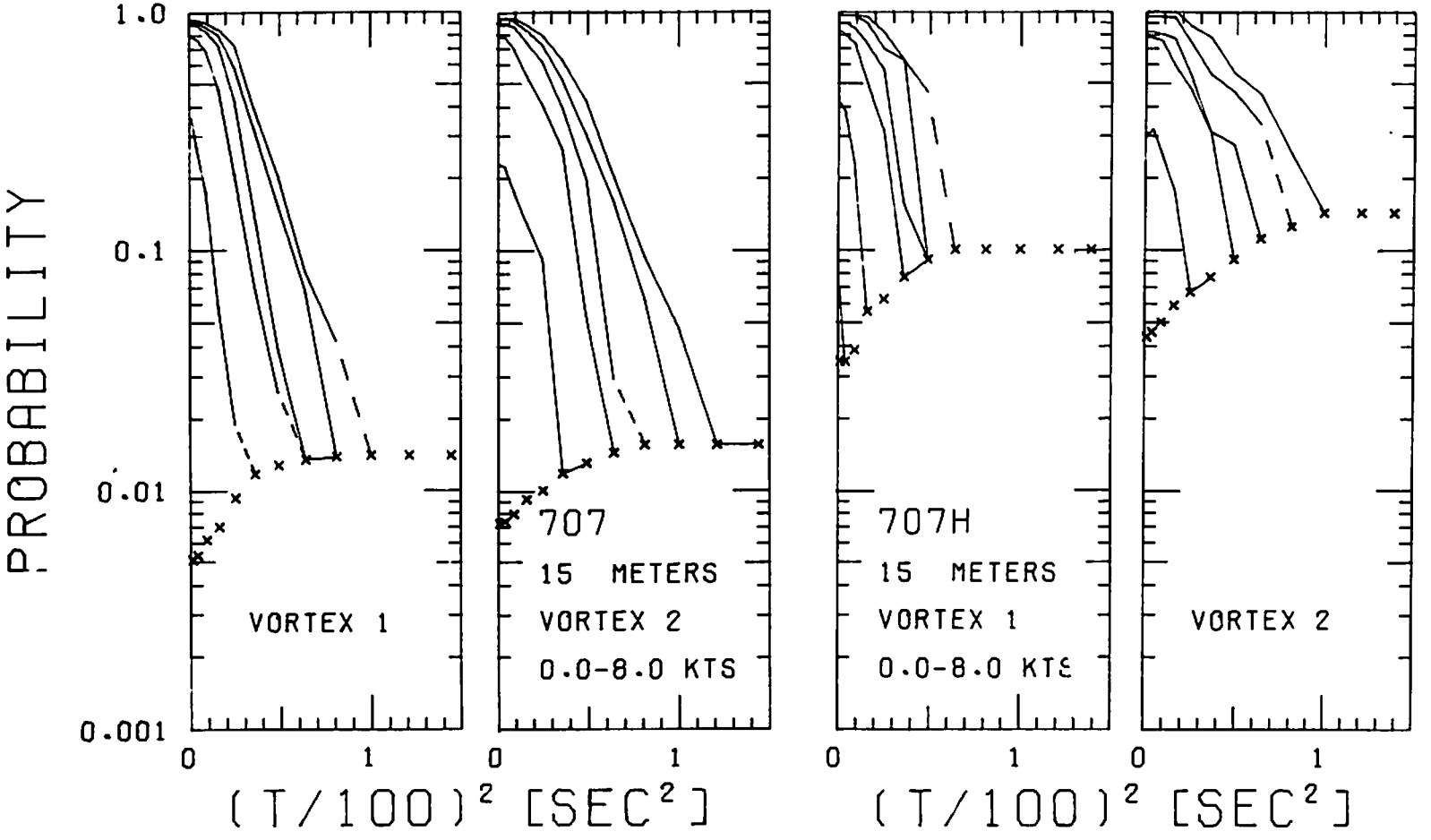

FIGURE 54. PROBABILITY OF DECAY, B-707 AND B-707H, WINDS LESS THAN 8 KNOTS, 15-m AVERAGING RADIUS

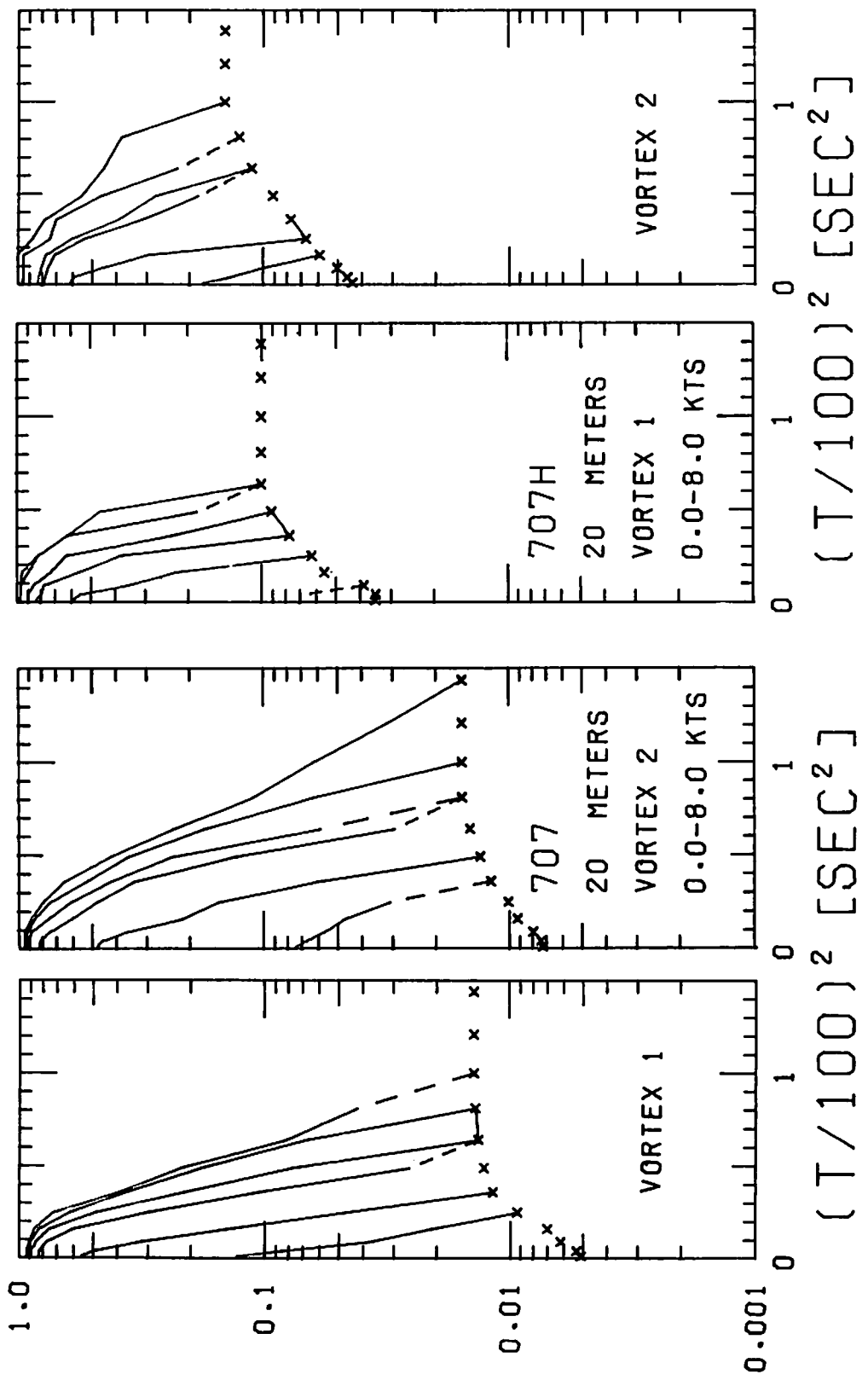

FIGURE 55. PROBABILITY OF DECAY, B-707 AND B-707H, WINDS LESS THAN 8 KNOTS, 20-m AVERAGING RADIUS

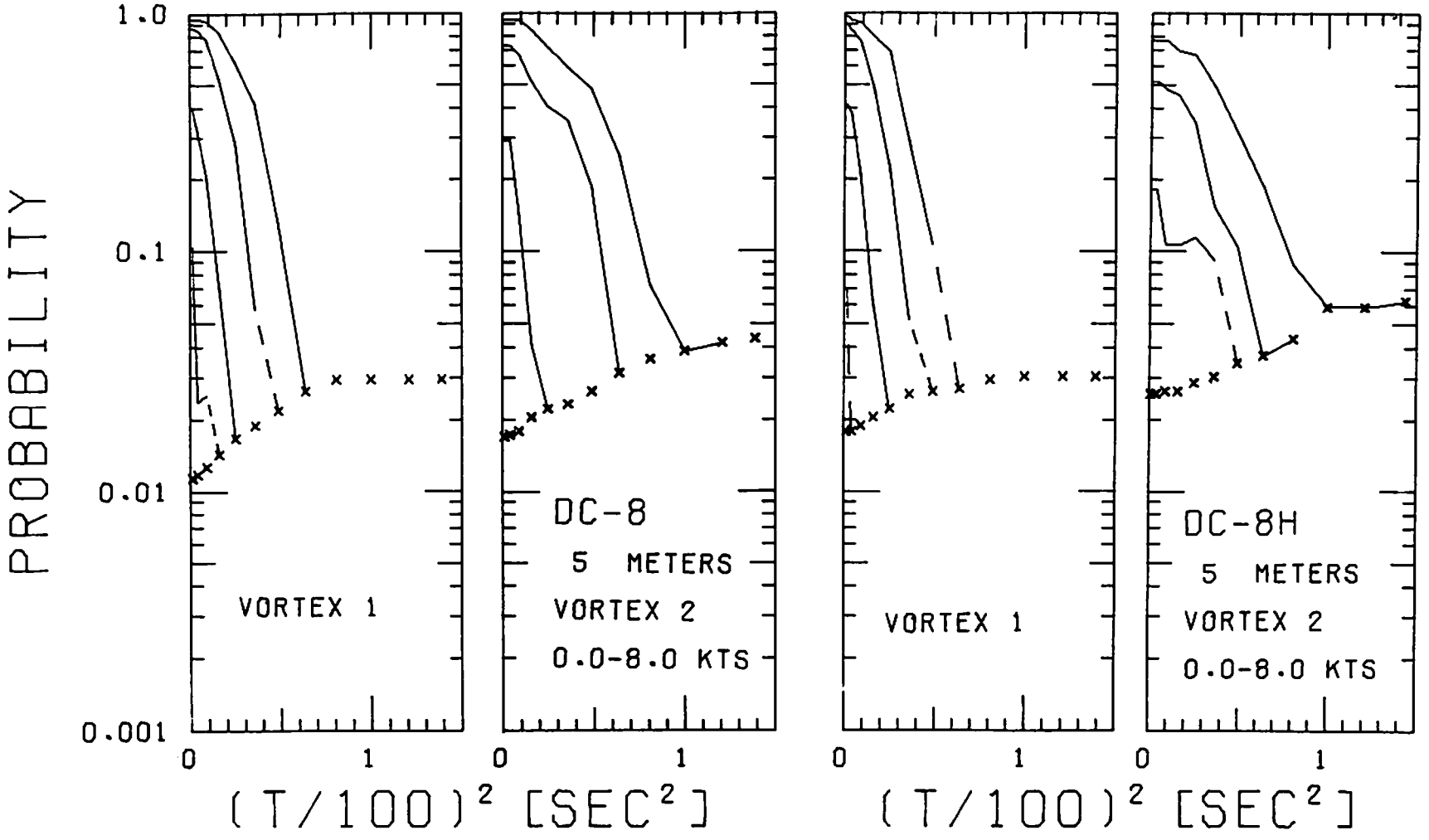

FIGURE 56. PROBABILITY OF DECAY, DC-8 AND DC-8H, WINDS LESS THAN 8 KNOTS, 5-m AVERAGING RADIUS

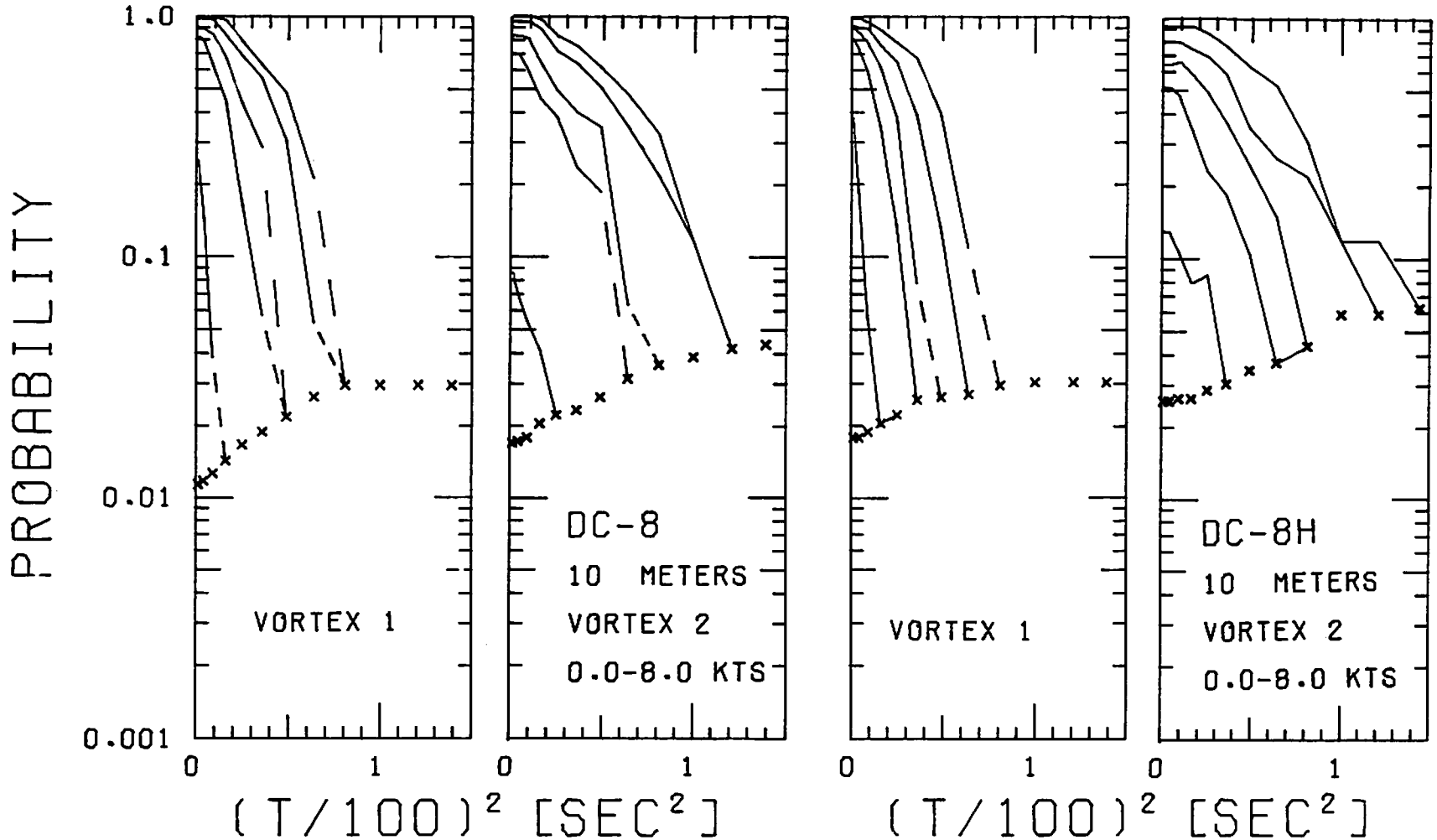

FIGURE 57. PROBABILITY OF DECAY, DC-8 AND DC-8H, WINDS LESS THAN 8 KNOTS, 10-m AVERAGING RADIUS

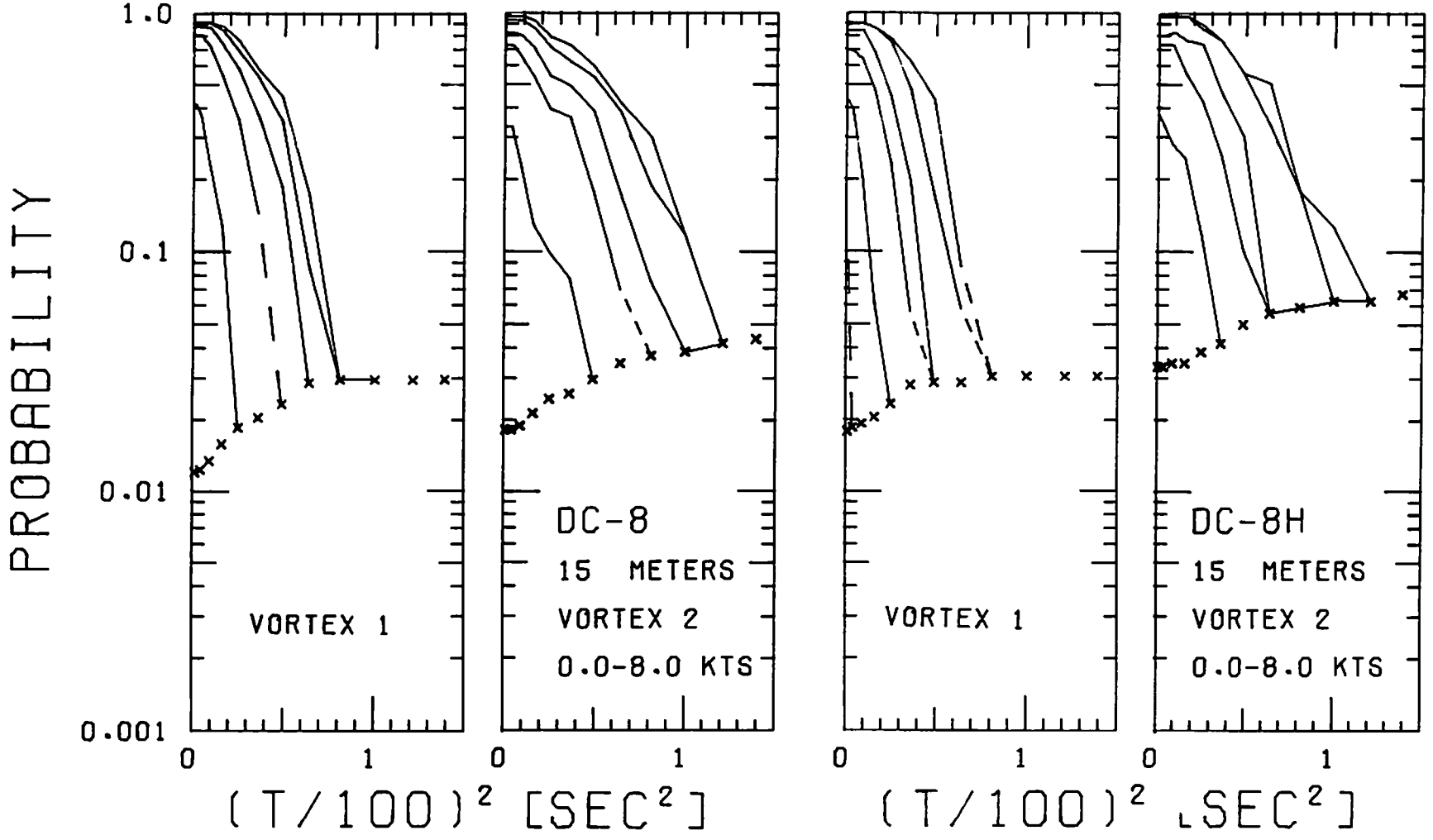

FIGURE 58. PROBABILITY OF DECAY, DC-8 AND DC-8H, WINDS LESS THAN 8 KNOTS, 15-m AVERAGING RADIUS

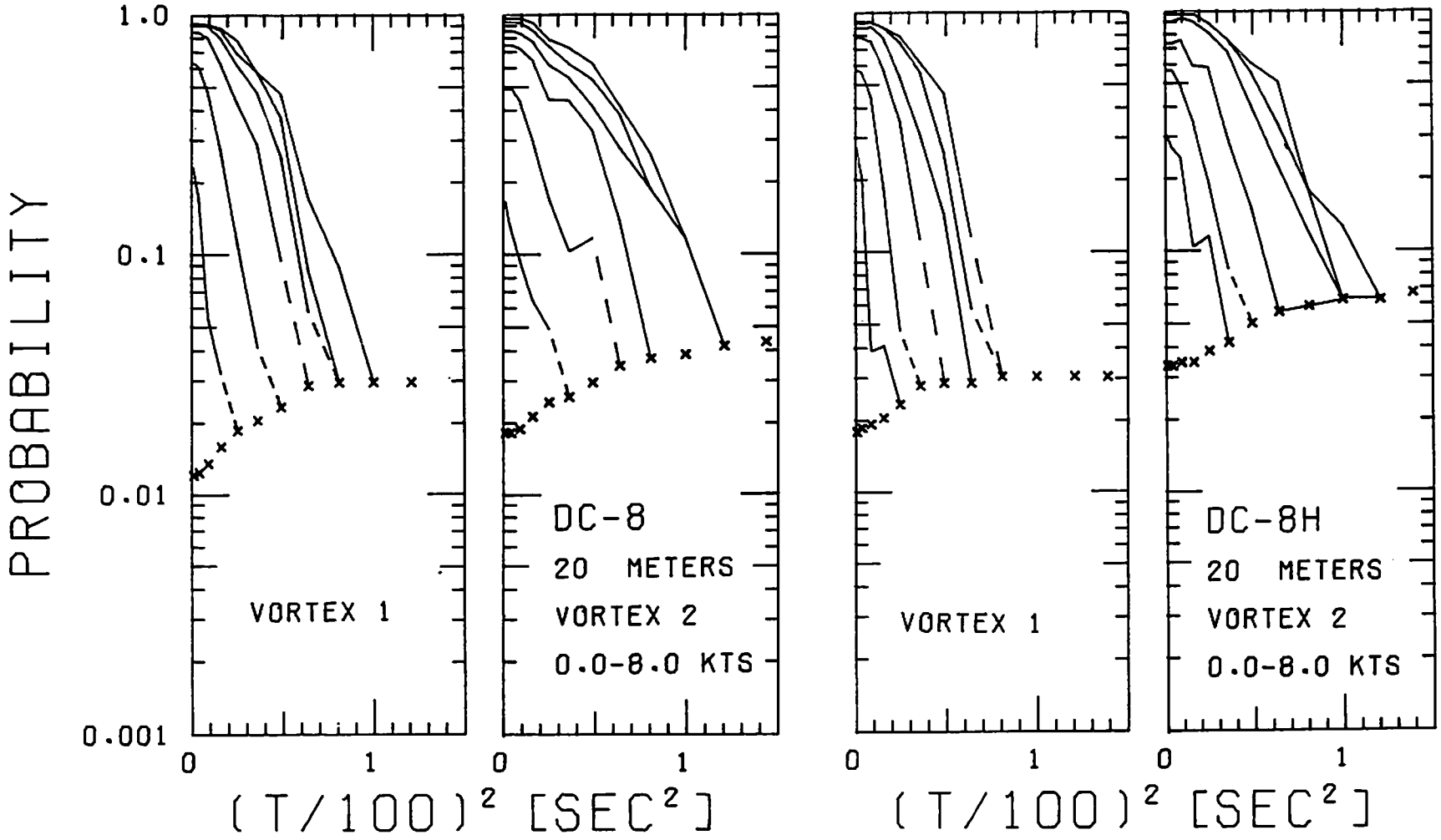

FIGURE 59. PROBABILITY OF DECAY, DC-8 AND DC-8H, WINDS LESS THAN 8 KNOTS, 20-m AVERAGING RADIUS

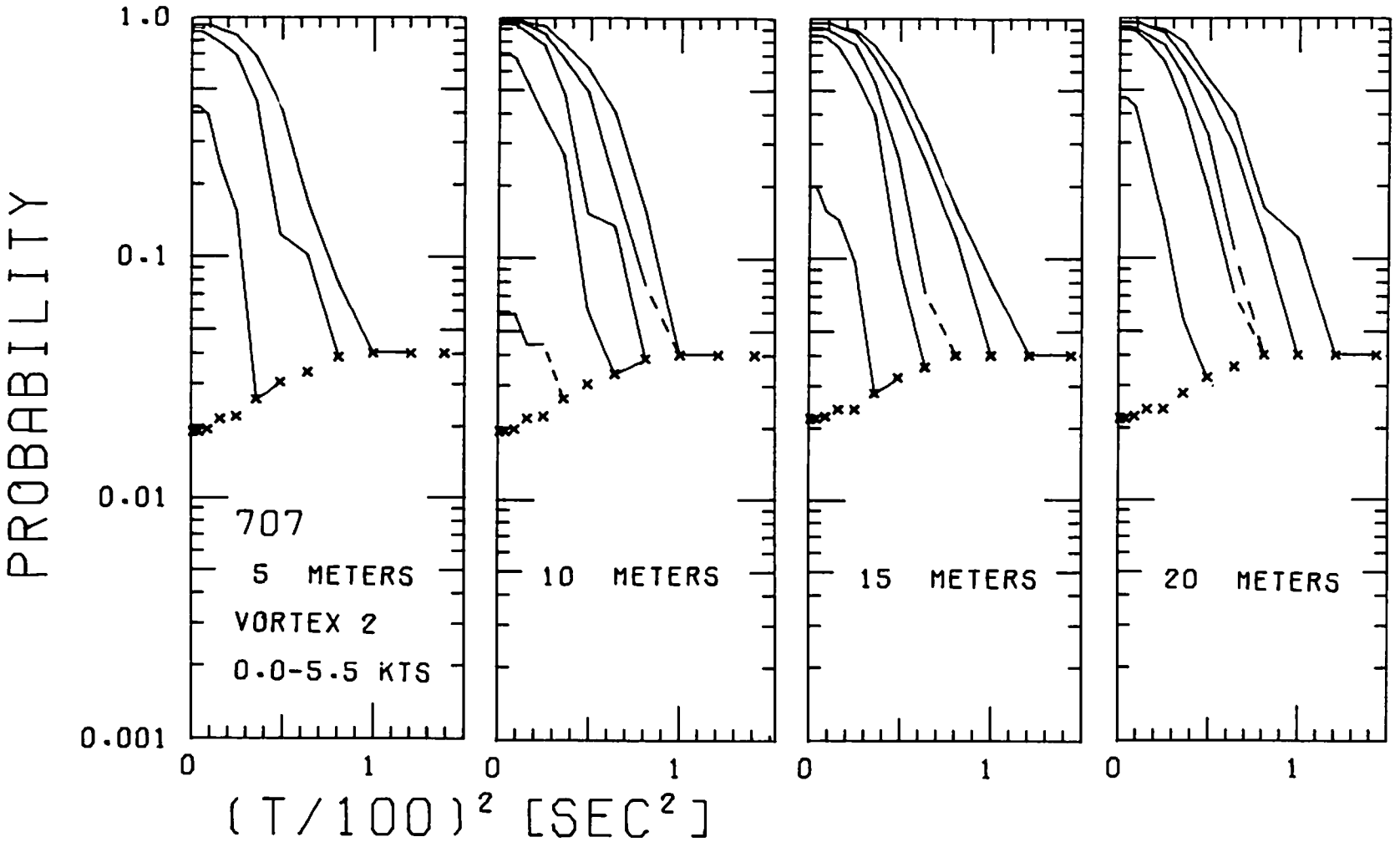

FIGURE 60. PROBABILITY OF DECAY, B-707, VORTEX 2, WINDS LESS THAN 5.5 KNOTS

APPENDIX D

STATISTICAL ERRORS IN VORTEX HAZARD PROBABILITY

This appendix estimates the statistical errors in the vortex hazard probability $F(\Gamma_T', t)$, which is the fraction of vortices whose strength is above the hazard threshold Γ_T' at time t. One can obtain the probability P(t) of a vortex falling below the threshold at time t as:

$$P(t) = - \frac{dF(t)}{dt} , \tag{D1}$$

where the explicit strength dependence of F has been dropped. The normalization of P(t) is

$$\int_0^\infty P(t)\, dt = F(0) - F(\infty) = 1. \tag{D2}$$

For the purposes of error analysis, take the functional form for F(t) as

$$F(t) = e^{-\alpha t^2} \tag{D3}$$

which gives a straight line on a plot of log F versus t^2. This expression can be rearranged to the form

$$\ell n\ F(t)/\ell n\ F(100) = (t/100)^2 \tag{D4}$$

where the coefficient α is replaced by the value of F at 100 seconds.

With this definition of the problem, one can generate ensembles of N vortex cases using a random number function to generate random times for the disappearance of the vortex hazard. A random number function RAN generates numbers between 0.0 and 1.0 with a uniform probability distribution. The probability of RAN falling between x and x+dx is dx.

Let

$$F(t) = x \tag{D5}$$

and one obtains the probability of disappearance times between t and dt of

$$dx = \frac{dF(t)}{dt}\ dt = P(t)dt. \qquad \text{(D6)}$$

Thus, equation (D6) leads to the desired probability P(t). Invert equation (D4) to get the time corresponding to a value of x = RAN:

$$t = 100\ (\ell n\ x/\ell n\ F(100))^{1/2}. \qquad \text{(D7)}$$

An ensemble of N cases will have N disappearance times t_i. The resulting value of $F_j(t)$ (for the j-th ensemble) is simply the ratio of the number of cases with $t_j > t$ to the total number of cases N. Now compute the mean value

$$\overline{F}\ (t) = \frac{1}{M} \sum_{j=i}^{M} F_j(t) \qquad \text{(D8)}$$

and the standard deviation σ

$$\sigma^2(t) = \frac{1}{M-1} \sum_{j=1}^{M} (F_j(t) - \overline{F}(t))^2 \qquad \text{(D9)}$$

by evaluating M ensembles.

Numerical evaluation shows that $\overline{F}(t) = F(t)$, the original function as long as many samples are included with $t_j > t$. The quantity $N\sigma^2(t)$ is found to be independent of N under the same conditions. In addition, the value of $\sigma(t)$ shows no dependance upon F(100). Figure 61 plots the $\sigma(t)$ results. It can be seen that for $F<0.1$, the calculated values are consistent with the solid line which corresponds to the equation

$$\sigma = (F/N)^{1/2}. \qquad \text{(D10)}$$

The simple form of this equation suggests that an analytical derivation should be possible. Equation (D10) can be rewritten in the form:

$$\sigma = (FF_N)^{1/2}$$
$$\sigma/F = (F_N/F)^{1/2} \qquad \text{(D11)}$$

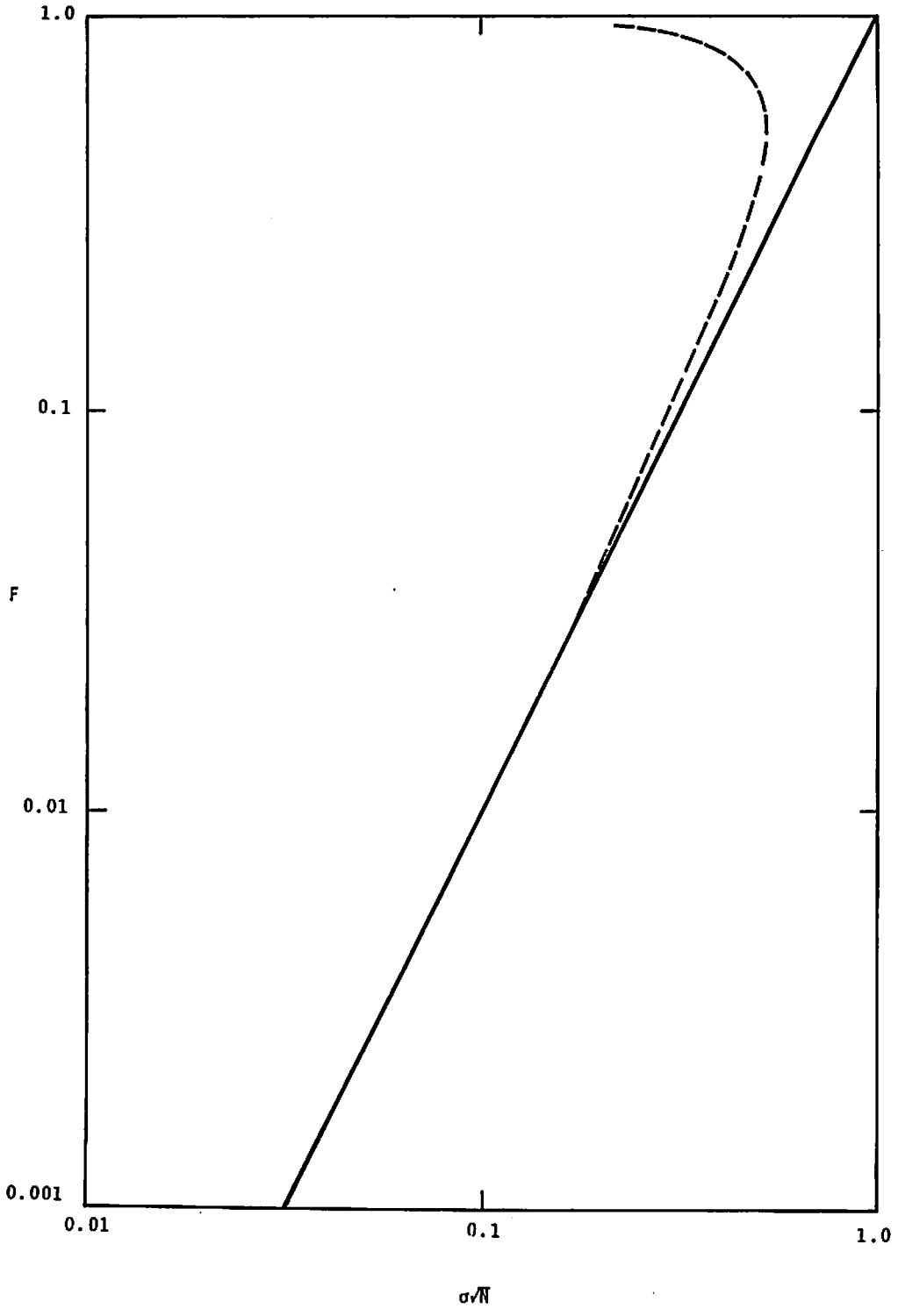

FIGURE 61. PLOT OF F VERSUS $\sigma N^{1/2}$

where $F_N = 1/N$ is the lowest probability which can be plotted on a log F versus t^2 plot for N cases. Thus, the error bars (σ/F) on an log F versus t^2 plot (see Fig. 62) depend only upon the ratio of F to F_N, the last point plotted (assuming N roughly constant). At the last point the standard deviation equals the probability. Figure 62 shows what the standard error bars look like for N = 10, 100, and 1000. One should note that the probability distribution for F cannot be Gaussian when σ is near in value to F since F cannot be negative.

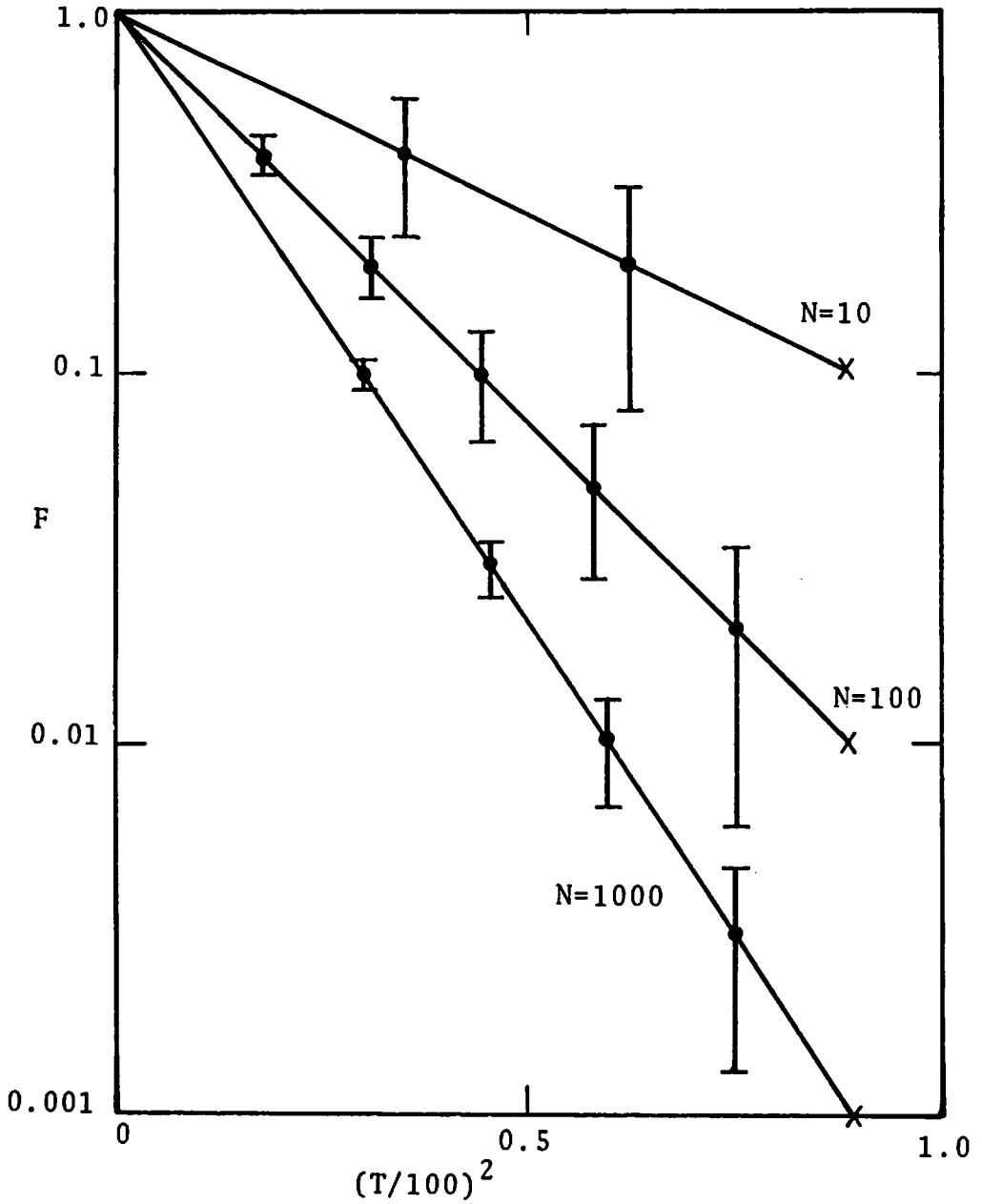

FIGURE 62. PLOT OF F VERSUS $(T/100)^2$ WITH ERROR BARS

APPENDIX E

FOUR LONG-LIVED B-707H VORTICES

This appendix contains the MAVSS processing displays for the four long-lived vortices from Heavy B-707 aircraft (Figures 63 to 70). Table 9 shows the parameters for these cases. In addition to showing cases which are important to the analysis of this report, they also serve to illustrate the type of data collected.

The display figures are described in detail in Volume I of this report. The first figure of each set shows the vortex detections (vertical lines) obtained by a correlator designed to match the vortex signature. The second figure of each set shows the velocity and spectral width profiles on the left hand side and the vortex trajectories (height and lateral position versus time) on the right hand side.

TABLE 9: LONG-LIVED B-707H CASES

TAPE	RUN	LONG-LIVED VORTEX	WEIGHT	TIME FOR $\Gamma'(5\ m) = 50\ m^2/s$
3153	123	#2	201,000 lb	98 sec
3156	151	#2	N.A.	85 sec
3142	51	#1	198,000 lb	78 sec
3158	67	#1	185,000 lb	71 sec

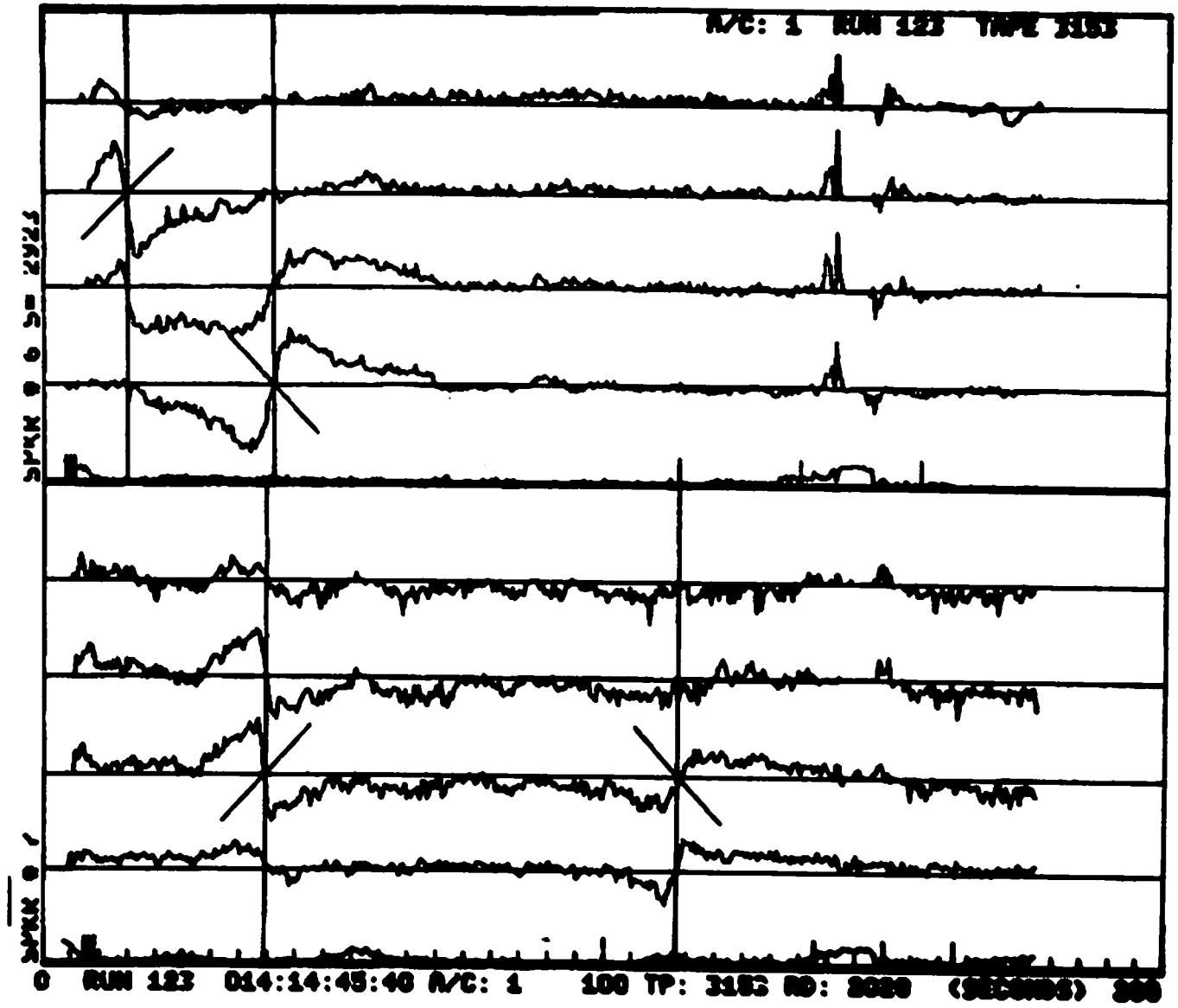

FIGURE 63. HARD COPY OUTPUT: TAPE 3153, RUN 123, VORTEX DETECTIONS

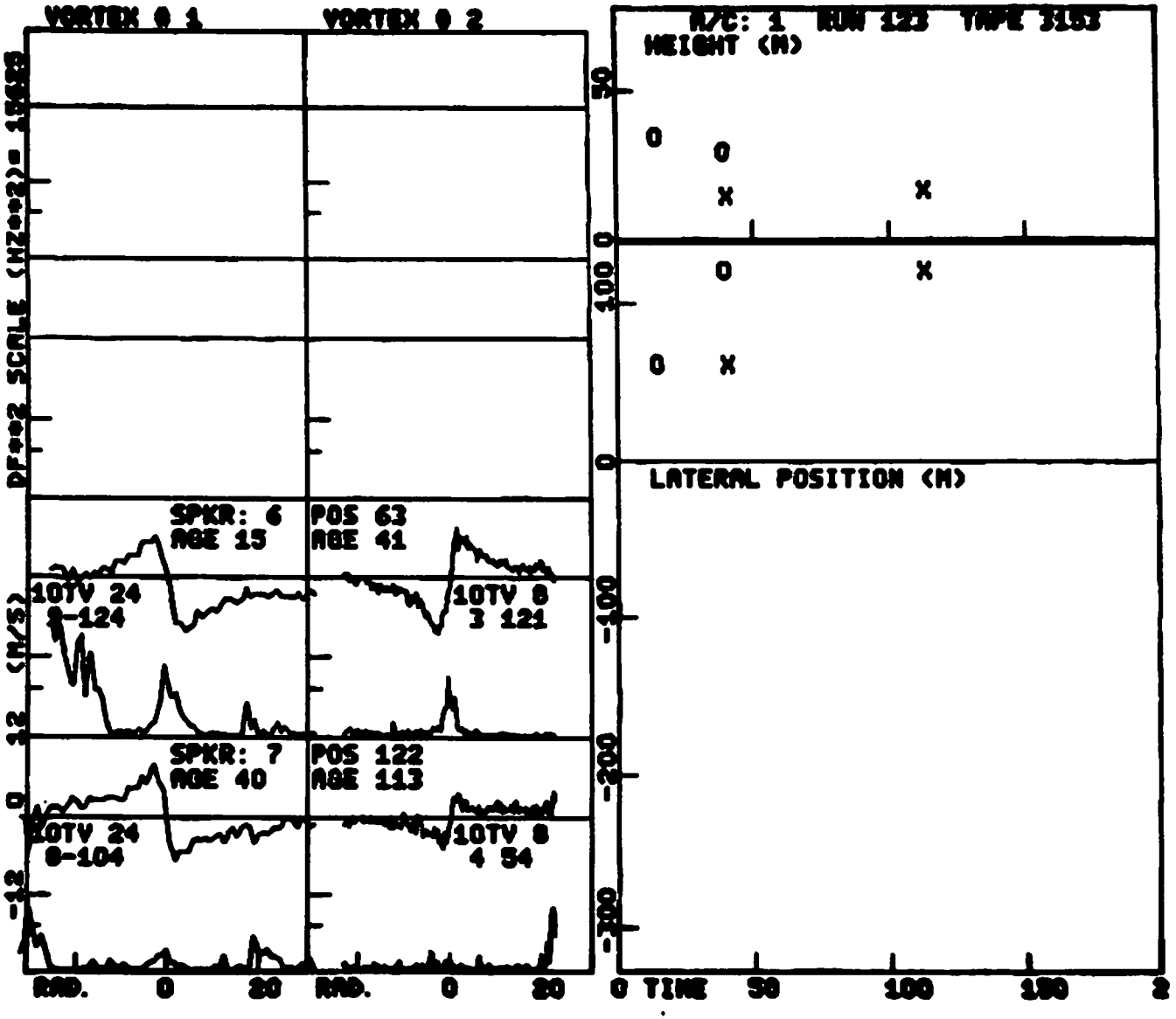

FIGURE 64. HARD COPY OUTPUT: TAPE 3153, RUN 123, VELOCITY SPECTRAL WIDTH PROFILES AND VORTEX TRAJECTORIES

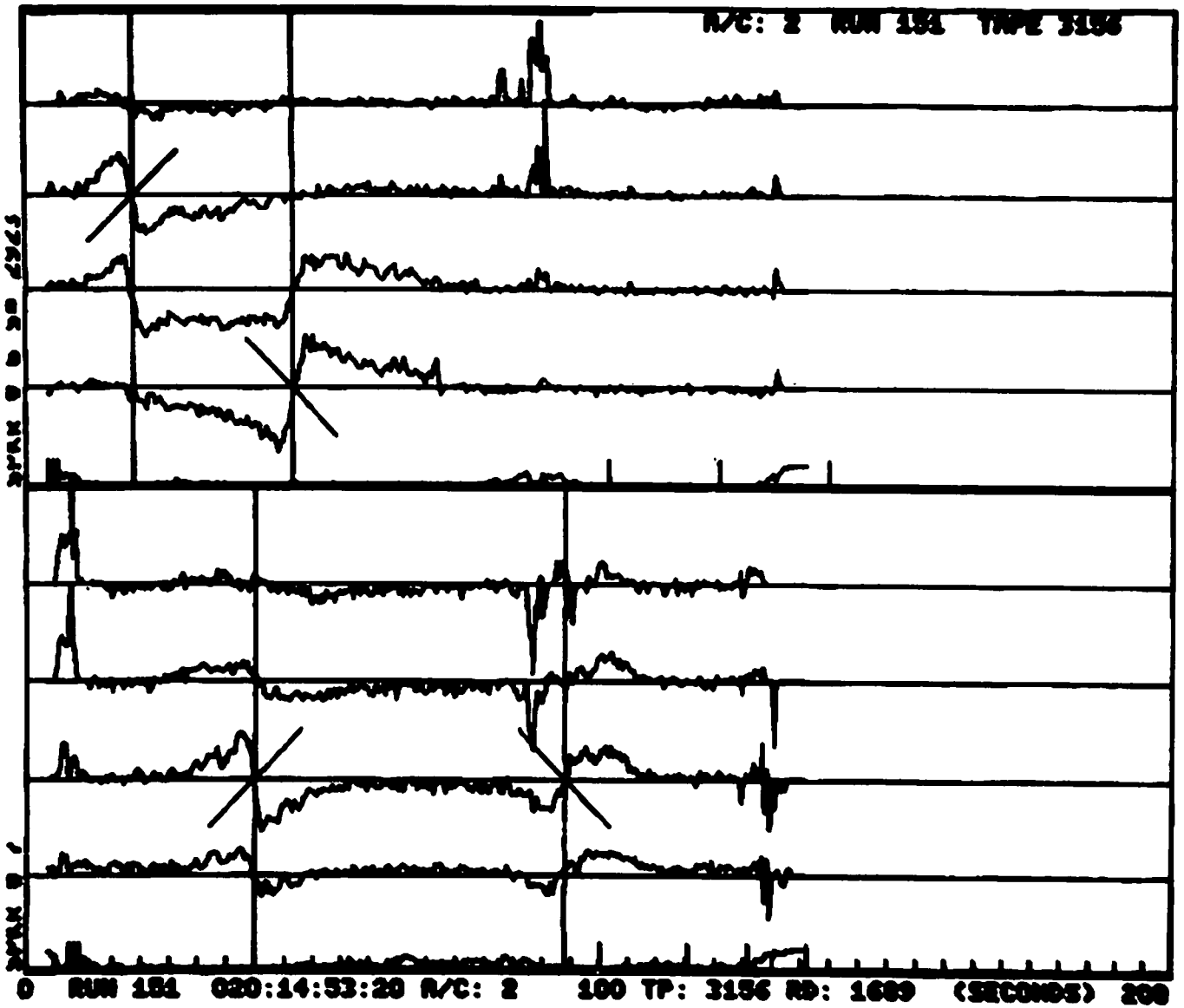

FIGURE 65. HARD COPY OUTPUT: TAPE 3156, RUN 151, VORTEX DETECTIONS

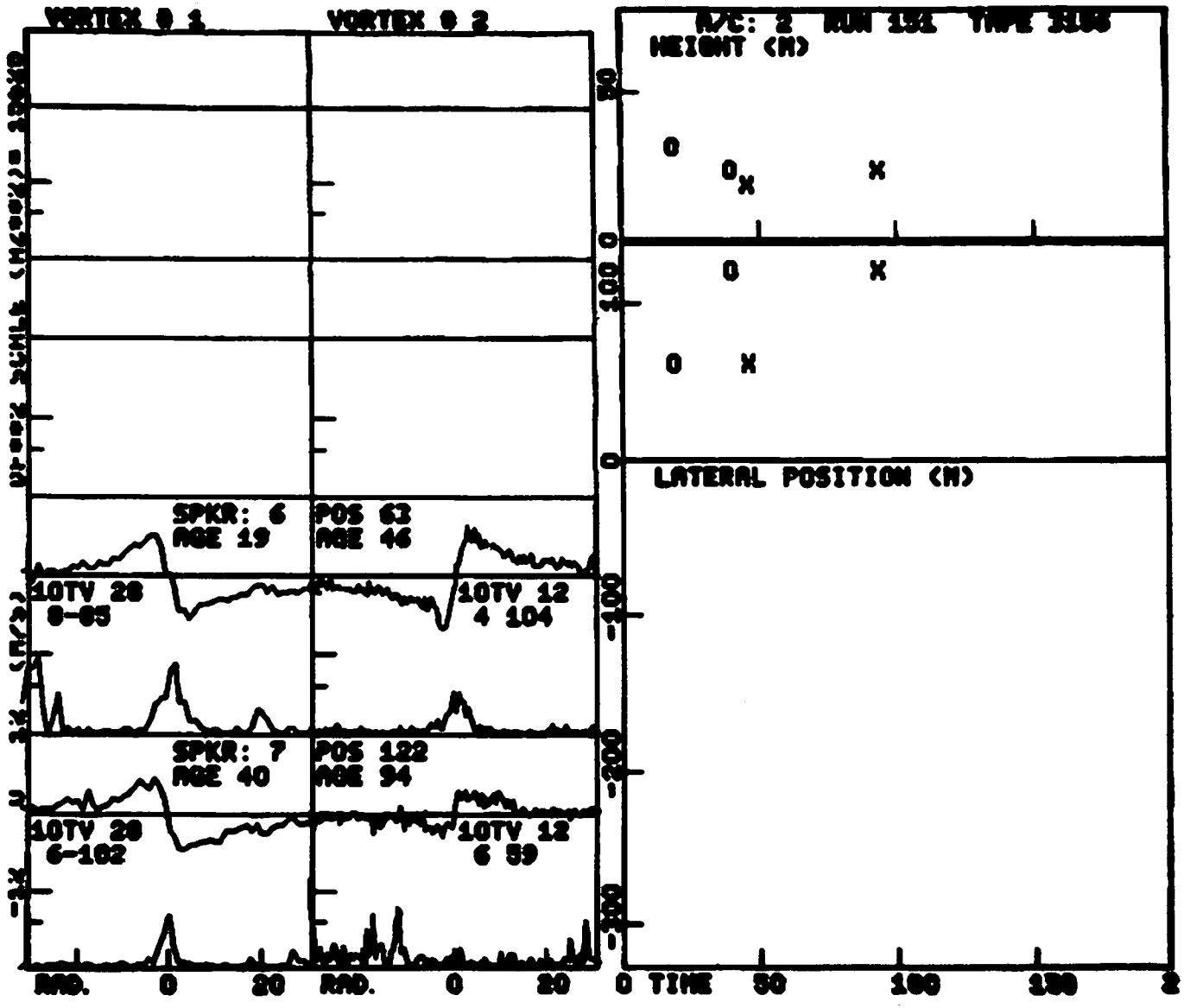

FIGURE 66. HARD COPY OUTPUT: TAPE 3156, RUN 151, VELOCITY SPECTRAL WIDTH PROFILES AND VORTEX TRAJECTORIES

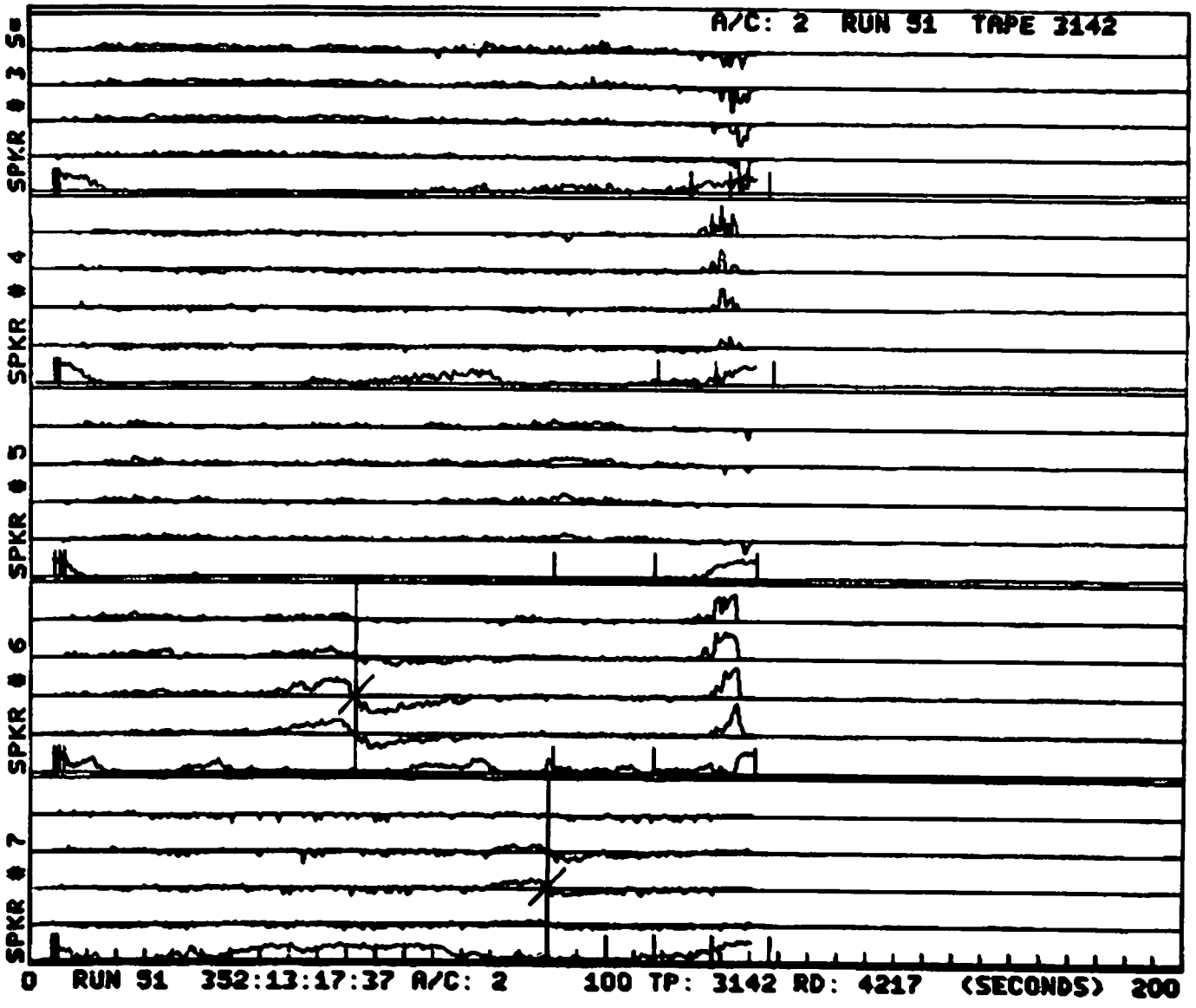

FIGURE 67. HARD COPY OUTPUT: TAPE 3142, RUN 51, VORTEX DETECTIONS

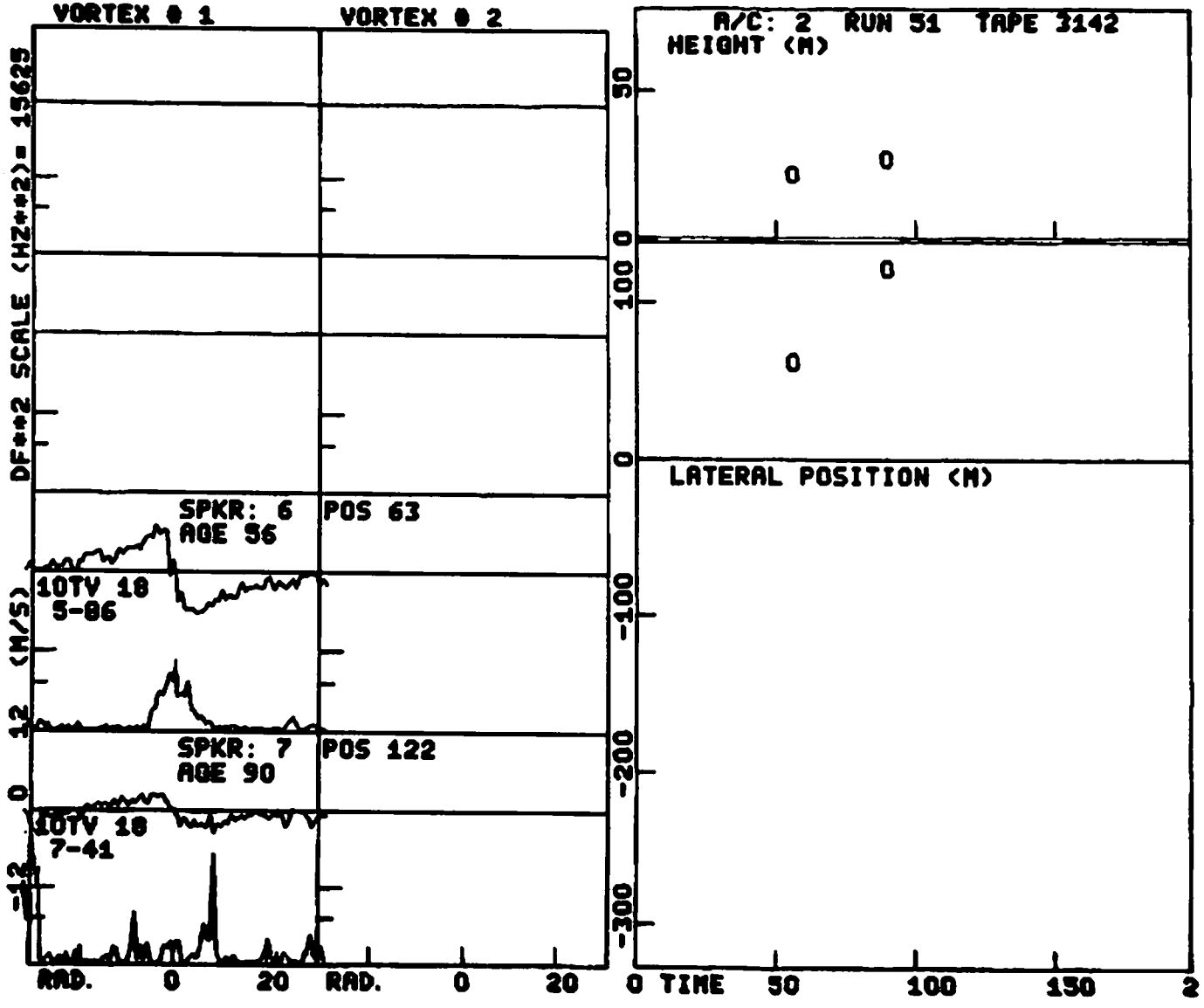

FIGURE 68. HARD COPY OUTPUT: TAPE 3142, RUN 51, VELOCITY SPECTRAL WIDTH PROFILES AND VORTEX TRAJECTORIES

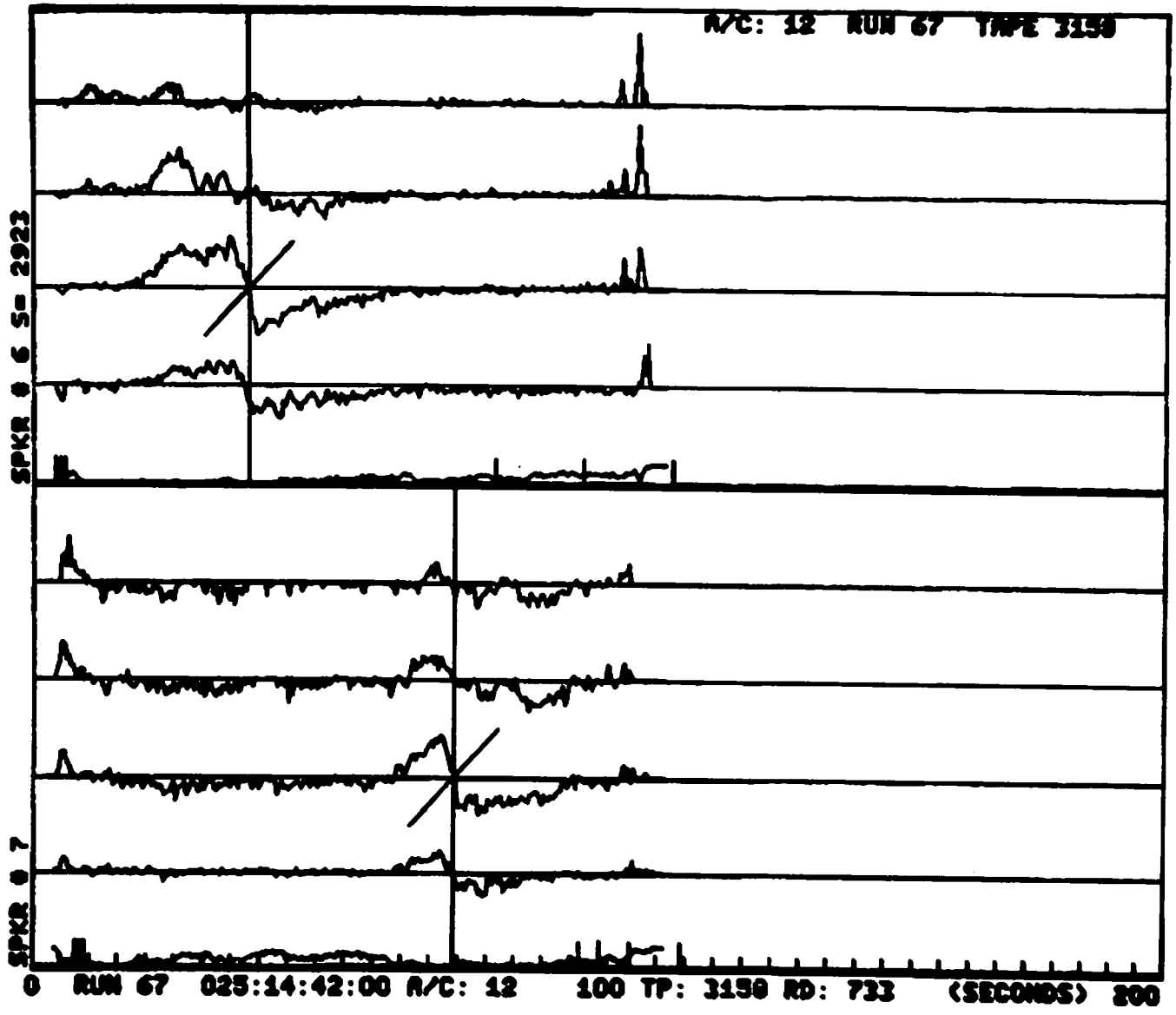

FIGURE 69. HARD COPY OUTPUT: TAPE 3158, RUN 67, VORTEX DETECTIONS

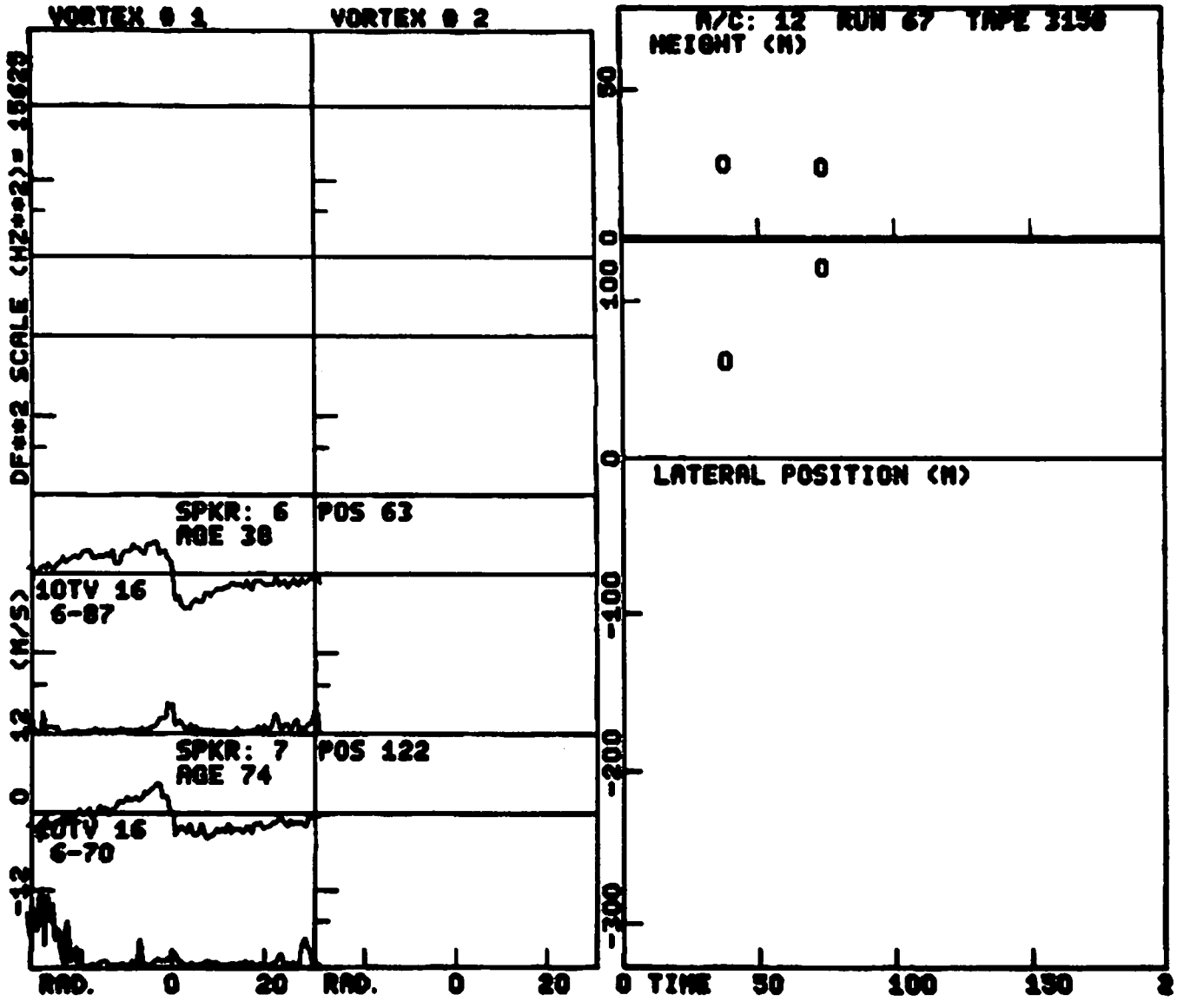

FIGURE 70. HARD COPY OUTPUT: TAPE 3158, RUN 67, VELOCITY SPECTRAL WIDTH PROFILES AND VORTEX TRAJECTORIES

APPENDIX F

WEIGHT DEPENDENCE OF VORTEX STRENGTH AT LONG TIMES

This appendix describes an attempt to use the time history data (Figure 3c) to analyze the weight dependence of vortex strength at long times. The analysis of Section 4.1.2 is of limited use beyond 40 or 50 seconds. Using the time histories produces a much larger number of valid cases at any given time and also deals consistently with the decay of vortex strength below the detection threshold. The cost of these advantages is the uncertainty introduced by the extrapolation of vortex strength to zero. The statistical analysis of Section 4.1.2 was applied to the ensemble of vortex time-history data at time increments of 10 seconds. The results are plotted in Figures 71 to 73.

Figure 71 shows the decay in mean vortex strength with age. The straight line in the plot corresponds to decay as the inverse square of the age (a functional dependence observed in analyses of Volume III of this report). The measured decay shows approximate agreement with this dependence after 40 seconds. At long times the decay rate increases.

The weight versus strength power law is shown in Figures 72 and 73. The open symbols show the basic data and the solid symbols show the results of reassigning the categories according to landing weight (Section 2.2). The most notable feature of these results is the rapid increase in the power n with vortex age. At first glance this effect would indicate that the vortex decay is slower for heavier aircraft. In fact, an analytical analysis (developed below) shows that this increase can be attributed to the assignment of zero strength to vortices below the detection threshold. Because of this problem, the time-history data were also processed with the exclusion of zero strength data. Points with more than 20 cases are plotted in Figures 72 and 73 with crossed symbols. Excluding $\Gamma' = 0$ data reduces the values of n and introduces more scatter because of the reduced number

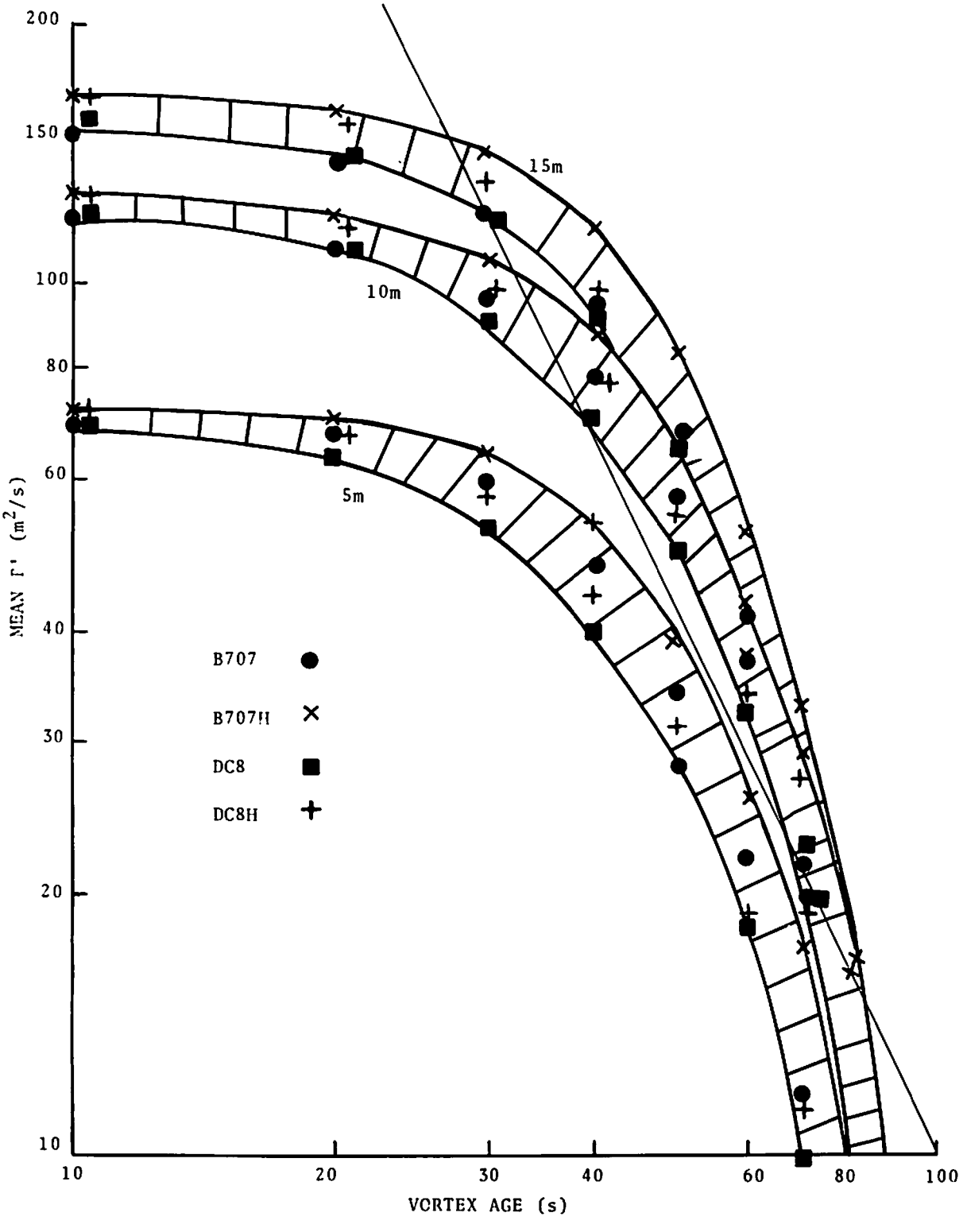

FIGURE 71. MEAN VORTEX STRENGTH VERSUS AGE

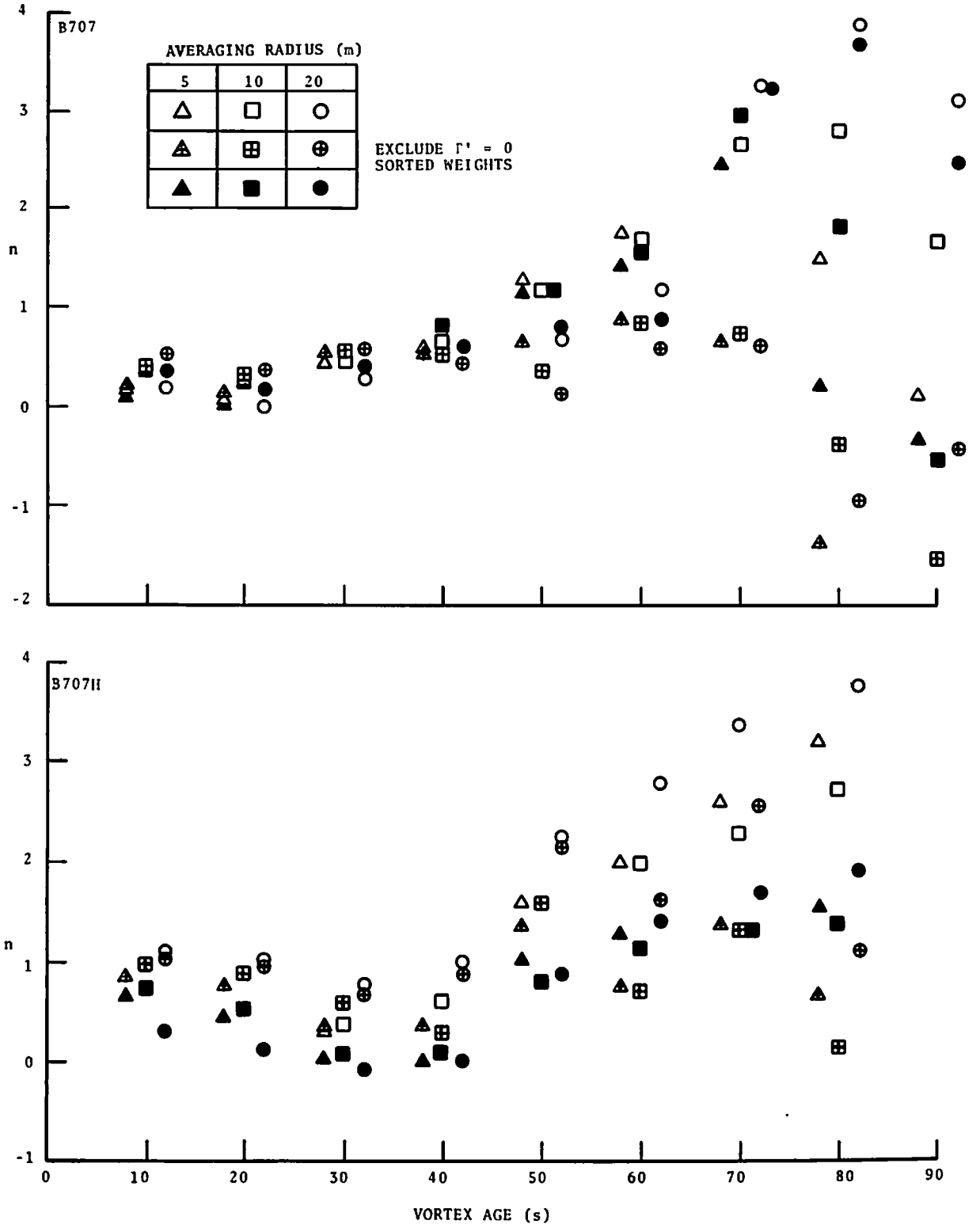

FIGURE 72. STRENGTH VERSUS WEIGHT POWER FOR THE B-707

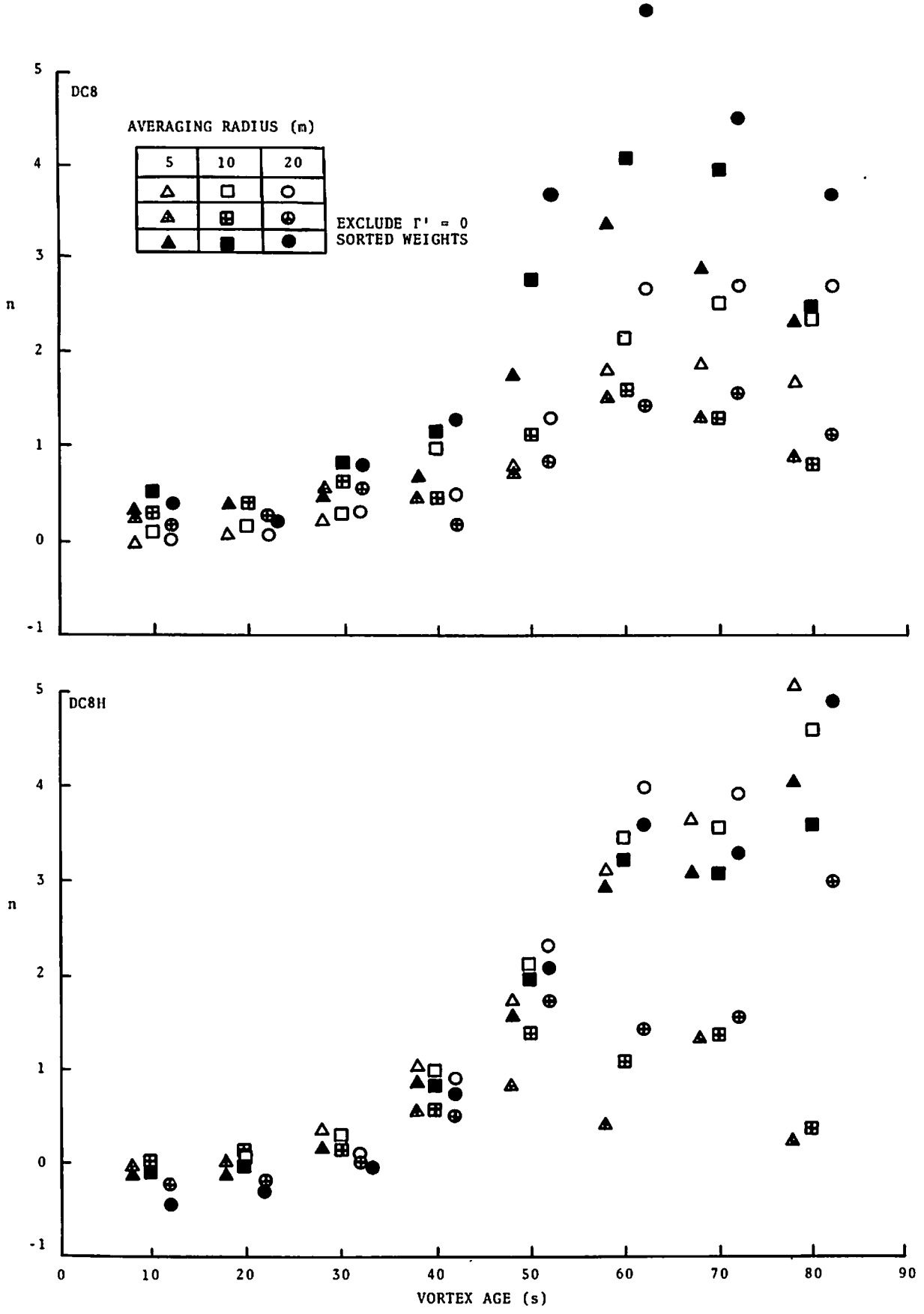

FIGURE 73. STRENGTH VERSUS WEIGHT POWER FOR THE DC-8

of cases. The vortex decay curves in Figure 71 and the power dependence curves in Figures 72 and 73 are undoubtedly strongly influenced by the time history extrapolation procedure (Section 2.1) and thus must be regarded of limited usefulness.

Now examine the effect of a vortex detection threshold on the measured power n. According to the analysis in Volume III, the distribution function $P(\Gamma)$ for the vortex strength can be modeled as

$$P(\Gamma) = \exp\ (-\Gamma/\overline{\Gamma}), \tag{F1}$$

where $\overline{\Gamma}$ is the average strength. If we have a strength detection threshold Γ_T below which the strength is zero, then one obtains the measured average strength as

$$\overline{\Gamma}_1 = \int_{\Gamma_T}^{\infty} \Gamma \exp\ (-\Gamma/\overline{\Gamma}) d\Gamma \Big/ \int_{o}^{\infty} \exp\ (-\Gamma/\overline{\Gamma}) d\Gamma \tag{F2}$$

$$= (\ \Gamma_T + \overline{\Gamma}\ ) \exp(-\Gamma_T/\overline{\Gamma})$$

when all cases are included, or

$$\overline{\Gamma}_2 = \int_{\Gamma_T}^{\infty} \Gamma \exp\ (-\Gamma/\overline{\Gamma})\ d\Gamma \Big/ \int_{\Gamma_T}^{\infty} \exp\ (-\Gamma/\overline{\Gamma}) d\Gamma \tag{F3}$$

$$= \Gamma_T + \overline{\Gamma}$$

if the cases with zero strength are excluded. The power n can be expressed as

$$n = \frac{d\overline{\Gamma}}{dW} \left(\frac{W}{\overline{\Gamma}}\right) . \tag{F4}$$

The corresponding expressions for n with a threshold are

$$n_1 = n \left(\frac{1}{1 + \Gamma_T/\overline{\Gamma}} + \frac{\Gamma_T}{\overline{\Gamma}} \right) \tag{F5}$$

for all cases, and

$$n_2 = n \left(\frac{1}{1 + \Gamma_T/\overline{\Gamma}} \right) \qquad \text{(F6)}$$

for zero strength cases excluded. In this model the value n_1 for all cases is greater than n and the value n_2 for zero strengths excluded is less than n. The errors can become large when $\overline{\Gamma}$ is less than Γ_T. Although this model is not an accurate representation of the extrapolation process leading to zero strength, it does give the trend observed in the data of Figures 72 and 73.

APPENDIX G

REFERENCES

1. Andrews, W.H., Robinson, G.H., and Krier, G.E., "Flight-Test Evaluation of the Wing Vortex Wake Generated by Large Jet-Transport Aircraft," FWP-18, Apr. 1970, NASA Flight Research Center, Edwards, CA.

2. Gupta, V.P., "Capacity Impact of Revising Aircraft Categories and Final Approach Separation Standards," MTR-7183, Mar. 1976, Mitre Corp., McLean, VA.

3. Burnham, D.C., "Chicago Monostatic Acoustic Vortex Sensing System, Volume I: Data Collection and Reduction," FAA-RD-79-103,I, Oct. 1979, DOT Transportation Systems Center, Cambridge, MA.

4. Aviation Week & Space Technology, 12 March 1979, p. 129.

5. Jane's All the World's Aircraft, edited by J.W.R. Taylor, Jane's Yearbooks, London, 1977/1978 and 1968/1969.

6. "Aircraft Data," Advisory Circular 150/5325-5B, July 30, 1975.

7. Tietjens, O.G., Applied Hydro- and Aeromechanics, Dover, New York, 1957, pp. 158-163.

8. Crow, S.C., "Stability Theory for a Pair of Trailing Vortices," AIAA J., Vol. 8, No. 12, Dec. 1970, pp. 2172-2179.

9. Bossel, H.H., "Inviscid and Viscous Models of the Vortex Breakdown Phenomenon," Ph.D. Thesis, Report A.S. 67-14, Aug. 1967, Univ. California, Berkeley, CA.

10. Hallock, J.N., "Vortex Advisory System Safety Analysis, Vol. I: Analytical Model," FAA-RD-78-68,I, Sep. 1978, DOT Transportation Systems Center, Cambridge, MA.

11. Gupta, V.P., "Vortex-Related Accidents over the Ten Year Period 1964-1973," FAA-EM-75-6, Apr. 1975, Mitre Corp., McLean, VA.

12. Piggott, B.A.M. and Pask, J.A. "Wake Vortex Incidents Reported in the UK 1972-1976," CAA Paper 77012, June 1977, Civil Aviation Authority, London, England.

13. Wonnacott, T.H. and Wonnacott, R.J., Introductory Statistics, Second Edition, John Wiley, New York, 1972, pp. 247-274.

220 copies

* U.S. GOVERNMENT PRINTING OFFICE: 1981 500-204/199

U.S. Department
of Transportation

**Research and
Special Programs
Administration**

Kendall Square
Cambridge, Massachusetts 02142